PERFORMANCE EVALUATION OF A CASCADED H-BRIDGE MULTI LEVEL INVERTER FED BLDC MOTOR DRIVE IN AN ELECTRIC VEHICLE

A Thesis

by

SRIRAM SARMA EMANI

Submitted to the Office of Graduate Studies of
Texas A&M University
in partial fulfillment of the requirements for the degree of

MASTER OF SCIENCE

May 2010

Major Subject: Electrical Engineering

PERFORMANCE EVALUATION OF A CASCADED H-BRIDGE MULTI LEVEL INVERTER FED BLDC MOTOR DRIVE IN AN ELECTRIC VEHICLE

A Thesis

by

SRIRAM SARMA EMANI

Submitted to the Office of Graduate Studies of
Texas A&M University
in partial fulfillment of the requirements for the degree of

MASTER OF SCIENCE

Approved by:

Chair of Committee,	Mehrdad Ehsani
Committee Members,	Karen Butler-Purry
	Shankar P. Bhattacharyya
	Mark Holtzapple
Head of Department,	Costas Georghiades

May 2010

Major Subject: Electrical Engineering

ABSTRACT

Performance Evaluation of a Cascaded H-Bridge Multi Level Inverter Fed BLDC Motor Drive in an Electric Vehicle. (May 2010)

Sriram Sarma Emani, B.Tech., Jawaharlal Nehru Technological University, India

Chair of Advisory Committee: Dr. Mehrdad Ehsani

The automobile industry is moving fast towards Electric Vehicles (EV); however this paradigm shift is currently making its smooth transition through the phase of Hybrid Electric Vehicles. There is an ever-growing need for integration of hybrid energy sources especially for vehicular applications. Different energy sources such as batteries, ultra-capacitors, fuel cells etc. are available. Usage of these varied energy sources alone or together in different combinations in automobiles requires advanced power electronic circuits and control methodologies.

An exhaustive literature survey has been carried out to study the power electronic converter, switching modulation strategy to be employed and the particular machine to be used in an EV. Adequate amount of effort has been put into designing the vehicle specifications. Owing to stronger demand for higher performance and torque response in an EV, the Permanent Magnet Synchronous Machine has been favored over the traditional Induction Machine.

The aim of this thesis is to demonstrate the use of a multi level inverter fed Brush Less Direct Current (BLDC) motor in a field oriented control fashion in an EV and make it follow a given drive cycle. The switching operation and control of a multi level inverter for specific power level and desired performance characteristics is investigated. The EV has been designed from scratch taking into consideration the various factors such as mass, coefficients of aerodynamic drag and air friction, tire radius etc. The design

parameters are meant to meet the requirements of a commercial car. The various advantages of a multi level inverter fed PMSM have been demonstrated and an exhaustive performance evaluation has been done.

The investigation is done by testing the designed system on a standard drive cycle, New York urban driving cycle. This highly transient driving cycle is particularly used because it provides rapidly changing acceleration and deceleration curves. Furthermore, the evaluation of the system under fault conditions is also done. It is demonstrated that the system is stable and has a ride-through capability under different fault conditions. The simulations have been carried out in MATLAB and Simulink, while some preliminary studies involving switching losses of the converter were done in PSIM.

DEDICATION

This thesis is dedicated to my mother for her love, my father for his wisdom and my brother for his support

ACKNOWLEDGEMENTS

I take this opportunity to thank my advisor Dr. Mehrdad Ehsani for his guidance and support during this thesis. He is a great mentor, an excellent teacher and the ideal guide for research. His insightful criticisms and patient encouragement aided the successful completion of this thesis. I would also like to thank Dr. Yimin Gao for his support in this work. I would like to show my appreciation to Dr. Karen Butler-Purry, Dr. Shankar Bhattacharyya and Dr. Mark Holtzapple for serving on my committee.

I am grateful to my colleagues Billy Yancey, Ronald Barazarte, Guadalupe Gonzalez, Richard Smith, Joshua Hawke, and Ali Eskandari for their support and contribution to knowledge. Credit goes to Tammy Carda and Jeanie Marshall for their help. I would like to thank my cousin Srihari Yamanoor for his suggestions. Special appreciation goes to Sangeeta for her encouragement and the innumerable conversations that kept me going through graduate school. I would like to thank all my friends for their companionship and encouragement.

My graduate studies would not have been possible without the support of my parents. I would like to thank my mother for her love and prayers, my father for his sage advice and wisdom, and my brother for his faith in me.

NOMENCLATURE

APOD	Alternative Phase Opposition Disposition
BLAC	Brush Less Alternating Current
BLDC	Brush Less Direct Current
BMS	Battery Monitoring System
CCA	Cold Cranking Amperes
CHB MLI	Cascaded H-Bridge Multi Level Inverter
CHB	Cascaded H – Bridge
CM	Common Mode
DTC	Direct Torque Control
EMF	Electro – Motive Force
EV	Electric Vehicle
FC	Flying Capacitor
FOC	Field Oriented Control
HEV	Hybrid Electric Vehicle
IM	Induction Motor
IPD	In-Phase Disposition
IPM	Interior Permanent Magnet
LSMM	Level Shifted Modulation Method
MLI	Multi Level Inverter
NO	Normally Open

NPC	Neutral Point Clamped
PI	Proportional Integral
PM	Permanent Magnet
PMSM	Permanent Magnet Synchronous Motor
POD	Phase Opposition Disposition
PPS	Primary Power Source
PSMM	Phase Shifted Modulation Method
PWM	Pulse Width Modulation
RMS	Root Mean Squared
RPM	Rotations Per Minute
SOC	State Of Charge
SRM	Switched Reluctance Motor
THD	Total Harmonic Distortion

TABLE OF CONTENTS

Page

Page

Page

Page

LIST OF FIGURES

Page

Page

Page

LIST OF TABLES

Page

1. INTRODUCTION

For the better half of the 20th century, Electric Vehicles (EVs) have been thought of, designed and developed to suit a variety of applications; from concept cars to advanced military vehicles. EVs specifically as pertaining to the commercial car market have been gaining lots of prominence because of ecological reasons to reduce air pollution and vehicle emissions. The economic depression of 2008-2009 has also caused many automobile majors to undergo a massive restructuring within their respective organizations to engage in further research in electric vehicles and introduce successful and competitive products. As the automobile industry evolves to introduce increased number of efficient vehicles, the suitable path is towards EVs. This transition is happening through an intermediary stage of Hybrid Electric Vehicles, but as technologies in automobile industry progress the move towards EVs is happening faster than previously imagined. The main challenges facing EVs today are improved battery technology, public recharging infrastructure and extending mileage range.

The latest improvements in control systems, transducers & instrumentation, and smart vehicle technology are enabling vehicles to be more and more automated. Universities of international repute such as Texas A&M University, Stanford University and Massachusetts Institute of Technology hold competitions for building and racing EVs. Concept cars that run on a variety of energy sources and exhibiting remarkable efficiencies and performance are displayed at such symposiums. The mandate for fuel efficient vehicles with active participation especially in states such as California, USA along with richer incentives for green technologies has brought in the right time for increased number of EVs on the road. Some states have imposed regulations proposing a minimum number of cars per year with zero emissions, which can be met by the EVs.

This thesis follows the style and format of *IEEE Transactions on Power Electronics*.

1.1 Motivation

Multi Level Inverter (MLI) topologies have been widely used in the motor drive industry to run induction machines for high power and high voltage configurations. Traditional multi level converter topologies such as Neutral Point Clamped (NPC) MLI, Flying Capacitor (FC) MLI, and Cascaded H-Bridge (CHB) MLI have catered to a wide variety of applications. The CHB MLI is probably the only kind of multi level inverter where the individual energy sources (capacitors, batteries etc) can be completely isolated DC sources. Induction Motors (IMs) have been traditionally used for nearly all types of industrial and vehicular applications. However in the last 10 years active research has shown that vehicular applications demand high performance which might be delivered by motors other than IMs. These include Brush Less DC, Permanent Magnet Synchronous Machines, Switched Reluctance machines etc.

The obvious reasons for traditionally using Induction Motor is that the motor technology and control methodologies are well understood both by the academia and the industry. The paradigm shift towards the use of Permanent Magnet Synchronous Machines and Brushless DC Machines has been due to the increased demand in high performance, faster torque response and enhanced speed and efficiency from vehicles.

The MLI offers advantages in vehicular electronic applications that other converters cannot. MLIs allow a scalable system with modularity that provides for more flexibility and reliability. Depending on the type of switching modulation strategy used, it is possible to have switching redundancies which facilitate easier control and also lower switch stresses. CHB in particular allows the use of isolated DC sources which further reduces any potential electric hazards, since the smallest individual voltage across any one battery terminal is small.

Literature has suggested different means to connect various DC sources to power a motor drive to run an electric vehicle; however the emerging and efficient one turns out to be the one using multi level converters. Significant work has been previously done in the area of MLIs as employed in industrial motor drives. Most of these applications

utilized Induction Motors as the traditional choice to be the power horse. More demanding and specialized applications which require excellent performance and fast torque response are turning towards Permanent Magnet Synchronous Machines since they deliver much better than Induction Machines.

The choice of motor is Permanent Magnet Synchronous Motor (PMSM) as opposed to the traditional Induction Motor (IM). Some important reasons for this are the higher speeds achievable by PMSM. The Electro-Magnetic Interference (EMI) from the inverter is much lesser in PMSM as compared to IM. The inverter for an IM driven system might experience 'shoot-through' and would require dead time circuits and compensation. The PMSM offers smooth rotation without torque ripple and high efficiency. PMSMs offer high performance and speed characteristics that are vital for modern electric vehicles, which are not achievable by the use of IM. PMSMs avoid the use of slip rings, hence it is simpler and maintenance free. Apart from these reasons, taking into consideration the comparable cost per HP of the motor, the PMSM is already becoming the favorite choice of all automobile majors in manufacturing EVs.

Work has never been done before in employing a standard drive cycle to test an actual on-road system performance by exploring the design of an electric vehicle right from the details of power electronics through the motor parameters.

Brushless DC Motors using high energy magnets offer a further substantial weight reduction and efficiency improvement. It is also very firmly believed that in the next decade there would be a steep fall in costs owing to more manufacturers entering the industry. Another reason for improvement would be due to richer investments in lower rare earth magnets to achieve higher energy density. Employing Samarium Cobalt (SmCO) rare earth magnets allow the PMSMs to be constructed smaller than reluctance motors, thus saving a lot in the frame size. This reduces both weight and size while providing improved operational benefits. Rare earth magnets with high coercive force are used to prevent the motors from demagnetizing in an over-voltage and/or over-temperature condition.

Simulation allows for exhaustive experiments to be carried out on the proposed system in a virtual environment. The system can be tested only when it is run to perform standard drive cycles like FTP-75, New York City urban etc. Simulation studies were performed for the vehicle using a simple acceleration and deceleration drive cycle, an FTP-75 urban drive cycle, and a commuter drive cycle. Various performance parameters generated during the simulation studies are graphically presented in the thesis.

1.2 System Specifications

The average continuous power range is expected to be 150-300 kW, while it might be larger for big military vehicles or mass transit systems. The design of the motor, switching circuitry, switch ratings etc all depend on the power capacity of the vehicle. Since the vehicle envisaged is an EV, the entire vehicle acts as a load for the electric motor. The design of the motor power and battery packs is a result of the calculations from vehicle design.

1.3 Power Electronics Implementation

The MLI is a unique type of inverter that is popular for high power applications that do not necessarily need stringing together various power sources to employ high voltage. Some of the salient features include modularity, flexibility and extended control over the system architecture. What was difficult earlier in terms of embedded control using microprocessors or microcontrollers has become easier because of use of DSPs and FPGAs.

1.4 Research Objectives

Based on the motivation for the research problem taken up, and literature survey carried out, the proposed objectives of this thesis work are as follows:

a) To design a Multi Level Inverter (MLI) fed Brush-Less DC (BLDC) motor drive for an Electric Vehicle (EV) application. This design also involves design of the EV in complete detail i.e. the electrical, mechanical and physical specifications of the entire system including the motor, battery packs, voltage levels etc.

b) To explore the feasibility of the MLI in a Cascaded H-Bridge configuration and explore both symmetrical and asymmetrical fashions.
c) To subject the designed system to a standard drive cycle, evaluate its performance like torque response, acceleration and closed loop speed control.
d) To explore the BLDC motor drive in a Field Oriented Control (FOC) technique to achieve the closed loop speed control for the EV to closely follow the reference drive cycle.
e) To evaluate the performance of the batteries during charge and recharge cycles, especially during regeneration which is achieved through the electrical braking.

1.5 Demand for Electric Vehicles

In a popular survey carried out by a website, 'Demand for Electric Vehicles' as opposed to other forms of similar transportation such as Hybrid Electric Vehicles (HEV), Plug-in Hybrid Electric Vehicles (PHEV) and the traditional gasoline engine vehicles, the EV was the most popular choice for future transportation scoring about 56%. A total of about 745 respondents were asked their choice of the most appealing alternative fuel vehicle. The battery powered EV is the kind which is fit with rechargeable batteries so that the vehicle can charge itself during braking or coasting, though with a limited driving range for each charge. It requires no gasoline and can cover about 300-400 km or 200-250 miles per charge. The HEV is a combination of EV and gasoline, typically has lesser driving range and uses gas to travel longer distances. The PHEV is the kind of HEV that can be charged from specific charging outlets typically which should be made available to public similar to gasoline stations. They provide a driving range of about 100 km and run on gas for longer distances or need to be charged again (usually both).

The EVs are vehicles which in theory drive with zero emissions contingent on the origin of how and where the electricity is produced. Although this is the most attractive option to many, it is not yet available as a bulk-produced vehicle. Most EVs currently on the market are not within the means of the middle class and face many different obstacles in order to stay in business. However this particular scenario is rapidly changing owing to

political reasons such as favorable government policies and economic stimulus funding. It is very interesting to see that a majority of the sampled population is still very interested in the battery powered EV as compared to the more common hybrid vehicle.

The question that plagues most supporters and critics of EVs is whether there is adequate infrastructure to support mass produced EVs. The answer to this question is that development in EV technology and infrastructure has to go hand in hand so they can complement each other well.

1.6 Outline of the Thesis

The following sections investigate the use of a multi level inverter to run a BLDC motor drive in an electric vehicle.

Section 2 gives a description of the state-of-the-art technologies in this research area. An exhaustive literature survey has been carried out to understand what has been already attempted, what efforts can be carried out to implement the proposed system and also improve it to make it better than previous work. This includes a thorough background of multi level inverters, permanent magnet synchronous motors, drive control techniques, and design.

Section 3 deals primarily with multi level inverters. A detailed explanation of the types of MLI, the relevant topologies along with their merits and demerits is given. The fundamental theory of operation and control of MLI is explained with relevant examples. Some light is thrown on the types of switching modulation strategies that can be employed to drive MLI.

In Section 4, the design of the proposed system is undertaken. This work involves designing the electric vehicle including all mechanical and electrical parameters, sizing of energy source (battery packs) and motors, transmission gear ratio etc. The equations governing the design are also provided.

Section 5 discusses the simulation modeling and implementation of the above designed system. The simulation models are explained in detail, while some parametric values are

left to be listed in the appendix. The interconnections of the various sub-system blocks to achieve the simulation are shown.

Section 6 discusses the results of the simulation implementation. A fault analysis has been conducted in order to test the implemented system's tolerance in the presence of faults. The results of this analysis are also discussed and illustrated.

Section 7 discusses the implications of the simulation results. It talks about the conclusions drawn, scope for future research and recommendations.

2. LITERATURE SURVEY

2.1 Survey of AC Motors

The induction motor (IM), thanks to its well-known advantages of simple construction, reliability, ruggedness, and low cost has found very wide industrial applications. Furthermore, in contrast to the commutation dc motor, it can be used in an aggressive or volatile environment since there are no problems with spark and corrosion. These advantages, however, are superseded by control problems when using an IM in industrial drives with high performance demands. This is where the Permanent Magnet Synchronous Motor (PMSM) comes in, because it serves very well for high performance vehicular applications (especially on-road commercial cars) where a driver is more concerned about factors such as efficiency, speed, reliability and acceleration. The PMSM is a rotating electric machine where the stator is a classic three-phase stator like that of an induction motor and the rotor has surface-mounted permanent magnets. In PMSMs there is no stator power dedicated to the magnetic field production. The work by Rais and Donsion in [1] describes the basic modeling and equivalent circuit representation of a PMSM in addition to the influence of its parameters on the operation of synchronization.

2.1.1 Permanent Magnet Synchronous Motor

PMSMs have a variety of applications in many areas such as automobiles, robotics, traction, and aerospace technology. PMSMs have extensive industrial and robotic applications due to their high efficiency, low inertia and high torque-to-volume ratio and this is due to its several advantages like high efficiency, compactness, fast dynamics and high torque to inertia ratio. A detailed comparison and reasons for choosing PMSM over the IM is better explained by the authors of [2] in the following two tables. The first one (Table 1) describes the features of the motors, while the second one (Table 2) describes the attributes of the converters driving the respective motors.

Table 1. Quantitative comparison of induction, switched reluctance and PM brushless motors for electric vehicles

Parameters	Induction Motors		Switched reluctance motors		PM brushless motors	
	Value	*Deviation*	*Value*	*Deviation*	*Value*	*Deviation*
Efficiency, %	93.4	1.8	93.0	2.8	95.2	1.6
Output power to mass, KW/Kg	0.7	0.5	0.7	0.6	1.2	1.1
Torque ripple, %	7.3	6.3	24.0	14.5	10.0	4.1
Overload capacity factor	2.43	0.56	1.86	0.57	2.12	0.54
Volume to output power, l/KW	1.8	1.6	2.6	1.8	2.3	1.6
Maximum speed, rpm	12700	6300	12400	8200	9400	4670

Table 2. Quantitative comparison of induction, switched reluctance and PM brushless motor converters for electric vehicles

Parameters	Induction Motor converters		Switched reluctance motor converters		PM brushless motor converters	
	Value	*Deviation*	*Value*	*Deviation*	*Value*	*Deviation*
Efficiency, %	95.0	2.1	96.1	2.0	95.9	1.9
Output power to mass KW/Kg	1.8	1.2	1.3	0.2	1.7	0.6
Volume to output power, l/KW	1.6	1.2	1.0	0.0	0.9	0.3

Of late PMSMs are being manufactured to possess characteristics such that they are more powerful with lower mass and having lower moment of inertia. In this respect, the PMSM is equivalent to an induction motor where the air-gap magnetic field is produced

by a permanent magnet. The use of a permanent magnet to generate a substantial air-gap magnetic flux makes it possible to design highly efficient PM motors. The power density of a PMSM is greater than that of an induction motor with the same ratings.

In theory, a permanent magnet brushless motor with any back-EMF waveform (depending on the conduction angle used) can be employed in either BLAC or BLDC mode. However, in practice, it is advantageous for a BLAC motor to have a sinusoidal back-emf and a BLDC motor to have a trapezoidal back-EMF waveform. This is so as to maximize the efficiency and torque capability and minimize the torque ripple. In a BLAC motor drive, the phase current is regulated by a pulse width-modulation (PWM) inverter so as to obtain a sinusoidal waveform and hence vector control is often employed. Alternatively in a BLDC motor drive, the PWM phase current possesses a rectangular wave form. BLDC motors often use concentrated windings, as it results in shorter end windings. This is preferred for getting superior efficiency and high torque density. Furthermore, BLAC drives require a precision rotor position sensor such as Hall devices in order to sense the current commutation points that occur in repetition every 60 electrical degrees. So in general for the above reasons, BLDC motor drives are cheaper when compared with BLAC motor drives.

BLDC machines are used in applications ranging from servo to traction drives owing to several distinct advantages such as high power density, excellent efficiency, large torque-to-inertia ratio, and enhanced controllability. These have been explained well by Toliyat in [3]. Brushless DC motor (BLDC) fed by two phase conduction scheme has higher power-to-weight and torque-to-current ratios. The well known method to control BLDC motors is through PWM current control in which a two-phase feeding scheme is utilized with a variety of PWM modes such as soft switching, hard-switching etc. Therefore, a relatively cheaper drive is obtained when compared to a PMSM drive with expensive high resolution position sensor, such as an optical encoder.

2.2 Control Methodology

According to Buja [4], motor control methods can be broadly categorized into scalar and vector control methods. The general classification of the variable-frequency methods is presented in (Figure 1).

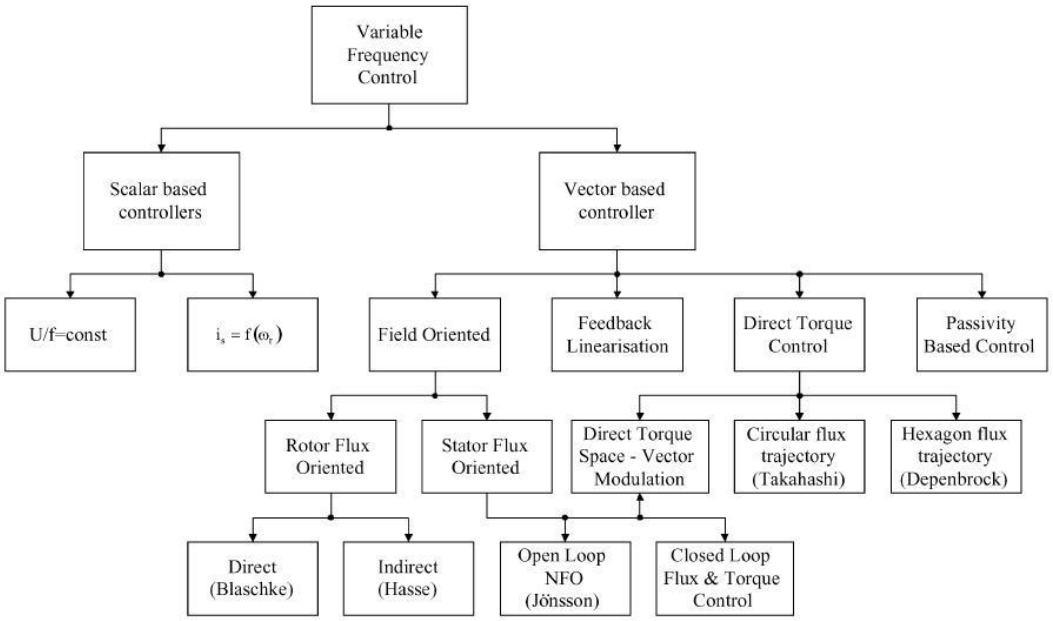

Figure 1. Classification of control methods

In scalar control, which is based on relationships valid in steady state, only magnitude and frequency (angular speed) of voltage, current, and flux linkage space vectors are controlled. Thus, the scalar control does not act on space vector position during transients. Contrarily, the vector control is a versatile and general control philosophy. It is based on relations valid for dynamic states, not only magnitude and frequency (angular speed) but also instantaneous positions of voltage, current, and flux space vectors are controlled. Thus, the vector control acts on the positions of the space vectors and provides their correct orientation both in steady state and during transients.

The most well known method known as field oriented control (FOC) or vector control, was expounded by Blaschke [5], and gives the induction motor a very good performance. The same principles can be applied to PMSM and this approach is explored. In the vector control methodology, the equations governing the motor are transformed into a coordinate system which rotates in synchronism with the rotor flux vector with new coordinates called field coordinates. In field coordinates—under constant rotor flux amplitude—there is a linear relationship between control variables and torque. Also, similar to that in a separately excited dc motor, the reference for the flux amplitude is reduced in the field-weakening region in order to limit the stator voltage at high speed. Transformation of equations in the field coordinates has a good physical basis because it corresponds to the decoupled torque production in a separately excited dc motor. However, from the theoretical point of view, other types of coordinate transformations can be selected to achieve decoupling and linearization of the motor equations. This led to other methods such as nonlinear control, feedback linearization control and input–output decoupling methods as described in [6, 7] .

Direct Torque Control (DTC) adjusts motor torque and stator flux magnitude in a closed-loop fashion where the feedback values are estimated from stator voltage and current vectors in stator-fixed coordinates. Therefore, it is a general control strategy independent of rotor parameters and can be applied to Induction Motor (IM) and also to all types of synchronous motors including PMSMs. In either case, both hysteresis-based DTC [8, 9], and DTC-SVM schemes can be used.

2.2.1 Direct Torque Control of PMSM

When compared with IMs, the initial parametric value of the stator flux in PMSMs is not zero and is instead dependent on the rotor position. In motion-sensorless PMSM drives, the initial position of the rotor is not known and this often causes troubles such as initial backward rotation, torque ripple and problems of synchronization. For non-salient (with surface-mounted magnets) PMSMs, reliable position estimation is more difficult than for salient (with buried or inserted magnets) construction [10], where the initial position can

be calculated in a definitive manner by exploiting the sinusoidal inductance variation. For a non-salient PMSM to start with light loads, a simple low-pass filter instead of a pure integrator in the flux estimator can be used [11]. This solves the problem of flux initial conditions.

Direct Torque Control as applied to PMSM has been explained well by Liu et al. in [12]. This paper studied the application of direct torque control, to a three-phase BLDC drive operating in the 120 degrees conduction mode (i.e., two phases conducting) to achieve instantaneous torque control, improved system performance and reduced torque ripple. The popular control method for BLDC drives is current control, which essentially assumes that the torque is proportional to the phase current. One must remember that in practice the above relationship i.e. that between torque and phase current is nonlinear. Hence various current control strategies have been suggested in previous literature to minimize torque pulsations. An instantaneous torque controller based on variable structure control in the d-q reference frame was projected in [13, 14]. Other relevant literature has also suggested means such that electro-magnetic torque pulsations were reduced with the aid of a torque controller in which the torque was estimated by utilizing the product of the instantaneous back-EMF and current. The real-time estimation of the back EMF employing a model reference adaptive method was reported in [15] which used a variable structure torque controller with space-vector PWM.

Direct torque control (DTC) was initially developed for IM drives and directly controls the flux linkage and electromagnetic torque. A relationship is established between the flux and the torque and an optimal switching strategy is devised for the inverter so as to accomplish a fast torque response. It is less sensitive to parameter variations, and is basically simple to implement. DTC has been effectively applied to IMs and in recent times to BLAC machines. The authors in [16] analyzed the DTC of a BLDC with non-sinusoidal back-emf. In [12] the voltage space vectors in a two phase conduction mode are explained and the electromagnetic torque equation based in a stationary reference frame is derived for surface-mounted PMSMs with non-sinusoidal back-EMF (BLDC).

2.2.2 Field Oriented Control of PMSM

The Field Oriented Control (FOC) method is one of the most popular high-performance control strategies for PMSM. The vector control theory of electrical drives is based on the control of the magnitude and phase of each phase current and voltage. It is possible to realize far more precise and accurate digital vector control algorithms with the introduction of high computational power silicon devices into the market, such as the TMS320F240 from Texas Instruments (TI). The primary principle in controlling a PMSM drive is based on field orientation. Since the magnetic flux generated from the PM rotor is fixed in relation to the rotor shaft position, the flux position in the coordinates can be determined by the shaft position sensor. FOC machines need two constants as input references. They are the torque component (aligned with the q co-ordinate) and the flux component (aligned with d co-ordinate). FOC scheme is an extremely popular and accurate vector control method in view of the following:

1. Capability of performing direct torque control
2. Handling system limitations and
3. Achieving higher power conversion efficiency

The FOC scheme is founded on three major points:

1. The machine current and voltage space vectors
2. The transformation of a three phase speed
3. Time dependent system into a two co-ordinate time invariant system and effective Pulse Width Modulation pattern generation

The control resembles three separate single-phase system controls rather than one control of a three-phase system. The FOC controls the stator currents represented by a vector and this control is based on projections, which transforms a three-phase time and speed dependent system into a two co-ordinate (d and q co-ordinates) time invariant system. These projections lead to a structure that is similar to a DC machine control. As FOC is based on projections, the control structure handles instantaneous electrical quantities, which makes the control accurate in every working operation (steady state and transient) and independent of the limited bandwidth mathematical model. Thus, the

FOC solves the classic problems by easily reaching constant reference (torque component and flux component of the stator current). It helps apply direct torque control because in the (d,q) reference frame the expression of the torque is: $m \propto \psi_R i_{sq}$.

The basic working diagram of the FOC scheme is shown in (Figure 2).

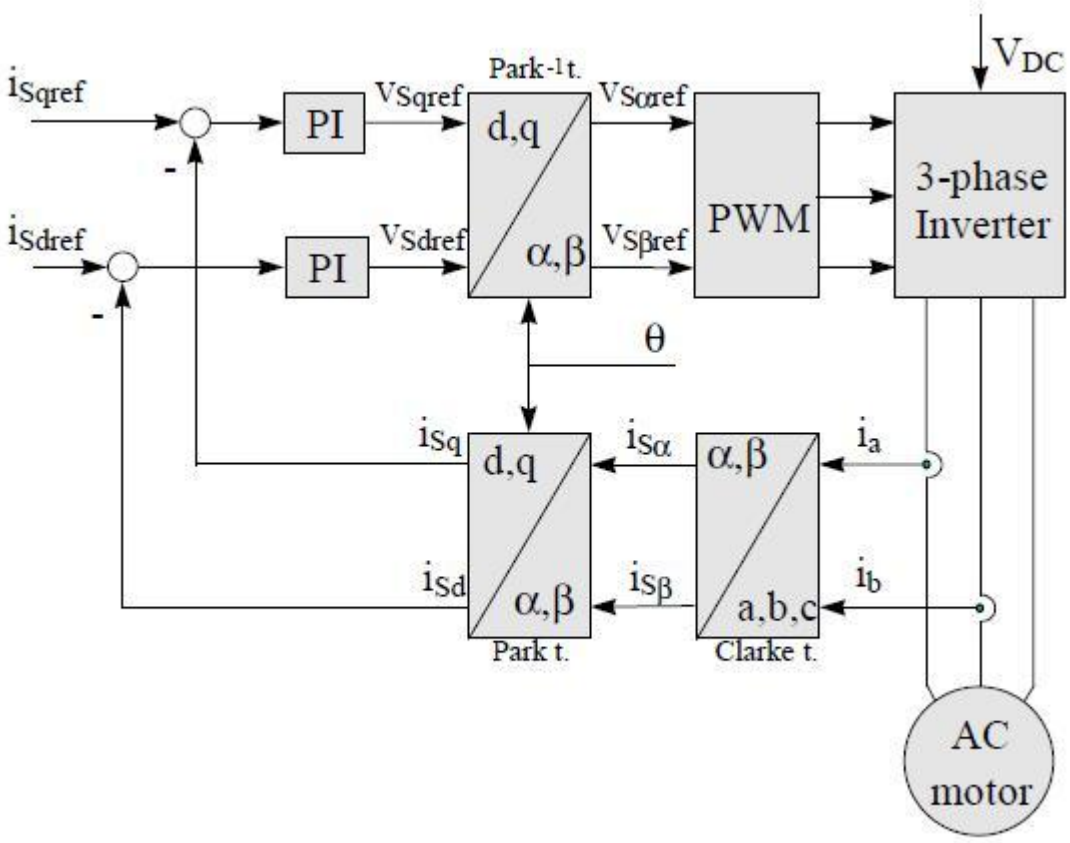

Figure 2. Basic scheme of FOC for AC motor

By maintaining the amplitude of the rotor flux (ψ_R) at a constant value one can generate a linear relationship between torque and torque component (i_{sq}). Thus the torque can be commanded, by controlling the torque component of stator current vector. Two motor phase currents are measured and these measurements feed the Clarke transformation module. The outputs are designated $i_{sα}$ and $i_{sβ}$ which are then used as the inputs for the

Park transformation that gives the current in the d,q rotating reference frame. The i_{sd} and i_{sq} components are compared to the references i_{sdref} (the flux reference) and i_{sqref} (the torque reference). At this point, this control structure displays an interesting advantage: it can be used to control the synchronous machine by simply changing the flux reference and obtaining rotor flux position. As in a PMSM, the rotor flux is fixed (determined by the magnets). Hence, when controlling a PMSM, isdref should be set to zero.

The torque command i_{sqref} could be the output of the speed regulator when we use a speed field oriented control scheme. The outputs of the current regulators are v_{sdref} and v_{sqref} and are applied to the inverse Park transformation. The outputs of this projection are $v_{s\alpha ref}$ and $v_{s\beta ref}$ which are the components of the stator vector voltage in the a,b stationary orthogonal reference frame and these become the inputs of the Space Vector PWM. The outputs of this block are the signals driving the inverter. It may be noted that both Park and inverse Park transformations need the rotor flux position and obtaining this rotor flux position depends on the AC machine type (synchronous or asynchronous).

The two fundamental requirements for the FOC are:

1. A knowledge of two phase currents (as the motor is star-connected, the third phase current is also known, since $i_a + i_b + i_c = 0$), and
2. The rotor flux position.

The measured phase currents i_a and i_b are sampled and then converted by A/D converter and the correct working of the FOC depends on the true measurement of these currents. In the synchronous machine the rotor speed is equal to the rotor flux speed. Then θ (rotor flux position) is directly measured by position sensor or by integration of rotor speed.

In summary, AC machines controlled in the FOC scheme enjoy every advantage achieved by DC machine such as instantaneous control of the separate quantities allowing accurate transient and steady state management. In addition they also succeed in solving the mechanical commutation problem inherent with DC machines.

3. MULTI LEVEL INVERTERS

3.1 Introduction

A brief introduction to the three main types of multi level converters involves an analysis of diode-clamped, capacitor-clamped and cascade H-Bridge converters. For this study, the cascade MLI is considered for use in large EV drive systems mainly because the available batteries make this inverter the favorite choice. Additional features such as its battery management capability, redundant switching states in inverter operation, and scalability make the cascade inverter the MLI of choice.

MLIs divide the main dc supply voltage into several dc sources which are used to synthesize an ac voltage into a stepped approximation of the desired sinusoidal waveform. The stepped approximation is also popularly known as the staircase model. An exhaustive literature survey was done to investigate the research work previously done in the area of MLIs. It is believed that the oldest reference to multi level power conversion is often stated to start with the paper presented by Nabae et al. [17]. Baker [18] patented a method of employing a programmed switching system for an inverter with cascaded stages.

The number of stages (cells or capacitors depending on the respective topology) helps decide the power capacity of the converter as a whole. Suitable connections either in series or shunt mode or both are done to achieve higher voltage and/or current ratings. One of the biggest advantages of using a MLI is that the transformer can be eliminated and this helps enhance efficiency and cost effectiveness.

The three popular topologies in MLI are as follows:

1. Neutral Point Clamped (NPC) Multi Level Inverter
2. Flying Capacitor (FC) MLI
3. Cascaded H-Bridge MLI

While a more detailed description of these specific inverters and their basic operation principles is given in the next section, the basic MLI topologies are shown in (Figure 3). Furthermore, the favored choice of MLI for this application is explained along with appropriate reasons and interpretation.

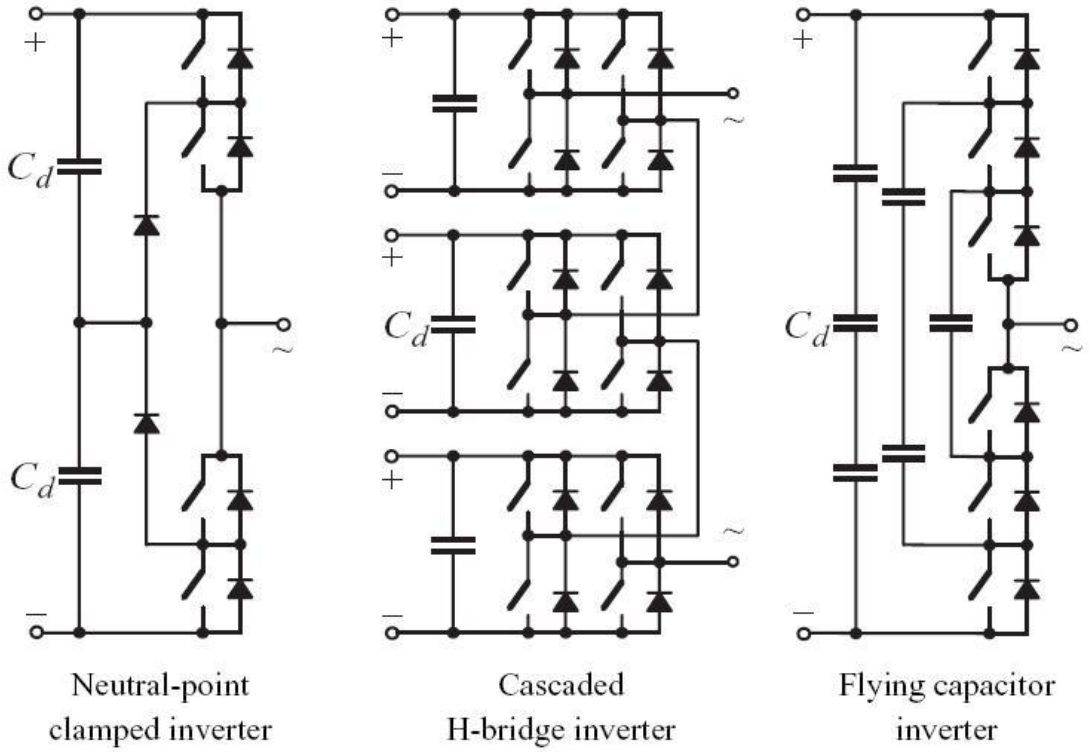

Figure 3. Multi level inverter topologies

The most attractive features of MLIs are as follows:

1. They can achieve voltage operation above usual limits of classic semiconductors, low harmonic distortion, low EMI, near sinusoidal outputs together with small dv/dt's for the power devices.
2. The generalized MLI topology can balance each voltage level by itself regardless of load characteristics [19].

3. They draw input current with very low distortion and better wave-shape.
4. They produce smaller common-mode (CM) voltage, thus minimizing the stress in the motor bearings. Further, using sophisticated modulation methods such as those suggested by Enjeti et al. in [20], CM voltages can be completely eliminated.
5. They can operate with a reduced switching frequency [21].
6. The modularity and flexible design allows for easy expansion, reconfiguration and retrofitting of most systems.

3.1.1 Neutral Point Clamped Multi Level Inverter

The generally popular diode-clamped inverter is known as the Neutral Point Clamped inverter (NPC) [22, 23]. The NPC consists of two pairs of series switches (upper and lower) in parallel with two series capacitors where the anode of the upper diode is connected to the midpoint (neutral) of the capacitors and its cathode to the midpoint of the upper pair of switches; the cathode of the lower diode is connected to the midpoint of the capacitors with its anode connected to the midpoint of the lower pair of switches. These clamping diodes are also called anti-parallel diodes. The simplest NPC topology i.e. three level schematic was shown in (Figure 3).The capacitor voltage mismatch may be controlled using a back-to-back topology as illustrated by Tolbert et. al. [24, 25] connecting resistors in parallel with capacitors, or using redundant voltage states. The characteristics of a NPC (example three-level) converter are:

1. Lower line-to-line and CM voltage steps as compared to other topologies
2. More voltage steps in one carrier cycle, hence smoother waveform
3. In comparison to other MLI topologies, a lower ripple component in the output current, hence one can achieve better wave-shape and lesser distortion for the same carrier frequency

One major problem with the NPC approach as described in [26], is the unequal load distribution among the switches and capacitors, especially for higher level converters. The advantages and disadvantages of the NPC MLI (of say m levels) are as follows:

Advantages:

1. A large number of levels ‘m’ yields a small harmonic distortion
2. All phases share the same DC bus
3. Reactive power flow can be regulated
4. High efficiency for fundamental switching frequency
5. The control method is fairly simple

Disadvantages:

1. Real power flow is difficult because of the capacitors' imbalance problem
2. Excessive clamping diodes (m-1)(m-2) are required per phase
3. Different current ratings for switches are required due to their duty cycle

3.1.2 Capacitor Clamped Inverter / Flying Capacitor Inverter

The Flying Capacitor (FC) MLI is similar to the NPC topology. Also known as the capacitor-clamped MLI topology it allows more flexibility in waveform synthesis and helps balance voltage across the clamped capacitors. An example of FC MLI topology was shown in (Figure 3).

Additional clamping diodes not being required implies lesser power devices, hence an expected decrease in the converter’s switching losses. This topology promises low harmonic distortion, hence there would be no need of filters, their large number of storage capacitors can provide buffer capabilities during power outages. They provide switch combination redundancy for balancing different voltage levels, both real and reactive power flow can be controlled .

One of the biggest advantages of FC MLI over the NPC topology is that one capacitor replaces two diodes (clamping / anti-parallel diodes) resulting in a natural simplification of topology and reduction in overall losses. The advantages and disadvantages of the m-level FC MLI are as follows:

Advantages:

1. Comparatively lower switching and conduction losses in the converter than the NPC MLI owing to lesser number of power devices
2. Large ‘m’ utilizes capacitors extra energy during long discharge transient
3. Lower Total Harmonic Distortion (THD) when the number of levels is high
4. Presence of switch redundancies accommodates for balancing different voltage levels to acquire the required inverter output voltage amplitude
5. Both real and reactive power flow can be regulated.

Disadvantages:

1. Large number of capacitors are bulky and generally more expensive than the clamping diodes used in the diode clamped MLI
2. They require large number of storage capacitors
3. More complicated control as compared to the simpler control employed in NPC MLI is required to maintain the capacitors voltage balance in FC MLI
4. For higher power levels, the converter losses are comparable to that of a NPC MLI and efficiency is lower for real power transmission
5. Complex pre-charging circuits are required

3.1.3 Cascade H-Bridge Multi Level Inverter

The Cascaded H-Bridge (CHB) Multi Level Inverter (MLI) is a cascade of H-Bridges, or H-Bridges in a series configuration. A CHB MLI consists of a string of H-Bridge (single-phase full bridge configuration) inverter units in each of its three phases. An example of a CHB MLI is shown in (Figure 4(a)). The three-level converter has the same configuration as a single H-Bridge inverter, a single phase full bridge inverter used in unipolar PWM. The four switches S1, S2, S3 and S4 are operated within limits to generate three discrete outputs Vab with levels of -Vdc, 0 or +Vdc. When S2 and S3 are on the output is -Vdc, when either pair S1 and S2 or S3 and S4 are on the output is 0,

and when S1 and S4 are turned on the output is +Vdc. The simplest inverter i.e. a H-Bridge inverter is illustrated in (Figure 4(b)).

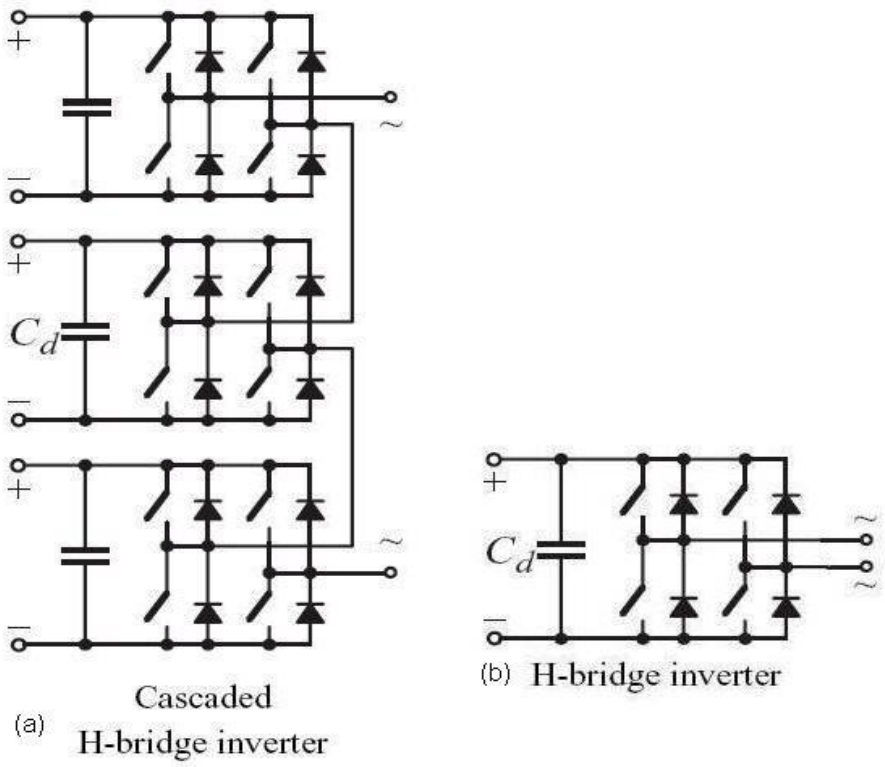

Figure 4. CHB MLI topology and H-Bridge inverter example

The advantages and disadvantages of a cascade H-Bridge MLI with a separate dc sources per phase are described as follows [27].

Advantages:

1. The series structure allows a scalable, modularized circuit layout and packaging since each bridge has the same structure.
2. Requires minimum number of components considering there are no extra clamping diodes or voltage balancing capacitors.

3. Switching redundancy for inner voltage levels is possible because the phase voltage is the sum of each bridge's output.
4. On an average, it is observed that the number of redundant switching states is more as compared to the NPC MLI or the FC MLI.
5. Due to the isolated / independent DC sources, the potential of electrical shock is greatly reduced which renders safer on-board wiring procedures
6. A very flexible scalability is achieved because the modularity in the system allows a racked up structure
7. The above features also allow for high reliability of operation

A known disadvantage is that it is limited to certain applications only where separate (isolated) DC sources are available, such as in EV or space shuttle.

Some additional advantages of EV drive systems using the CHB MLI are as follows:

1. redundant switching operation to balance battery use
2. rotation to ensure charge balance between batteries
3. ride through capability which operates using a minimal number of levels
4. worst case operability which maintains operation at a reduced performance

The batteries can be switched on in different ways to synthesize the required output voltage, thus enhancing EV drive system’s operability, and system’s management flexibility. A minimal number of sources may be applied to operate the drive system at reduced performance, which would default to a ride through or worst case mode [27].

3.2 Multi Level Inverters for Electric Vehicle Applications

Development of electric drive trains for large commercial vehicles will result in greater fuel efficiency, reduced emissions, and possibly better vehicle performance (acceleration, coasting and braking). MLIs are ideally suited for these applications because of the high VA ratings possible [24, 28]. For EVs, the highly advantageous CHB MLI can be used to drive the traction motor from a set of batteries or fuel cells.

This is well illustrated in (Figure 5), and is explained further here. Each H-Bridge unit in a CHB MLI has its own DC source (represented by E Volts here), which for an EV would be a battery unit or battery pack. The upper cell in one phase is denoted by H1 and the lower cell by H2.

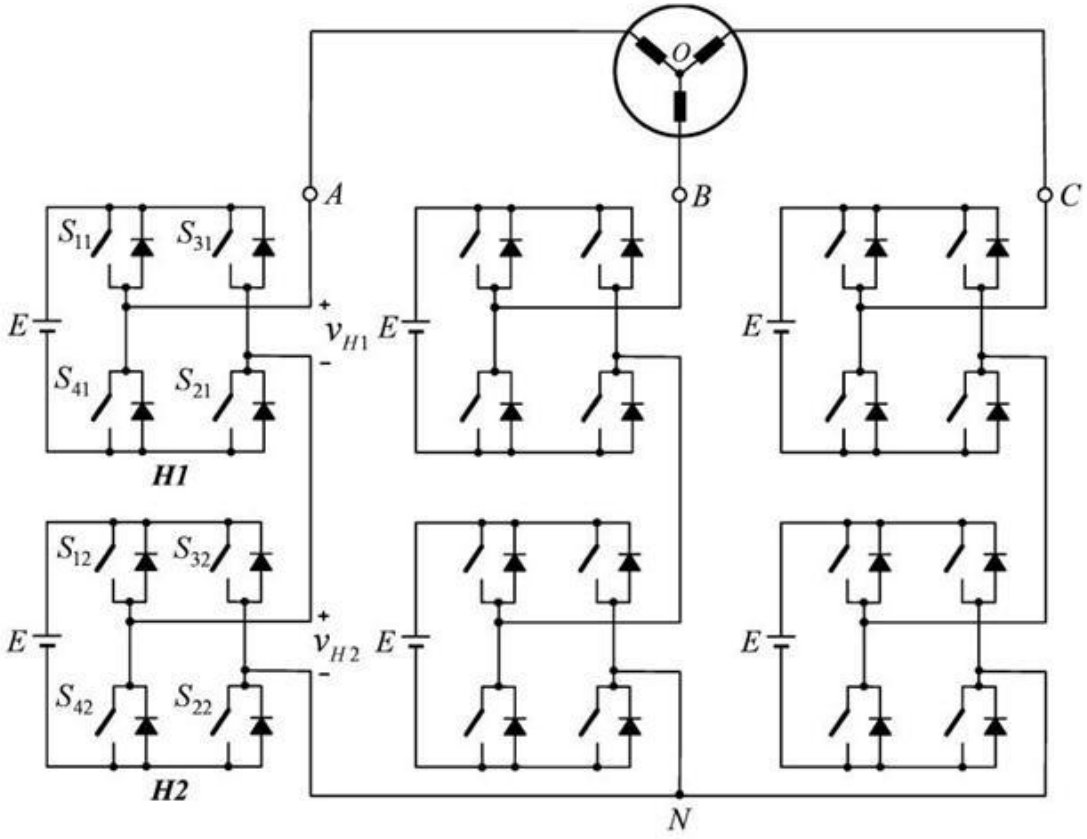

Figure 5. CHB MLI fed PMSM

The above figure portrays an important building block of the work accomplished in this work. Its implementation in MATLAB Simulink is explained in the later sections. This cascade inverter makes EVs more accessible/safer and open wiring is made possible for most of an EV's power system because each low voltage battery is isolated through switching devices. The switches' offstate leakage currents are within safe limits.

The way the individual DC sources are synthesized to construct the cumulative inverter output voltage using staircase modulation method was illustrated and explained by Tolbert in [24]. If the same pattern of duty cycles is used on a motor drive continuously, then one battery is cycled on for a much longer duration than another thus discharging sooner. Since the switches do not share the same load during the construction of the multi level waveform, the gate triggering of these switches must be rotated to actively share the duty cycle. However, by using a switching pattern swapping scheme among the various levels as explained in [24], all batteries will be equally used charged and/or discharged. The combination of the 180° conducting method or staircase modulation method and the pattern-swapping scheme make the cascade inverter's voltage and current stresses the same and battery voltage balanced. Identical H-Bridge inverter units can be utilized, thus improving modularity and manufacturability.

In the motoring mode, power flows from the batteries through the cascade inverters to the motor. In the charging mode, the cascade converters act as rectifiers, and power flows from the charger (inverter which acts as the AC source) to the batteries. For a drive cycle the motoring mode means the accelerating part, and the charging mode is the part where the vehicle coasts to a stop or decelerates. The cascade converters function as rectifiers to help recover the kinetic energy of the vehicle during regenerative braking.

3.3 Multiple Carrier Based Pulse Width Modulation Schemes

The carrier based modulation schemes for MLIs can be generally classified into two categories – (a) Level Shifted Modulation Method (LSMM) and (b) Phase Shifted Modulation Method (PSMM). Both these methods apply very well to CHB inverters. A brief description about these methods follows [29].

3.3.1 Level Shifted Modulation Method (LSMM)

The LSMM is similar to the PSMM in requiring (m-1) triangular waves for a m-level inverter however these waves are vertically disposed such that the bands they occupy are contiguous. The frequency modulation index is given by $m_f = f_{cr}/f_m$ which remains the same as that for the PSMM whereas the amplitude modulation index is given by

$m_a = \frac{\hat{V}_m}{\hat{V}_{cr(m-1)}}$ $for\ 0 \leq m_a \leq 1$ where $\hat{V}_m$ is the peak amplitude of the modulating wave v_m and $\hat{V}_{cr}$ is the peak amplitude of each carrier wave. This classic carrier-based sinusoidal PWM uses the level shifted technique to reduce the harmonics in the load hence, is preferred in industrial applications. The main LSMM techniques [29] which are popularly used in both NPC and FC MLIs are shown in (Figure 6).

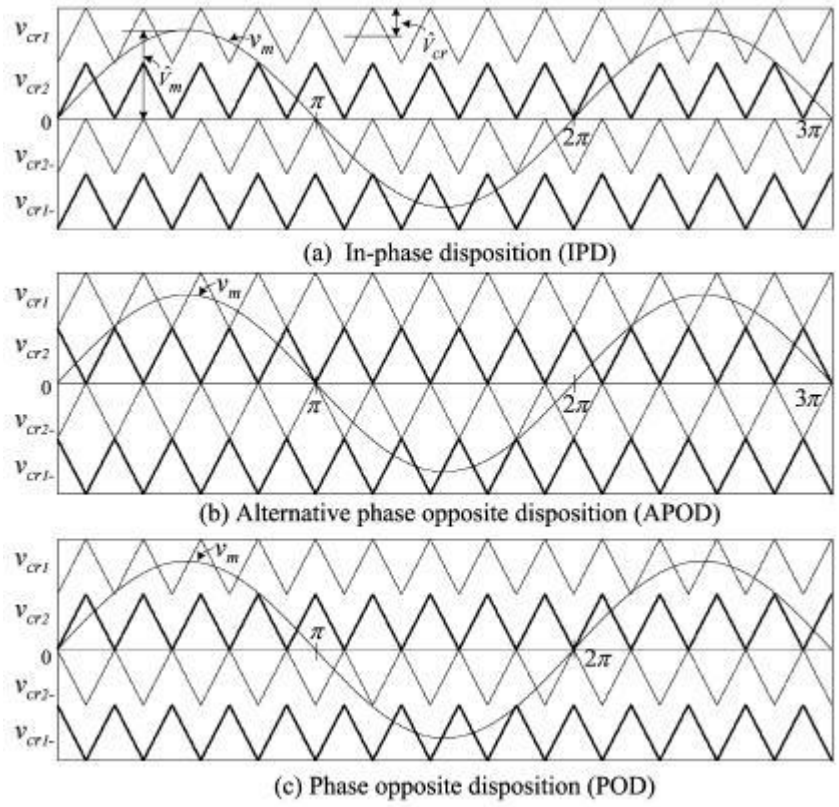

Figure 6. Level-shifted multicarrier modulation for five-level inverters

The three popular types of LSMM are as follows:

(i) In-Phase Disposition (IPD)

(ii) Phase Opposition Disposition (POD)

(iii) Alternative Phase Opposition Disposition (APOD)

3.3.2 Phase Shifted Modulation Method (PSMM)

In general a m-level MLI requires (m-1) triangular carriers. The PSMM can be better illustrated by an example from [29] as shown in (Figure 7).

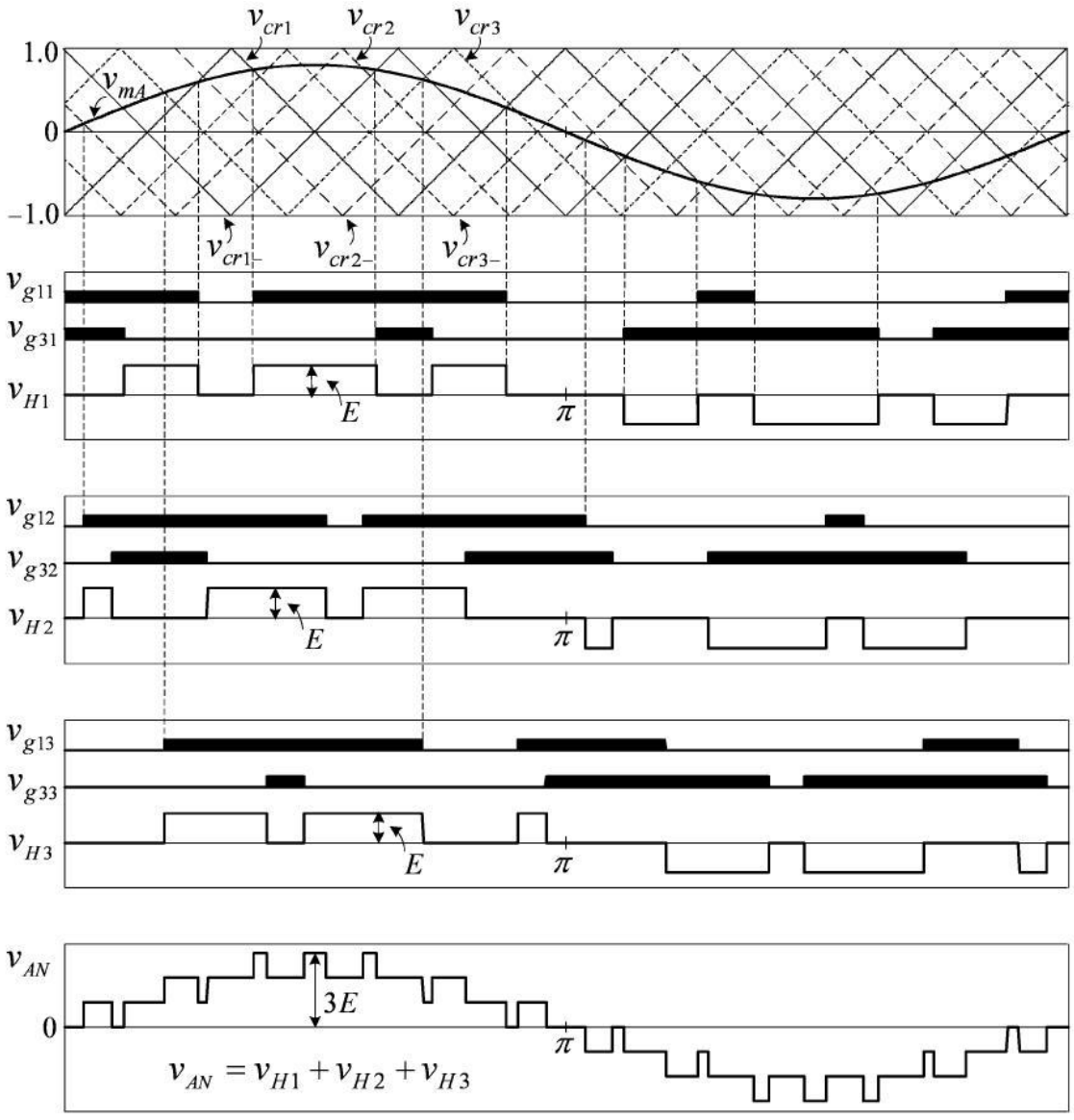

Figure 7. Phase-shifted PWM for seven-level CHB inverters (mf = 3, ma = 0.8, fm = 60Hz, and fcr = 180 Hz)

The above figure shows the multiple carrier waves for a seven-level MLI. In the PSMM, all the triangular carriers have the same frequency and peak-to-peak amplitude; however there is a phase shift between any two adjacent carrier waves given by $\varphi_{cr} = 360°/(m-1)$. It also shows how the final waveform is constructed as a result of the outputs of the individual cells. It can also be observed that these outputs VH1, VH2 and VH3 are identical except for a small phase displacement due to PSMM. The dominant harmonic's frequency in the inverter's output voltage represents its switching frequency.

3.3.3 Comparison between LSMM and PSMM

For the same operational switching frequency, a brief comparison has been made in order to evaluate the perfect candidate for this thesis. During this research, a thorough investigation of the application of both PSMM and LSMM (including IPD, POD and APOD) to the 5-level and 13-level MLI implementation was done.

One of the demerits of using LSMM is that there are periods of time when no switching occur in some cells in a phase. This means that in order to evenly distribute the switching and conduction losses of the converter, the switching pattern has to rotate. This is done in order to maintain a charge balance among the energy sources supplying the converter. On the other hand, in a system employing PSMM, the individual H-Bridge output voltages are almost identical except a small phase displacement among them. This also means that all the power devices operate at the same switching frequency and conduction time; hence an external method of rotating the switching pattern is not required simplifying the control of power electronics. In summary, the device conduction period and switching frequency can be kept same for all devices in PSMM but have to be different in the LSMM. However LSMM requires rotating of switching patterns. With regard to the line-to-line voltage THD, the LSMM is better than PSMM.

To sum up, this section discussed Multi Level Inverters in detail because the MLI forms the heart of the implementation. The topology, principle of operation and switching modulation strategies were discussed. The merits and demerits of modulation methods for use in a MLI were also briefly discussed.

4. DESIGN

4.1 Electric Vehicle Design

In order to evaluate the driving performance of an Electric Vehicle (EV), it is required to understand its acceleration time, maximum speed and gradeability. The EV's drive train design is done by involving the traction motor power rating and transmission parameters as these two are the primary considerations to meet the performance specification. The comprehensive design of all these parameters depends mostly on the torque-speed and power characteristics of the traction motor.

Typical characteristic curves for an adjustable speed drive in an electric vehicle would look like that shown in (Figure 8). This figure and other important design considerations are borrowed from the work done by Dr. Ehsani in [30].During the period of acceleration from zero speed to base speed, the torque is at maximum value and the power is ramping up. The first part of the graph is the low speed region (analogous to the low gear region of a vehicle) where it is in high torque and low speed mode in order to accelerate itself to the base speed. In the high speed region where the speed is more than the base speed, the system is in a constant power mode. This characteristic is also frequently described by the speed factor X which is defined as the ratio of the maximum speed to the base speed. This speed factor X is such that for an induction motor its value is around 4, for a PMSM it is about 2 to 4 and for a SRM it is at about 6. In general the higher the X, the better it is for an EV in terms of performance. The value of the X varies for the type of winding and construction that has been employed. In low-speed operation, the voltage supply to the motor increases with the rotor speed through the action of the inverter while the flux is kept constant. After the base speed, the power is constant hence the motor voltage is kept constant and the flux is weakened such that it drops hyperbolically with increasing speed.

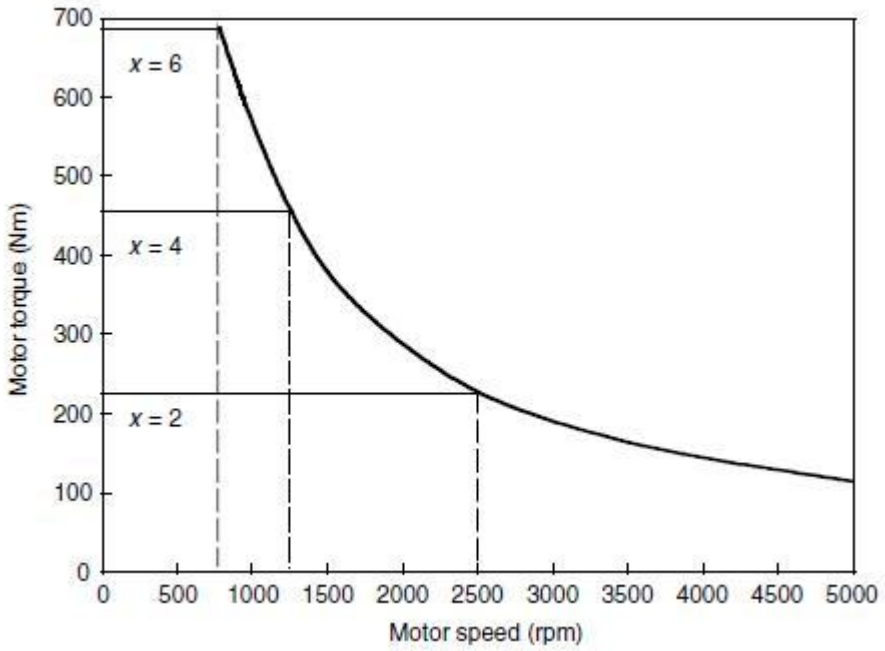

Figure 8. Speed-torque profile of an electric motor with X=2, 4, 6

It is observed in the above figure that the torque drops hyperbolically with the increasing speed. The longer the constant power region, the simpler is the transmission and the better is the performance in terms of gradeability and vehicle acceleration. Longer constant-power region allows for a higher maximum motor torque (during starting).

4.2 Design Problem

The problem at hand is to design the parameters of an electric vehicle. Given the parameters, it is required to find the specifications of the system including the design of the traction motor and battery capacity. Design of the traction motor includes calculating the required motor power capacity and other details such as coil inductance, resistance and ratio of voltage-to-speed. The design of the battery would be dealt in more detail. The following design equations have been borrowed from a reference book [30] authored by Dr. Ehsani.

4.2.1 Design of the Electric Vehicle

Mechanical and Environmental Parameters:

1. Mass of vehicle, $M = 1500$ kg
2. Coefficient of rolling friction, $f_r = 0.01$
3. Coefficient of Aerodynamic drag, $C_D = 0.3$
4. Front Area, $A_f = 2.2\ m^2$
5. Wheel radius, $r_d = 0.3$ m
6. Density of air, $\rho_a = 1.205\ kg/m^3$

Parameters of Velocities and Speeds:

1. $V_{max} = 160\ km/h = 44.44\ m/s$ where V_{max} is the maximum speed
2. $n_{m,max} = 10000$ RPM, where $n_{m,max}$ is the maximum RPM of the Motor
3. $w_{max} = \frac{2.\pi.n_{m,max}}{60} = 1047.198\ rad/s$, w_{max} is the maximum angular velocity
4. $V_f = 100\ km/h = 27.78\ m/s$ where V_f is the final speed
5. $n_f = 6521.75$ RPM, where n_f is the final speed RPM of the Motor
6. $V_b = \frac{V_{max}}{X} = \frac{160}{4} = 40\ km/h = 11.11\ m/s$ where V_b is the base speed
7. $n_{base} = \frac{n_{m,max}}{X} = 2500$ RPM, n_{base} is the base speed RPM of the Motor
8. $w_{base} = \frac{2.\pi.n_{base}}{60} = 261.8\ rad/s$, w_{base} is the base angular velocity

Parameters dealing with the kinematics of the system:

1. Time of acceleration, $t_a = 10$ sec
2. Acceleration, $\alpha = \frac{(V_f - 0)}{t_a} = \frac{(27.78 - 0)}{10}\ m/s^2 = 2.78\ \ m/s^2$

4.2.2 Design of Gear Ratio

The gear ratio is designed such that the vehicle reaches its maximum speed at the motor maximum speed.

From the expression $i_g = \frac{2\pi.n_{m,max}.\mathrm{r_d}}{60.V_{max}} = \frac{\pi.n_{m,max}.\mathrm{r_d}}{30.V_{max}}$ we have

i_g Gear ratio of transmission and i_0 gear ratio of final drive

n_t Efficiency from motor to wheel

Assume a single-gear transmission $i_0 = 1$ is used. Then, the designed gear ratio in this drive train can be acquired such as $i_g = 7.07$

$n_t = n_{gear} * n_{bearings} = 98\% * 98\% = 96.04\%$ (assuming appropriate values)

4.2.3 Design of Traction Motor

$mass\ factor, \delta = 1 + \delta_1 + \delta_2.(i_g.i_0)^2 = 1.165\ where\ \delta_1 \approx 0.04, \delta_2 \approx 0.0025$

Therefore $\delta = 1.165$, $\mathrm{V_b} = \frac{2\pi.\mathrm{N_{M,base}}.\mathrm{r_d}}{60.(\mathrm{i_g i_0})}\ (\mathrm{m/s}) = 11.11\ \mathrm{m/s}$, $\mathrm{V_f} = 27.78\ \mathrm{m/s}$

From the equation for tractive power, $\mathrm{P_t} = \frac{\delta.\mathrm{M_v}}{2.\mathrm{t_a}}\left(\mathrm{V_f^2} + \mathrm{V_b^2}\right) + \frac{2}{3}\mathrm{M_v g f_r V_f} + \frac{1}{5}\rho_a \mathrm{C_D A_f V_f^2}$ we can calculate the required traction motor size.

$\mathrm{P_t} = 78.214 + 2.725 + 0.123 = 81.062\ \mathrm{kW} \cong 90\ \mathrm{kW}$ (nominal power)

Thus the maximum motor torque and tractive effort is calculated as

$\mathrm{T_{M,max}} = \frac{\mathrm{P_{max}}}{\mathrm{w_{base}}} = \frac{90\ \mathrm{kW}}{2500*\frac{2\pi}{60}} = 343.775\ \mathrm{Nm}$, $\mathrm{T_{M,min}} = \frac{\mathrm{P_{max}}}{\mathrm{w_{max}}} = \frac{90\ \mathrm{kW}}{10e^3*\frac{2\pi}{60}} = 85.944\ \mathrm{Nm}$

$\mathrm{F_{t,max}} = \frac{\mathrm{T_{M,max}}*\mathrm{i_g}*\mathrm{i_0}*n_t}{\mathrm{r_d}} = 7.780\ \mathrm{kN}$, $\mathrm{F_{t,min}} = \frac{\mathrm{T_{M,min}}*\mathrm{i_g}*\mathrm{i_0}*n_t}{\mathrm{r_d}} = 1.945\ \mathrm{kN}$

The torque-speed-power characteristics of the electric motor are shown in (Figure 9). The tractive effort of the design as per values from above calculations and from the (Figure 9) gives the illustration (Figure 10).

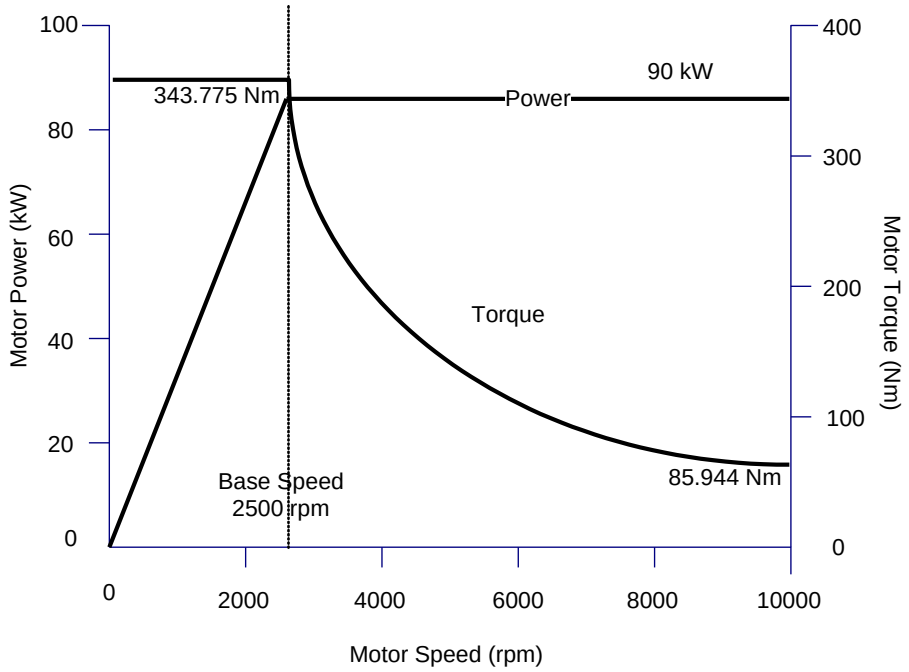

Figure 9. Torque - speed - power characteristics of the traction motor

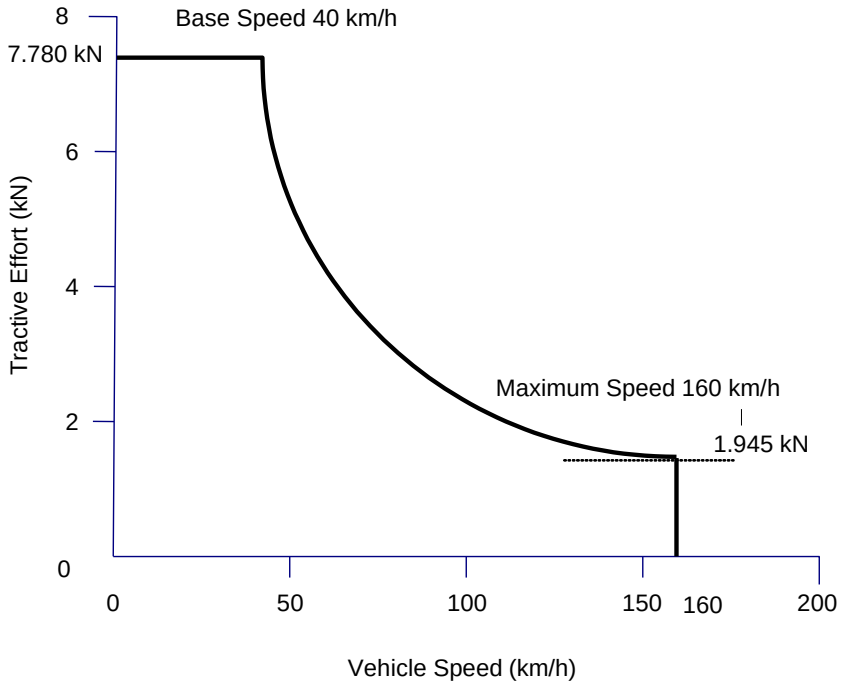

Figure 10. Tractive effort vs speed of the traction motor

4.2.4 Design of the Battery System

An investigation into the design and sizing of the Primary Power Source (PPS) i.e. battery pack for an EV involves understanding the parameters that define a battery [31]. These parameters are briefly discussed here to help understand all the different factors that affect the construction, operation and maintenance of batteries. The first three parameters namely power capacity, energy capacity and weight of the batteries are very important. It is important to understand that battery sizing is improved when using a MLI because of smaller inverters across each individual battery. It should also be noted here that a battery pack could mean a single battery or a cascaded configuration of series and parallel connection of multiple batteries. This is in order to achieve the required voltage amplitude and Ampere-Hour for one cell.

a) Design of the power capacity of PPS

Sum of output power of the engine/generator PPS should be greater than or equal to the input power of the traction motor

$$P_{pps} = \frac{P_{motor}}{n_{motor}} = \frac{90}{0.9} \cong 100 \text{ kW}$$, assume 90% for motor efficiency

b) Design of energy capacity of PPS

The whole energy capacity of the battery can be calculated using the following equations. In this case, the State-Of-Charge (SOC) is assumed to be varying between 0.3 and 0.8 hence ΔSOC is 0.5. A variation of 0.2 will limit the terminal voltage to 10% variation. The total storage energy for 600 seconds duration (FTP-75) can be calculated by $E_{pps} = \frac{\Delta E_{max}}{\Delta SOC} = \frac{100 * \frac{600}{3600}}{0.5} = 33.33\ kWh \cong 35$ kWh

c) Battery weight

Battery specific power = 500 W/kg given

$$Weight = \frac{Maximum\ power\ capacity}{Specific\ power} = \frac{100\ kW}{500\ \frac{W}{kg}} = 200\ kg$$

Let's say that the battery specific energy = 150 Wh/kg

$$Weight = \frac{Maximum\ energy\ capacity}{Specific\ energy} = \frac{35\ kWh}{150\ \frac{Wh}{kg}} = 233.3\ kg$$

d) Charge (or Amp-hour) capacity

The electric charge that a battery can supply is clearly a most vital parameter. The commonly used unit is the Amp-hour which implies one Amp flowing for one hour. For example, the capacity of a battery might be, say, 10 amp-hours or 10 Ah. This means it can provide 1 Amp for 10 hours, or 2 Amps for 5 hours or in theory 10 Amps for 1 hour. The capacity of the large batteries used in electric vehicles (traction batteries) is usually quoted for a 5 hour discharge.

e) Specific energy

Specific energy is the amount of electrical energy stored for every kilogram of battery mass, and the units are measured in $Wh.kg^{-1}$.

f) Specific power

Specific power is the amount of power obtained per kilogram of battery. It is a highly variable and rather anomalous parameter, since the power produced by the battery depends more on the load connected to it than the battery itself. The normal units are $W.kg^{-1}$. Some batteries have a very good specific energy, but have low specific power, which means they store a lot of energy, but can only give it out slowly. When applied to EVs, this means that these batteries can drive the vehicle very slowly over a long distance. High specific power normally results in lower specific energy for any particular type of battery. This is because, if the energy is taken out of a battery quickly, i.e. at high power, it reduces the energy available. This variation of specific power with specific energy for different battery types is important, and useful to understand in vehicular applications.

g) Energy stored

The primary job of a battery is to store energy so it can be used later. The energy stored in a battery depends on its voltage, and the charge stored. The stored energy reduces if

the battery is discharged quickly. The popularly used unit for energy stored by the battery is the Watthour and is the energy equivalent of working at a power of 1 Watt for 1 hour. The Watt-hour is equivalent to 3600 Joules and is compatible with the current use of the Amp-hour for charge, as it yields: *(Watt-hours) = Voltage x Amp-hours*.

h) Energy density

Energy density is the amount of electrical energy stored per cubic meter of battery volume, and is measured in units of $Wh.m^{-3}$. It is also an important parameter since the energy capacity of the battery (Wh) can be divided by the battery's energy density ($Wh.m^{-}3$) to calculate the volume of battery required.

i) Cell and battery voltages

Among the other parameters that describe a battery and its functioning is the terminal voltage. Batteries for traction applications like electric vehicles are usually specified at 6V or 12V, and these units are in turn connected in series to produce the desired voltage. When an output current is drawn, the voltage reduces; and during the charging of the battery, the voltage increases or rises. This is best expressed in terms of internal resistance. However, one should note that the open circuit voltage is not constant. This is because it is also affected by the SOC and external factors such as temperature.

j) Energy efficiency

This parameter is defined as the ratio of electrical energy supplied by a battery to the amount of electrical energy required to return it to the state before discharge.

k) Self-discharge rates

Most batteries discharge when left unused, and this is known as self-discharge. The rate varies with battery type, and with other external factors such as temperature; higher temperatures greatly increase self-discharge.

l) Battery geometry

The battery geometry is important keeping in mind the spacing consideration in an EV.

m) Battery temperature, heating and cooling needs

When choosing a battery for an EV the designer needs to be aware of its sensitivity to battery temperature, heating and cooling needs.

n) Battery life and number of deep cycles

Most rechargeable batteries will only undergo a few hundred deep cycles to 20% of the battery charge. However, the exact number depends on the battery type, and also on details of the battery design, and on how the battery is used. This factor reflects in the battery's lifetime, which in turn affects the EV running costs.

4.3 Design of the Multi Level Inverter

The design of the Multi Level Inverter involves deciding the number of cells per phase. An important consideration is the voltage amplitude for each cell, and the required line-to-line voltage at the output of the inverter to feed the motor drive. This output voltage is to be built up from the individual cells (H-Bridge inverters). The number of cells in a phase is an engineering design problem and needs to be dealt keeping in mind the cost, efficiencies, reliability and ruggedness of the system. More number of switches might mean lesser reliability however also means easier reparability. Due to modular nature, faster maintenance is possible. Scalability provides for potentially any number of cells to be used. The most standard power switches already available in the market at an inexpensive price can be employed, since high voltage switches are not particularly popular.

Following from the above discussion, the value of 1500V was found to be a desirable output MLI voltage. The simplest MLI configuration would involve 2 cells per phase. However a solution requiring a cell voltage of approximately 700V is not practical. Therefore 6 cells per phase MLI system has also been designed and simulated. It has been found to give similar results as given by the 2 cells per phase MLI system. Additionally the voltage and switching stresses are comparatively much lower, hence a more practical solution. The 6 cells per phase MLI is shown in the self explanatory (Figure 11).

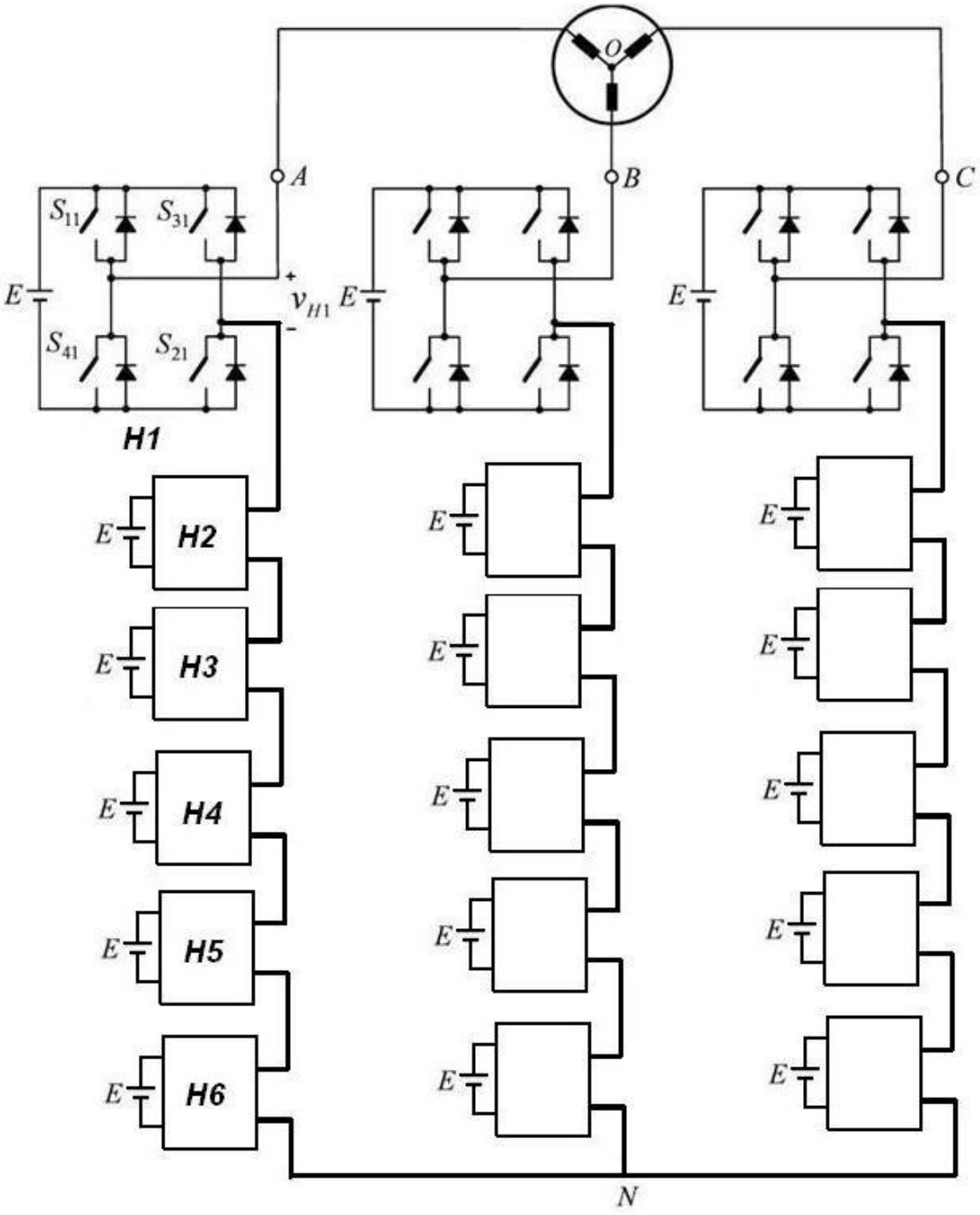

Figure 11. 6 cells per phase CHB MLI fed PMSM

In the above figure, it is seen that there are 6 cells (H-Bridge inverters) in each phase marked by H1 through H6 in the Phase A. The phase voltage V_{AN} would be the sum of the individual cell voltages V_{H1} through V_{H6} thus generating the required voltage to run the PMSM. In this particular design, each cell is fed by a battery (energy source) with terminal voltage of 250V. These six cells add up to give the 1500V amplitude, with the line-to-line voltage being higher. It is once again emphasized that the number of cells did not affect the performance in terms of acceleration, torque and speed responses.

4.4 Design of the Permanent Magnet Synchronous Motor (PMSM)

Regarding the design of the PMSM, one of the greatest advantages of PMSM is that it can be designed directly for low speeds without compromising on efficiency or power factor [1]. An induction motor with a mechanical gearbox can often be replaced with a direct PMSM drive. There is a saving in both space and cost, because the efficiency increases and the cost of maintenance decreases. Since a low-speed motor often requires a large amount of poles, the number of stator slots per pole and phase is typically low. Thus, the stator magneto-motive-force (mmf) contains a lot of large harmonic components. Especially the fifth and the seventh stator harmonics are very harmful and tend to produce torque ripple and can prove to be extremely detrimental to the performance at lowest speeds. The lack of excitation control is one of the most important features of permanent magnet motors, and as a consequence, the internal voltage of the motor rises proportionally to the rotor speed, and when the motor is working at constant horsepower mode its power factor becomes important.

4.4.1 DQ Model for PMSM

In recent years, compact and high-efficiency synchronous motors have been designed using high-energy permanent magnet (PM) in the rotor. Motors with PM mounted inside the steel rotor core known as interior permanent magnet (IPM) synchronous motor are popular in the industry. PMSMs are being manufactured and used increasingly in low to medium power range applications. Their merits can be further enhanced by design optimization, thus reducing production costs and improving the motor’s performance.

IPM motors with extra features of mechanical robustness, capability of flux weakening and high-speed operation are particularly suitable as variable speed drives in EVs.

A PMSM is driven by sine wave voltage coupled with the given rotor position. The generated stator flux together with the rotor flux which is generated by a rotor magnet defines the torque, and thus the speed of the motor. The sine wave voltage output has to be applied to the three-phase winding system in a way that the angle between the stator and the rotor flux is kept close to 90 degrees to get the maximum-generated torque. To meet this criterion, the motor requires electronic control for proper operation.

The equations of the PMSM are:

$$\begin{bmatrix} v_a \\ v_b \\ v_c \end{bmatrix} = \begin{bmatrix} R_s & & \\ & R_s & \\ & & R_s \end{bmatrix} . \begin{bmatrix} i_a \\ i_b \\ i_c \end{bmatrix} + \frac{d}{dt} \begin{bmatrix} \lambda_a \\ \lambda_b \\ \lambda_c \end{bmatrix}$$

$\begin{bmatrix} v_a \\ v_b \\ v_c \end{bmatrix}$ represents the stator phase voltages, R_s is the stator resistance

$\begin{bmatrix} i_a \\ i_b \\ i_c \end{bmatrix}$ represents the stator currents and $\begin{bmatrix} \lambda_a \\ \lambda_b \\ \lambda_c \end{bmatrix}$ represent the flux linkages

The mechanical equations are $J\frac{d\overline{\omega_m}}{dt} = T_{em} - B.\overline{\omega_m} - T_{load}$ and $\frac{d\theta_r}{dt} = \frac{P}{2}.\overline{\omega_m}$ where θ_r is the rotor electrical angle.

T_{load} is the load torque, and B is a coefficient, which is calculated from the moment of inertia J and the mechanical time constant T_{mech} as follows: $B = \frac{J}{T_{mech}}$

Using the d-q transformation, the voltage equations of a PM machine in the rotor reference frame are:

$$v_d = R_s i_d + \frac{d\lambda_d}{dt} - \overline{\omega_e}\lambda_q$$

$$v_q = R_s i_q + \frac{d\lambda_q}{dt} + \overline{\omega_e}\lambda_d$$

$$\lambda_d = L_d i_d + \lambda_m \text{ and } \lambda_q = L_q i_q$$

4.5 Power Device Requirements

Some ideal requirements of power devices for use in MLI are:

i. Adequate blocking voltage.
ii. High turn off current and surge current capabilities.
iii. Adequate isolation voltage withstanding capability.
iv. Reverse conducting and active switching in one module.
v. Low conduction and switching losses.
vi. Suitable for parallel and series operation
vii. Fast switching; tolerance to dV/dt and dI/dt.
viii. Good thermal performance
ix. Ease of protection and control
x. Fail-safe failure mode

In summary, this section discussed the detailed design of the system. This work involved the design of the EV including its mechanical, electrical and environmental parameters. Further detailed design included sizing of tractive power required, motor ratings and battery packs. The design of the MLI required the number of levels, and more importantly the number of cells per phase. The PMSM was described in the form of mathematical equations.

5. SIMULATION IMPLEMENTATION

Simulation modeling is a very significant step in any product development. This is because before the system can be modeled as a hardware prototype, it needs to be tested for actual operation, fault analysis, possible improvements etc. It should also be noted that all system variables are accessible to be studied in detail, and the dynamics of the system can be predicted. It is known that disturbances can be suppressed and parts of a system can be studied in isolation through simulations.

Some of the important reasons for performing a simulation before hardware implementation are that the latter is too expensive, might be unsafe since it has never been done before among other practical problems. Simulation allows for exhaustive experiments to be carried out. Simulation also facilitates learning about the system behavior under different operating conditions, providing realistic operator training and experiment under various load profiles.

Once the designs of the entire system and individual components have been finalized, as done in the previous section, the next step in the procedure is to develop a simulation model. This model would be a simulation implementation in order to demonstrate the working capability of the proposed system and the proof of principle of operation. The simulations have been carried out using MATLAB and Simulink software. The significance of various blocks is explained. Some of the blocks have embedded MATLAB code, which is presented in the appendices. The simulation parameters are given at the end of the section.

5.1 Simulation Models

(Figure 12) is basically a Simulink model of the system level implementation or system schematic showing the various interconnected components. Each of these components would be elaborated upon in complete detail assisted by illustrations and real time plots.

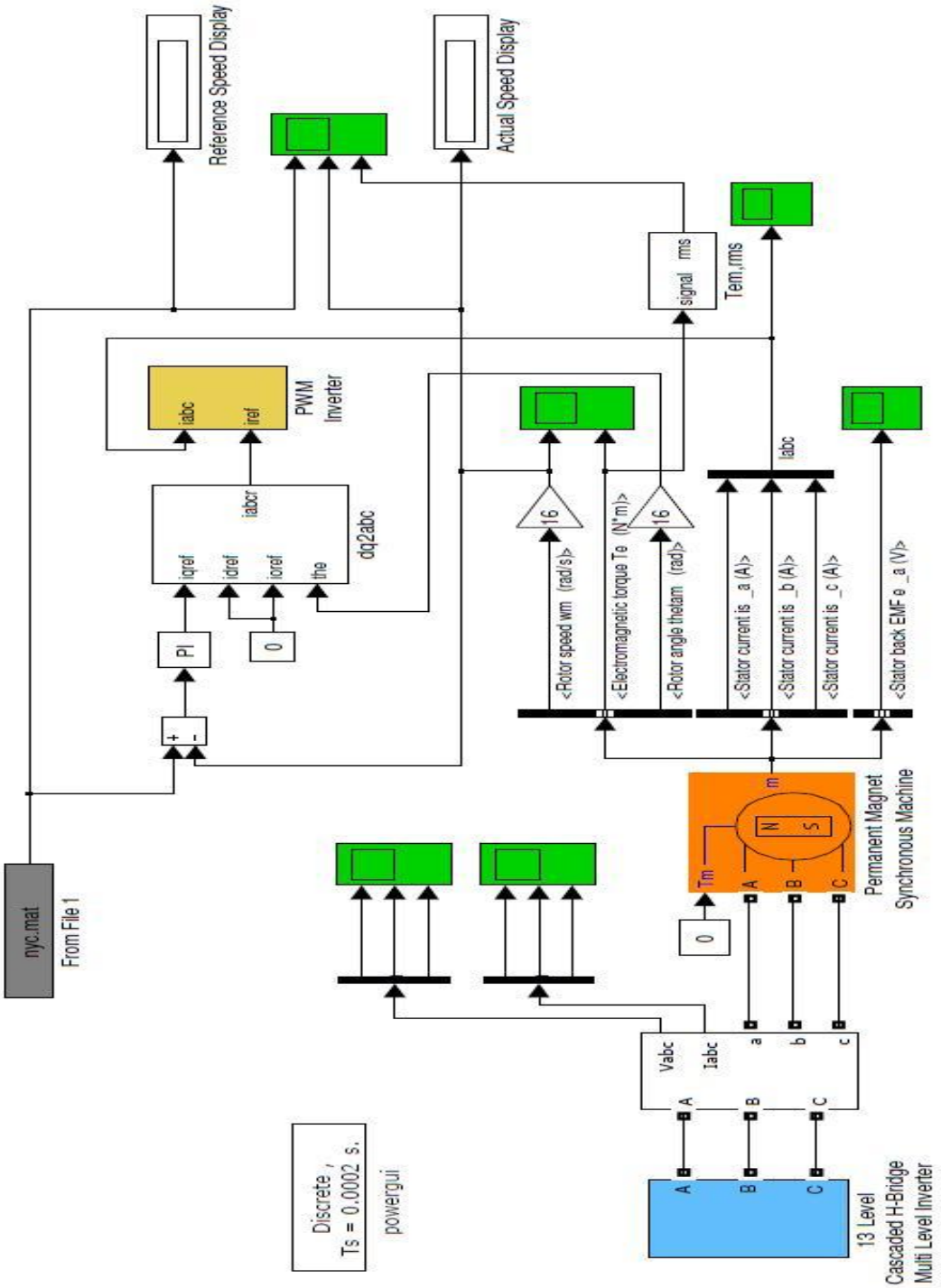

Figure 12. Simulink schematic of system level implementation

This parent model simulation shown in the above figure is given an elaborate explanation because it shows all the interconnections between the components of the system. One can observe the major components of the system to be the MLI (in blue color), the measurements block (all measurements are shown in green), the battery packs within the MLI, the controllers, the PMSM (in orange color) as the load on the MLI, the input reference driving cycle (shown in grey color) and the closed loop speed control (in yellow color) along with the FOC scheme implementation.

5.2 Battery Sub-System Model

The energy source capacity was designed in Section 4.2.3. The energy source in an EV i.e. a battery is employed in Simulink using the in-built models. The graphical masks for battery and PMSM are shown in (Figure 13).

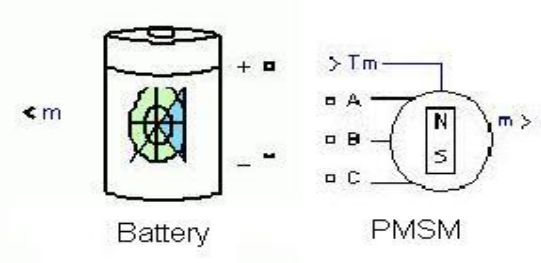

Figure 13. Battery and PMSM models in Simulink

The equivalent circuit of the battery underneath the masked sub-system model is shown in (Figure 14). These illustrations are borrowed from the MATLAB support documentation to help explain the battery's construction and functioning.

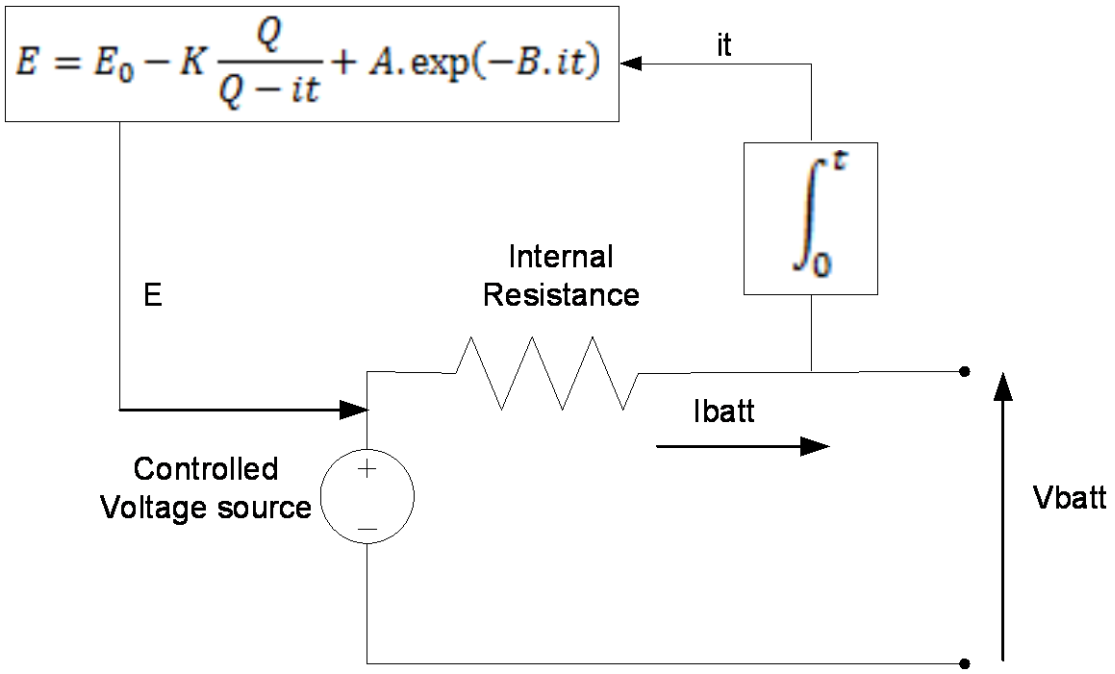

Figure 14. Battery equivalent circuit

The parameters defining the battery in the above circuit are as follows:

- E = No load voltage (V)
- E0 = Constant voltage (V)
- K = Polarization voltage (V)
- Q = Battery capacity (Ah)
- A = Exponential voltage (V)
- B = Exponential capacity (Ah)-1

The rated capacity is the minimum effective capacity of the battery. The typical discharge characteristic is shown in (Figure 15).

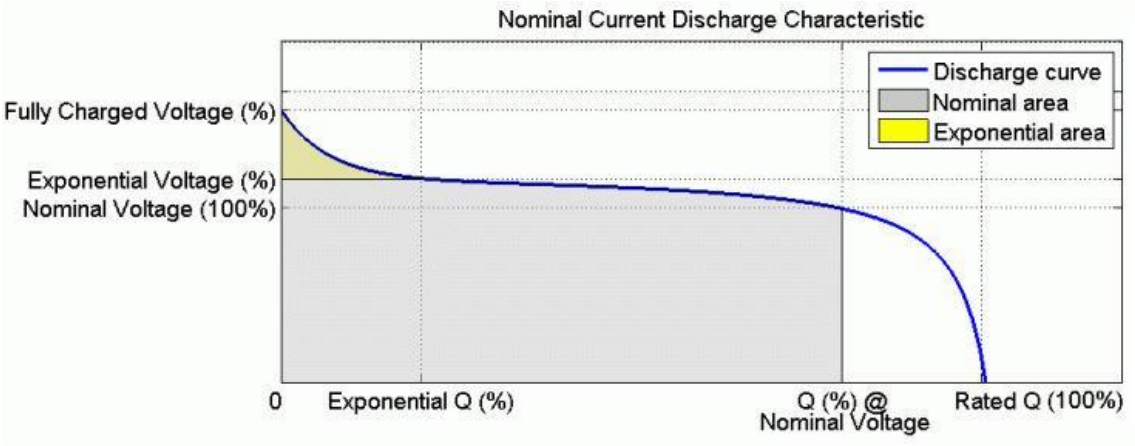

Figure 15. Battery discharge characteristics

Borrowing the same parameters to work in the system during the regenerative mode, the charging characteristics of the battery are illustrated in (Figure 16). In the charge characteristics, one can observe the battery SOC to be nearly flat during 30%-80%. Depending on the type of batteries currently employed, the SOC range during charge-discharge cycles is kept within 40%-60%.

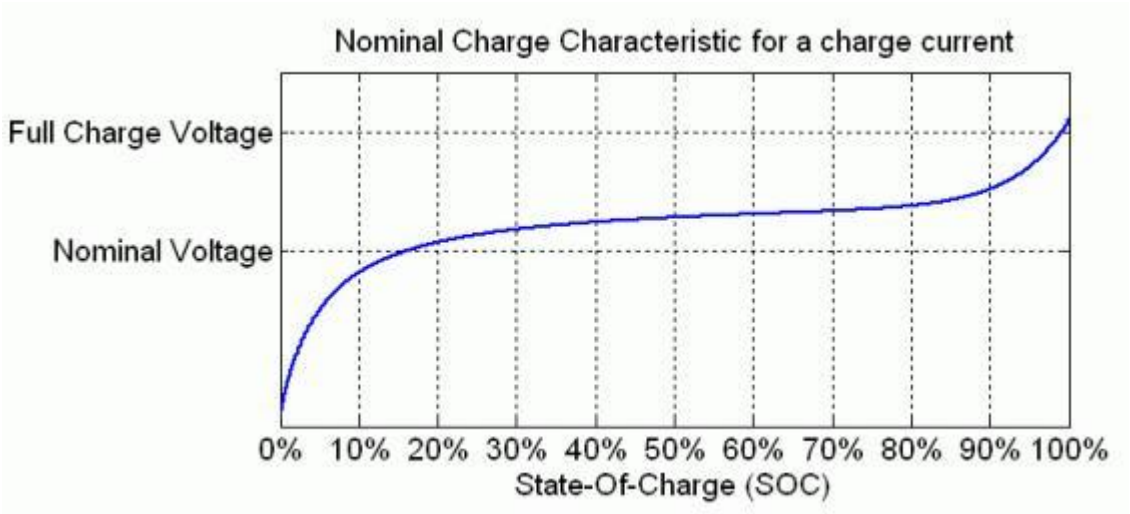

Figure 16. Battery charging characteristics

The parameters that are varied and manipulated for normal operation of the battery are described in some detail below:

1. Nominal Voltage is the nominal voltage of the battery (Volts).
2. Rated Capacity is the rated capacity (Q) of the battery in Ampere-Hour. The rated capacity is the minimum effective capacity of the battery. The maximum theoretical capacity (when the voltage crosses 0 volts) is generally equal to 105% of the rated capacity.
3. Initial State-Of-Charge (SOC %) of the battery, 100% indicates a fully charged battery and 0% indicates an empty battery. This is an initial condition for the simulation and does not affect the discharge curve.

5.3 Permanent Magnet Synchronous Motor (PMSM) Sub-System Model

The PMSM is modeled as a readily available Simulink block which was illustrated as an orange block in the right half of (Figure 13). The schematic shows that three phases feed the machine and the N-S magnet signifying the permanent magnets are housed within. In this particular system, the PMSM is run on mechanical torque input equaling zero since there is no separate load torque subjected on the motor. It should be understood that the load on the PMSM is the EV itself, since the entire vehicle has to be drawn by the motor.

The other parameters that describe the machine model in detail are:

R_s (Ω) is stator phase resistance, L_s (H) is stator phase inductance

Inertia is described by the combined machine and load inertia coefficient J (kg.m2). Friction factor defines the combined viscous friction coefficient F (N.m.s). Pole pair(s) describes the number of pole pairs.

The machine constant selection specifies the block parameterization:

1. Flux linkage established by magnets: The constant flux λ (Wb) induced in the stator windings by the magnets, in Webers.

2. Voltage Constant: The peak line to line voltage per krpm (or 1000 rpm). It is the peak open circuit voltage when the machine is driven as a generator at 1000 rpm.
3. Torque Constant: The torque per ampere constant which assumes that the machine is driven by an inverter which provides a perfect synchronization between the current and the Back-EMF.

When any one of the above is selected for varying, the other two parameters are appropriately calculated though inaccessible and only displayed for information.

Back EMF flat top area is the width of the flat top for a half period of the electromotive force F' (degrees). In the case of a trapezoidal machine it amounts to 120° while it is zero for sinusoidal machine.

The field for Initial conditions specifies the mechanical speed (rad/s), mechanical angle θ_m(degrees), and instantaneous stator current (A): [w_m, θ_m, i_a, i_b].

Note that since the stator is wye-connected, $i_a + i_b + i_c = 0$.

The following outputs available for the machine model measured by the in-built encoder-resolver into the machine, and are very vital inputs for the control loop.

1. Rotor speed w_m (rad/s)
2. Electromagnetic Torque T_e (N.m)
3. Rotor angle θ_m (rad)
4. Stator currents i_a i_b i_c (A), multiplexed into actual currents i_{abc} (A)
5. Stator back-emf EMF_A (V)

5.4 Multi Level Inverter Sub-System Model

The Multi Level Inverter (MLI) is a type of topology, and is not fixed in terms of levels or components; hence it is not an in-built block or system in Simulink. Therefore the sub-system model has to be built taking into consideration the theoretical background and design work accomplished in previous sections. While the basic CHB MLI topology and operation was explained in (Figure 4), the simulation implementation of the 13-level

CHB MLI of (Figure 12) shall be explained as a practical solution and extension to the 5-level MLI.

5.4.1 Three-Phase Five-Level Two Cells Per Phase MLI

The three-phase five-level MLI is constructed such that the three phases feed output connection ports namely A, B and C as shown in (Figure 17). These ports are pins on the MLI block as seen in the system level schematic (Figure 12).

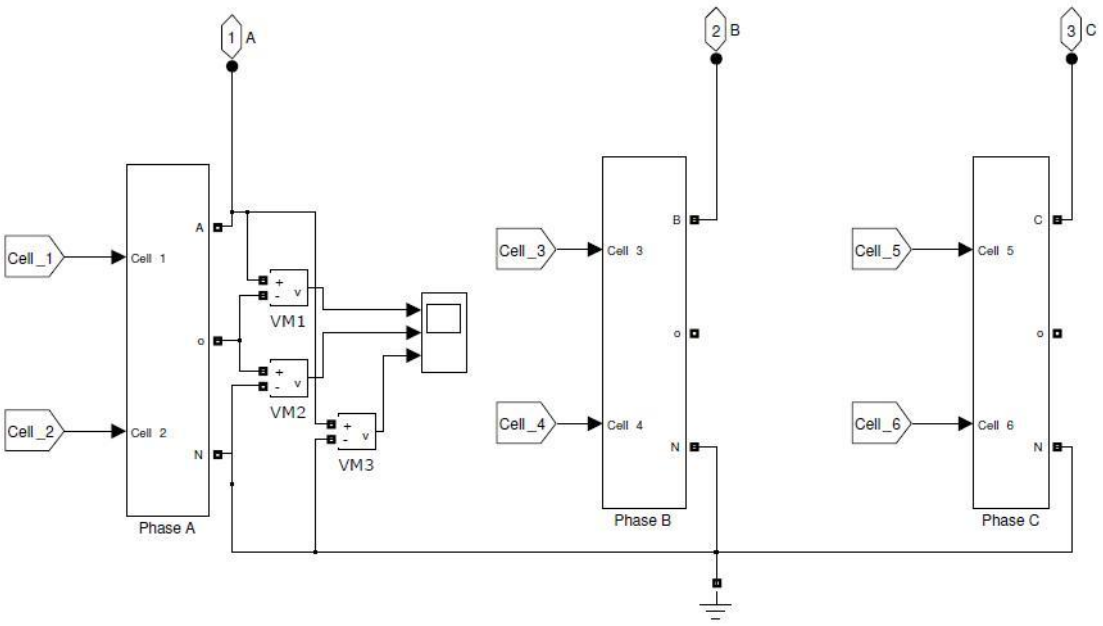

Figure 17. Simulink sub-system model of the 5-level multi level inverter

The above Simulink model is an implementation of the schematic shown in (Figure 5).It is observed that each of the three phase blocks are fed by global connection ports named Cell_1, Cell_2 etc. These are the gating signals that come from the signal generator so as to trigger the various switches. In the above figure, i.e. in (Figure 17) it is also seen that there are measurements being monitored. For sake of space and convenience, they are shown on only phase A. These measurements VM1, VM2 and VM3 measure the

respective cell output voltages. VM1 is the AC voltage output of the upper cell and is measured between nodes A and O. VM2 is the AC output voltage of the lower cell and is measured between O and neutral N. VM3 is the combined sum of VM1 and VM2, and is measured between as the phase voltage between A and N. The lower terminals or negatives of the three phases are tied together to the neutral N in a wye configuration (or star configuration).

A further investigation into the construction of each phase block as explained by the illustration (Figure 18) shows that there are two cells in each phase. One cell here is defined as a single H-Bridge. Each cell is fed by a battery and these batteries (energy sources for the inverter and also the EV as a whole) are kept inside the MLI block for reasons of convenience.

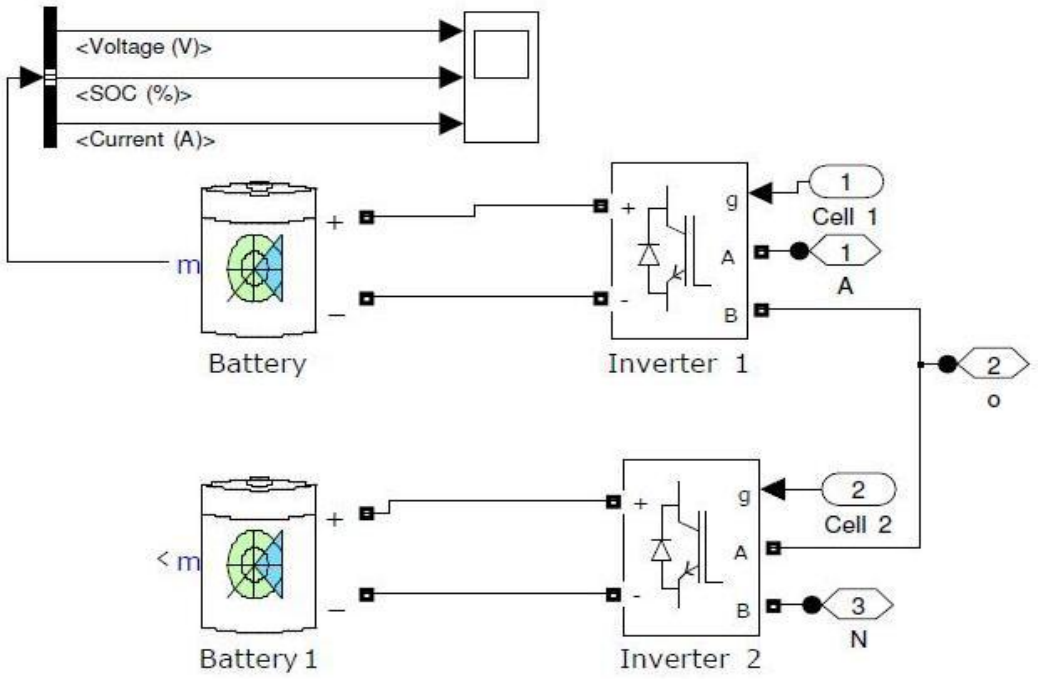

Figure 18. Simulink sub-system model of one phase of the 5-level MLI

5.4.2 Three-Phase Thirteen-Level Six Cells Per Phase MLI

The extension of the above concept to the six cells per phase as explained in the Section 4.3 and (Figure 11) was also implemented in simulation. The masked sub-system block for this implementation looks as shown in (Figure 19). It is observed that each phase is fed by 6 gating signals. The voltage measurement VM1 gives the output voltage of one cell, while VAN gives the phase voltage.

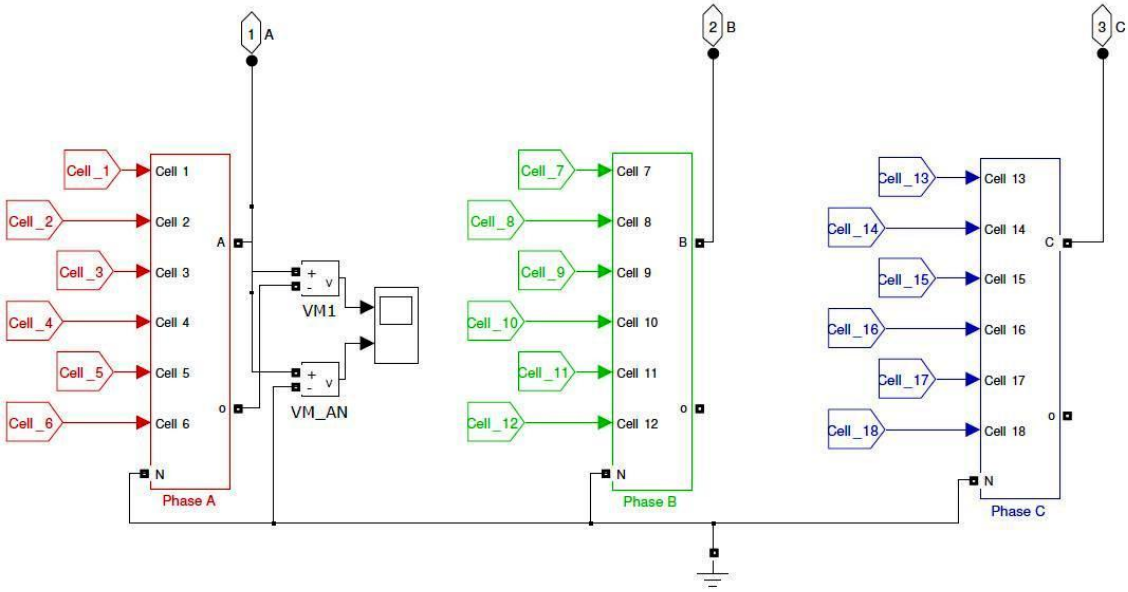

Figure 19. Simulink sub-system model of the 6 cells per phase MLI

An investigation into the construction of each phase block leads to the implementation shown in (Figure 20). The Battery Monitoring System (BMS) aboard a vehicle is very important in order to constantly monitor the health and functioning of the battery packs. Some common measurements are Voltage, State-Of-Charge (SOC) and current drawn. The last parameter is significant in terms of the driving range regenerative capability. The voltage generated is important in order to produce the desired speed. The battery voltage and current together also decide the power and energy available for the system.

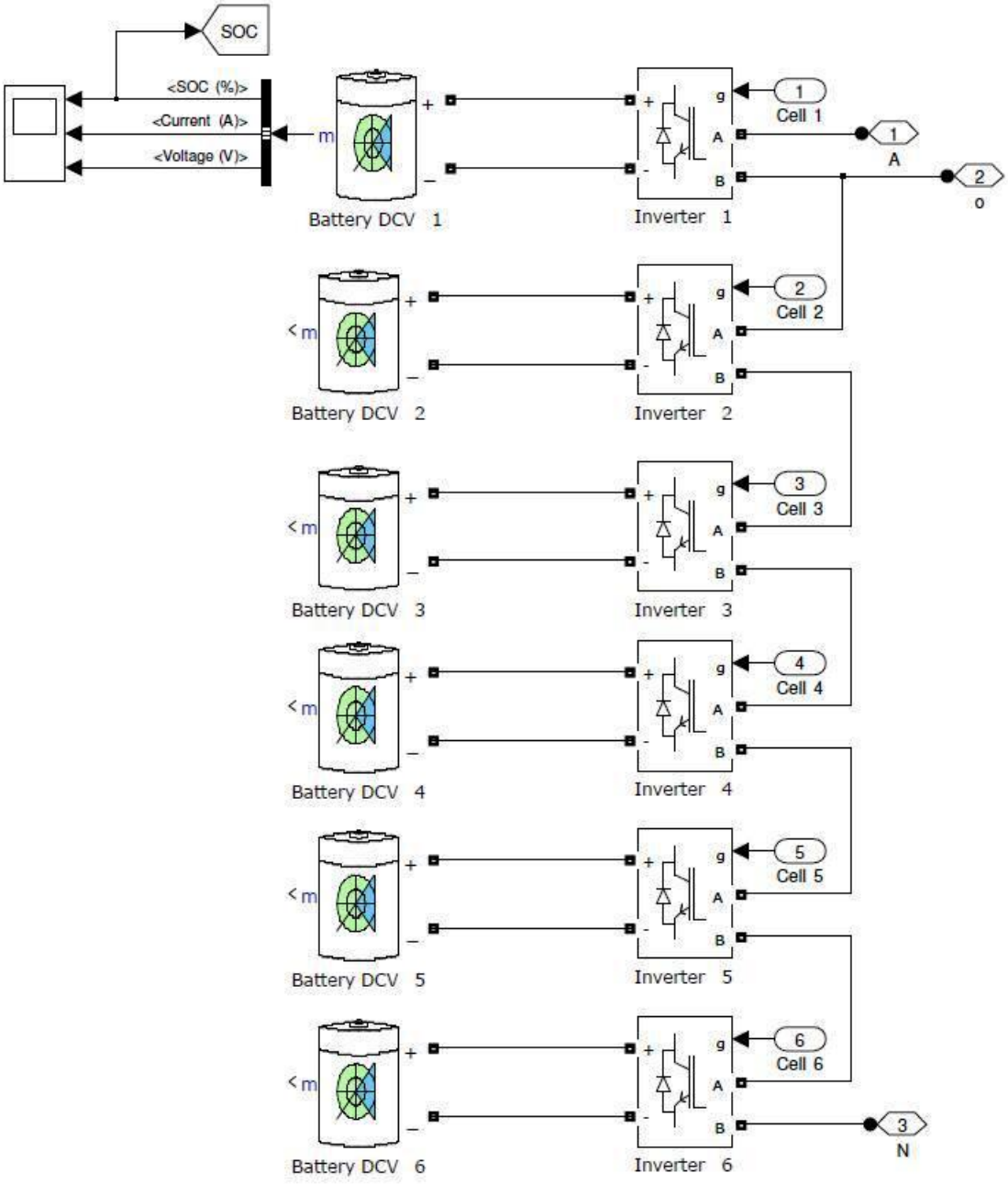

Figure 20. Simulink sub-system model of one phase of the 6 cells per phase MLI

The H-Bridge inverter is a block readily available in Simulink, the internal construction within the mask being shown in (Figure 21). One should understand that many

parameters are required to describe the inverter such as snubber resistance and capacitance values, on-resistance values etc. Each pair of switches is triggered by the gating pulse generator. Depending on the switching modulation strategy employed, each cell is fed by one pulse which determines the individual 4 gating signals for the switches within.

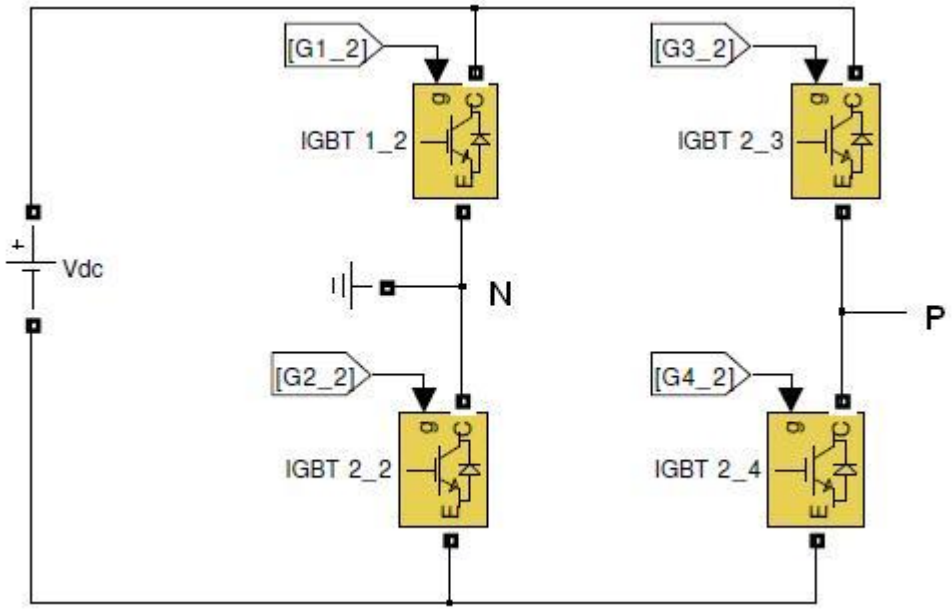

Figure 21. Simulink sub-system model of a H-Bridge inverter

5.5 Reference Inputs in Simulink

5.5.1 Driving Cycle

A driving cycle is a series of data points representing the speed of a vehicle versus time. In order to evaluate the performance of vehicles in various locations and different operating conditions, a popular method is to use driving cycles. For example the FTP-75 (New York urban) driving cycle has been employed in this study to evaluate the viability of the proposed system, and its performance characteristics. An important application for driving cycles is in vehicle simulations such as in this research work. They are

particularly used in propulsion system simulations (simulators designed specifically to model the drive system and predict performance of motors, transmissions, electric drive systems, batteries etc. Some driving cycles are a result of theory and equations, whereas others are direct measurements of a driving pattern deemed representative (such as the New York urban driving cycle).

There are two commonly known types of driving cycles:

1. Transient driving cycles: As the name suggests, they involve many transients or changes, demonstrating the constant speed changes typical of on-road driving. Popular examples are the American FTP-75, and the unofficial European Hyzem driving cycles.
2. Modal driving cycles involve protracted periods at constant speeds such as the official European NEDC and the Japanese 10-15 Mode cycles.

Drive Cycle Recognition (DCR) is an advanced vehicle control strategy that uses past driving information, as well as a library of representative drive cycles to extrapolate future vehicle control parameters. For example, the vehicle's computer can identify past driving history as one particular representative cycle and use the known information to improve vehicle performance. This control strategy is very valuable for EVs since it has a superior vehicle performance than the regular Internal Combustion Engine (ICE) driven vehicle.

5.5.2 Reference Drive Cycle

The closed loop speed control of the (Figure 12) is fed by the input from the driving cycle (or drive cycle). In hardware, this drive cycle represents the driving input from the driver according to the traffic conditions. Any typical drive cycle is made up of portions of acceleration, constant speed, stop-and-go, coasting and deceleration as illustrated in (Figure 22). The top part shows a typical drive cycle, the middle part explains the state of the battery whether charging or discharging and the last part displays the energy changes in the battery.

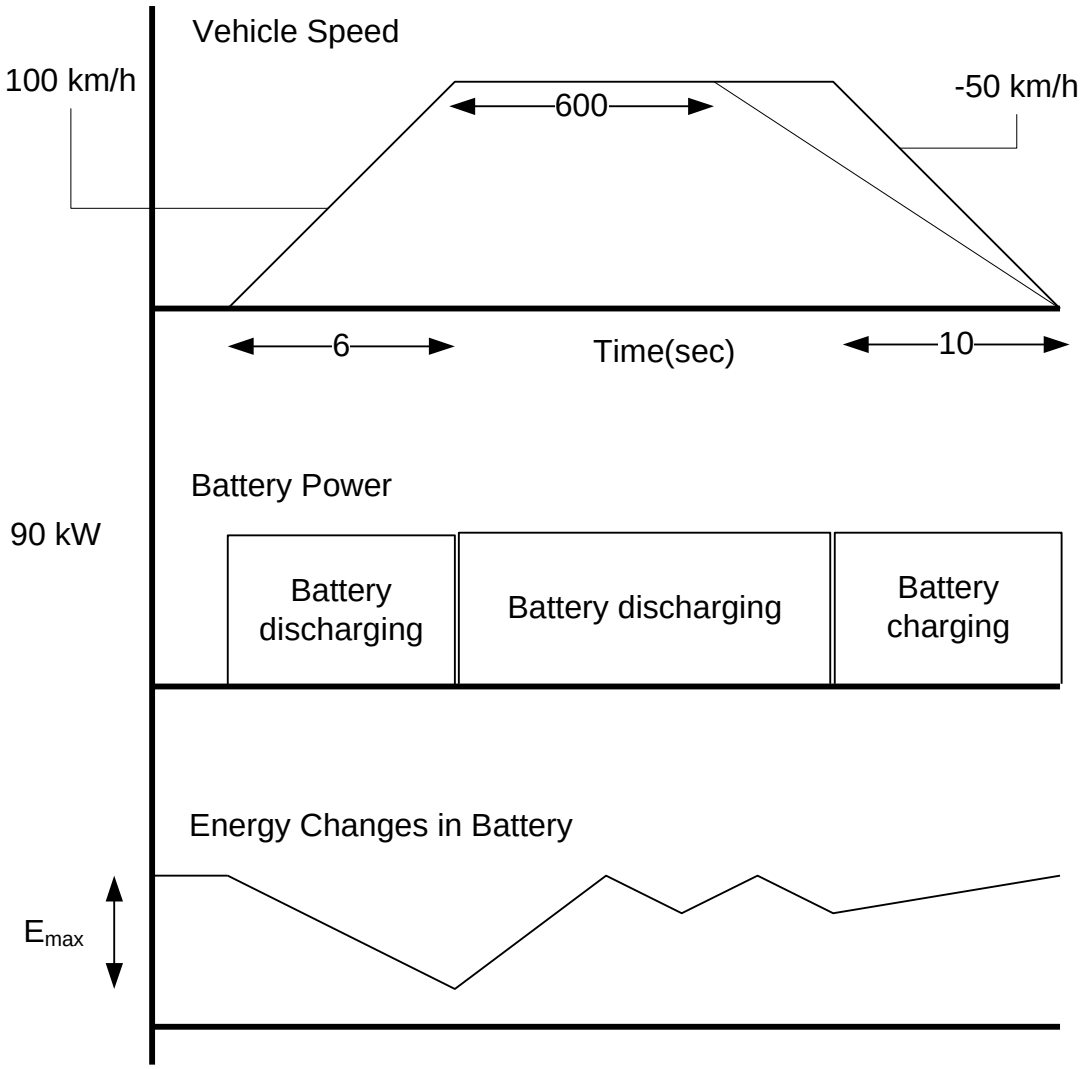

Figure 22. Typical drive cycle

The most common driving cycles are probably the European NEDC and the American FTP-75. This thesis employs the American FTP-75 driving cycle which represents the New York urban driving cycle. This is because it is believed that if the system implementation can run an urban driving cycle that is as transient as the FTP-75, then it should perform well in almost every urban scenario. The FTP-75 driving cycle is shown in (Figure 23).

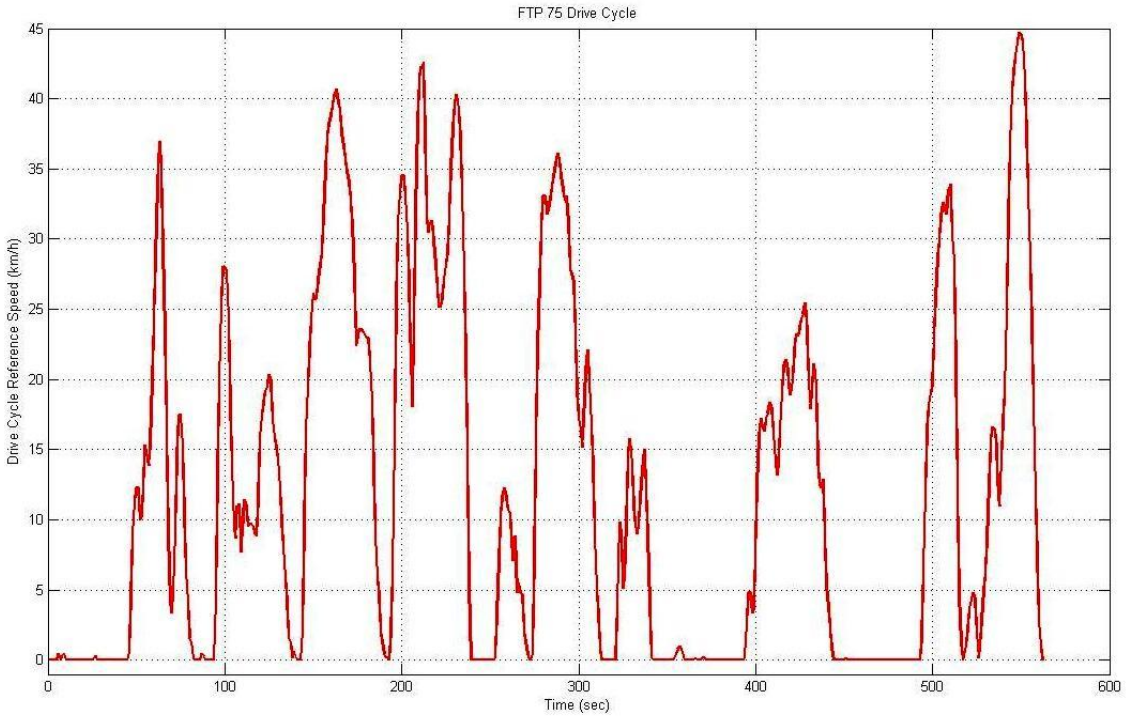

Figure 23. The American FTP-75 reference drive cycle

5.6 Drive System

The machine, inverter, feedback, and controllers constitute the PMSM drive system as shown in (Figure 12). All reference or commanded values are superscripted with a "*" in the diagram. The error between the reference and actual speeds is operated upon by the speed controller to generate the torque reference. In the constant air-gap flux mode of operation where $i_d^* = 0$, the torque reference divided by the motor torque constant gives the reference quadrature axis current. This goes through the inverse Park transform to generate the (a, b, c) stator reference currents. The PWM current controller using current feedback attempts to force the actual motor currents to equal the commanded values at all times. Current control is implemented by the appropriate firing of power devices (in the MLI). Both position and speed feedback can be obtained from a resolver/signal processor combination.

5.6.1 Speed Control

The typical speed controller is based on a PI regulator as shown in (Figure 24). The outputs of this regulator are set points (or reference values) for the torque as applied to the vector control block. It should be noted that in this particular research problem the torque is later transformed into reference current to be compared with actual current in the vector control block. Thus the coefficients of the PI regulator are manipulated to produce reference current values.

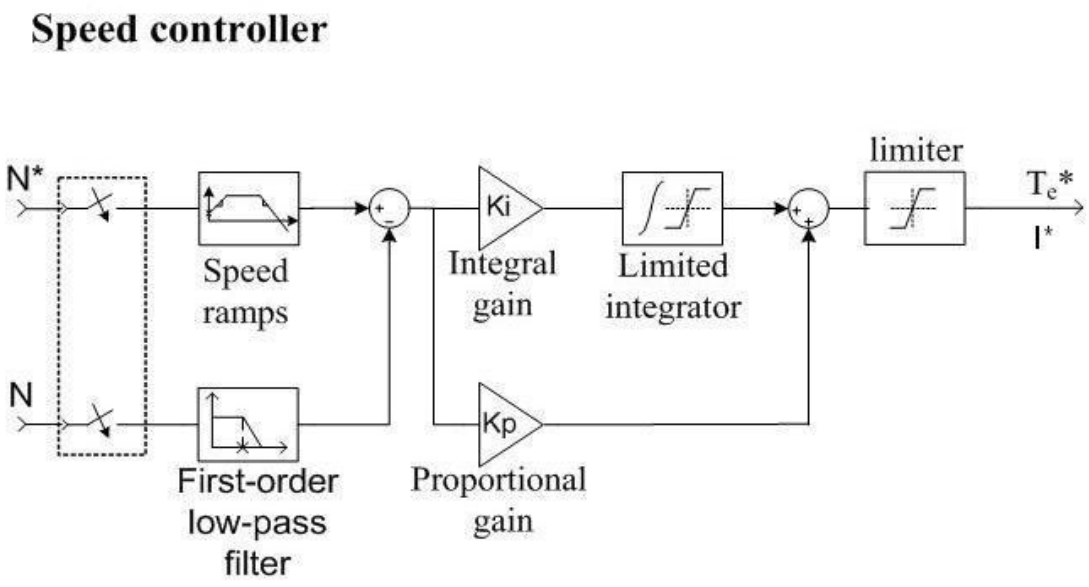

Figure 24. Typical speed controller

The value N* is the reference speed input which comes from the driving cycle. The actual speed of the vehicle is given by N, which is a result of the motor's traction in the face of inertia and friction. The two values N and N* are compared and the error is fed to a PI controller. The subsidiary blocks like speed ramps, low pass filter and band limiter are signal conditioners. The speed ramps block makes the speed signal to ramp up a defined slope to avoid abrupt changes. The first order low pass filter is placed to remove any high frequency components of the actual speed signal so it can be properly

compared with the reference signal. The band limiter (here applied for the current) keeps the signal within upper and lower bounds making it very practical.

The PI controller acts as the heart of the control system. It is a feedback controller which receives the error signal from the comparator, passes it through a proportional and integral block in such a way the steady state error moves towards zero. The proportional block helps respond quickly to changes in the error deviation. The integral block though slower than the proportional block helps reduce the offset between the plant output and reference signal. A basic PI regulator is shown in the (Figure 25). This is a realization of the expression given by the following transfer function, $\frac{U(s)}{E(s)} = K_P + \frac{K_I}{s}$.

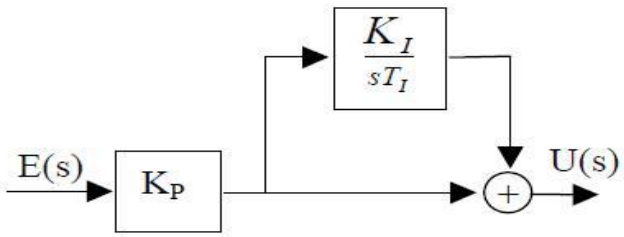

Figure 25. Basic PI regulator

5.6.2 Vector Control Block

Vector control is normally used in ac machines to convert them; performance wise, into equivalent separately excited dc machines with highly desirable control characteristics. PWM current controllers are used to ensure that the actual motor currents are as close as possible to the references. The advantage of the PWM current controller over hysteresis control is that the switching frequency is preset thus never exceeding the inverter switching capability. The vector control block shown in (Figure 26) consists mainly of inputs, dq-to-abc transformation block, current regulator and outputs. The output of the dq-to-abc block is the multiplexed form of the reference current signal denoted by I^*_{abc} .

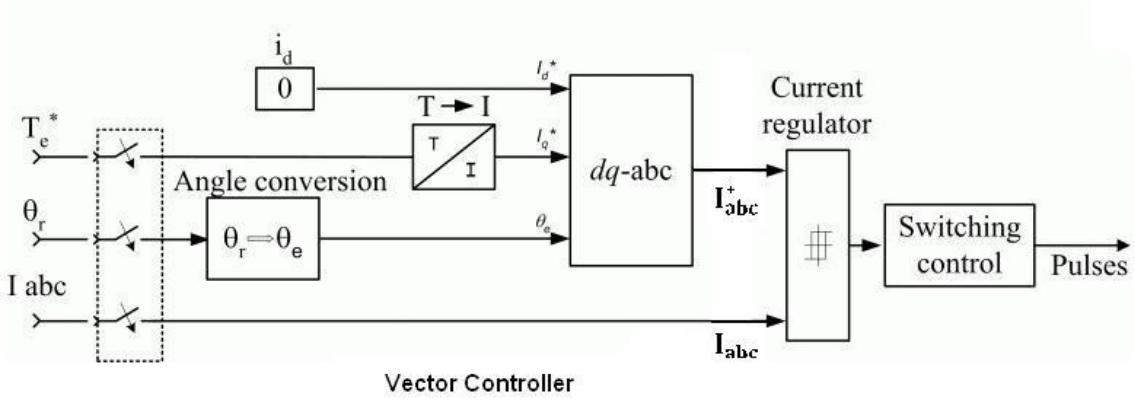

Figure 26. Vector controller

The inputs that feed into the dq-to-abc transformation block of (Figure 26) are:

1. The torque signal converted to an equivalent quadrature current, I_q^*
2. The rotor angle, θ_r
3. The actual values of stator currents, I_{abc}

The DQ transformation is basically a transformation of coordinates from the three-phase stationary coordinate system to the *dq* rotating coordinate system. This transformation is a two stage process:

a. a transformation from the three-phase stationary coordinate system to the two-phase, so-called *ab*, stationary coordinate system and
b. a transformation from the *ab* stationary coordinate system to the *dq* rotating coordinate system

The basic transformations including Park and inverse-Park are described in the self-explanatory illustration shown in (Figure 27).

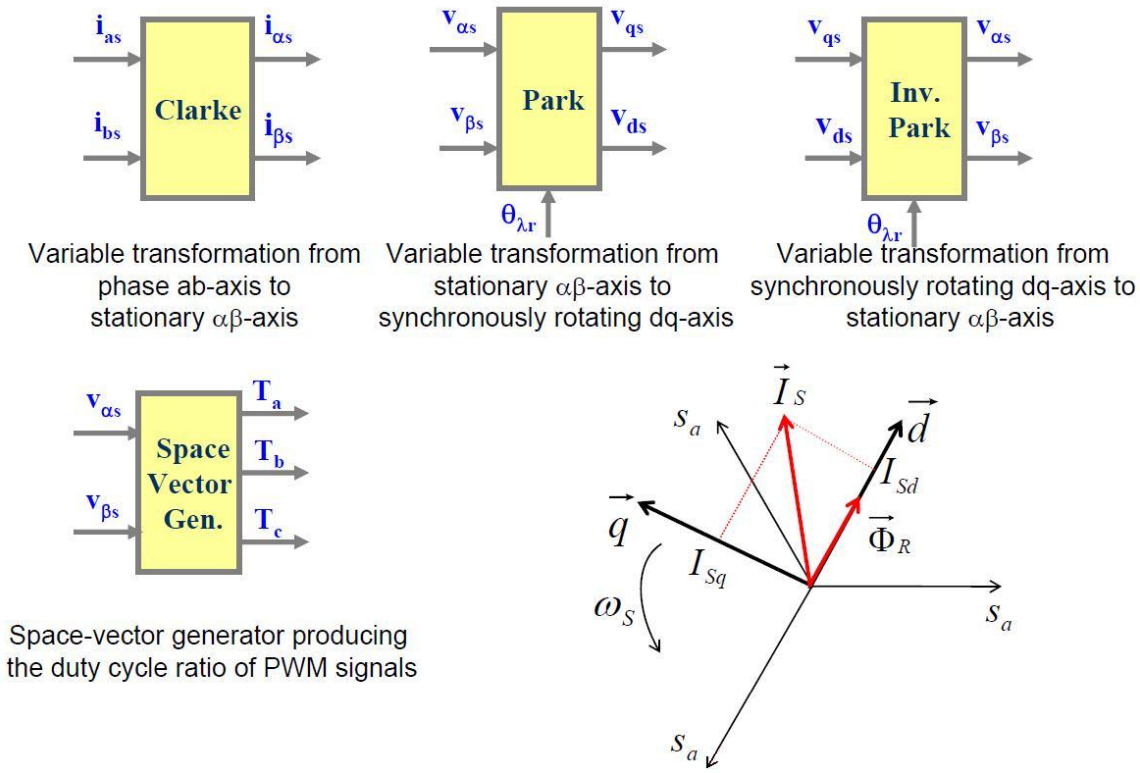

Figure 27. Vector matrix transformations

The inverse Park transformation matrix (from *dq* to *abc*) is defined as:

$$T' = \begin{bmatrix} \cos(wt) & -\sin(wt) \\ \cos(wt - \frac{2\pi}{3}) & -\sin(wt - \frac{2\pi}{3}) \\ \cos(wt + \frac{2\pi}{3}) & -\sin(wt + \frac{2\pi}{3}) \end{bmatrix}$$

The inverse transformation is calculated as $X_{abc} = T'X_{dq}$

The simulation implementation of the dq-to-abc control is shown in (Figure 28).

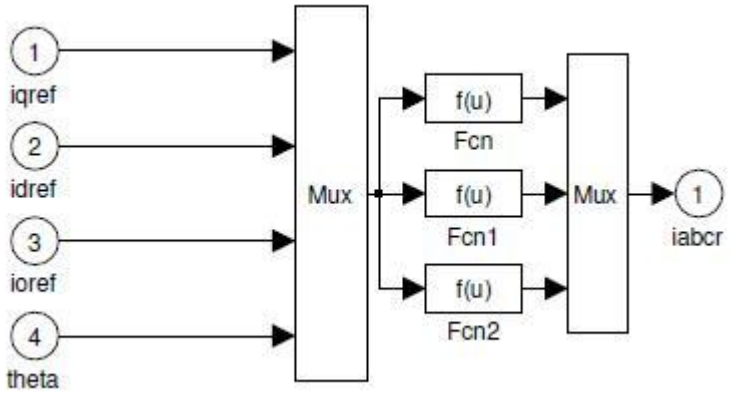

Figure 28. Simulink model of dq to abc transformation

The inputs to the above model are as follows:

1. iqref, which is a product of the PI as explained earlier
2. idref which is held at zero
3. ioref, held at zero
4. theta, is the rotor angle θ_r

The above signals are given to a multiplexor (mux) and then fed to the three functions shown in the above figure. These functions are actually a result of the inverse Park transformation as explained above. The resulting three signals are again fed to a mux in order to produce a three phase reference current signal.

5.7 PWM Current Controller

A popular method used to generate the required stator currents is to use a PWM current controller which requires rotor position feedback. The actual values of the currents are compared with the reference currents to generate error currents which are then compared to a sawtooth-shaped triangular wave as shown in (Figure 29). If the error signal is positive and larger than the sawtooth, the voltage is switched positively, while if the error signal is positive and smaller than the sawtooth, the voltage is switched negatively.

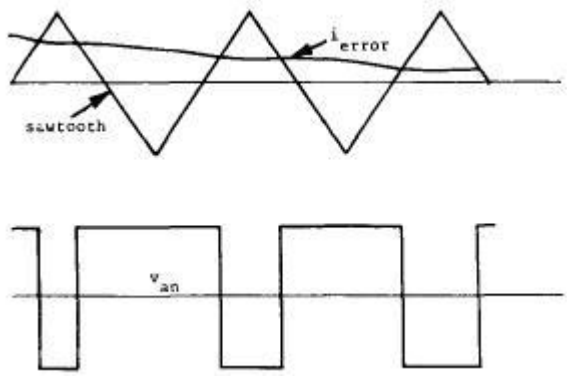

Figure 29. PWM current control

5.8 Switching Gate Signal Generator

The switching circuitry employs a unique form of a current comparator and gating signal generator. The current comparator works on two input current signals, the reference current signal (generated as a result of the dq-to-abc transformation block) and the actual current. This is well explained in the following illustration (Figure 30).

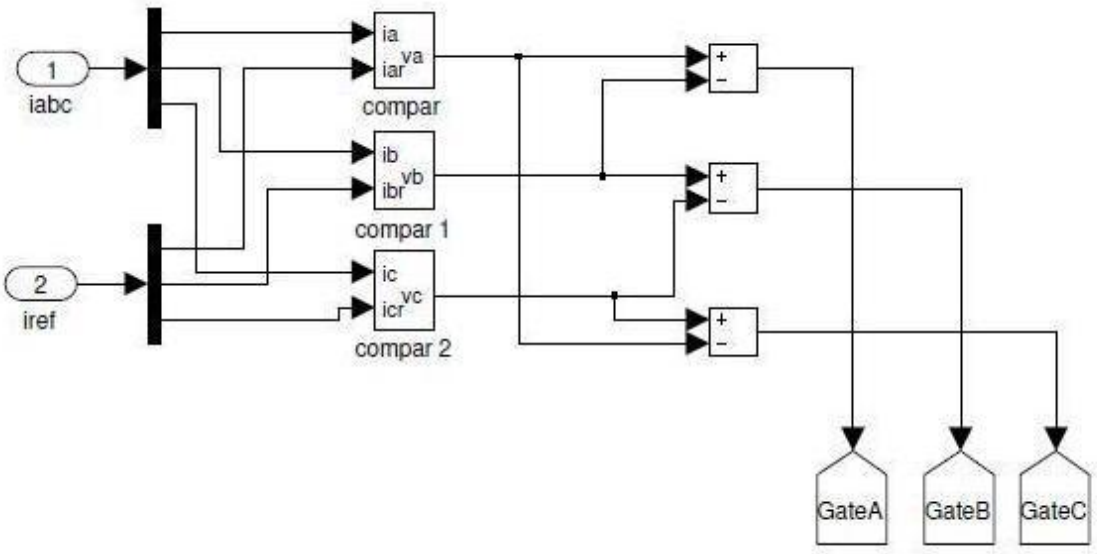

Figure 30. Switching gate signal generator

It can be observed in the above figure that the three-phase current signals go through a demultiplexor (demux) and produce individual phase currents. These currents pass through the current comparator to generate an equivalent voltage signal. The outputs become the reference gate signals called as GateA, GateB and GateC. These represent the reference gate signals for each phase of the inverter. A single signal for each phase is further computed and decoded to give the individual gating signals for each cell and the switches within.

The current comparator of (Figure 30) for one phase is constructed as shown in (Figure 31). *ia* and *iar* are the actual and reference current values respectively. The actual current value is passed through a first order low pass filter, in order to make it easier for comparison with the reference signal. The output of the comparator passes through a block called Relay block. The Relay block allows its output to switch between two specified values (courtesy The MATLAB support documentation made available by The Mathworks Inc). When the relay is on, it remains on until the input drops below the value of the Switch off point parameter. When the relay is off, it remains off until the input exceeds the value of the Switch on point parameter. The block accepts one input and generates one output. The output here is a small voltage signal *va* which was also observed earlier in (Figure 30).

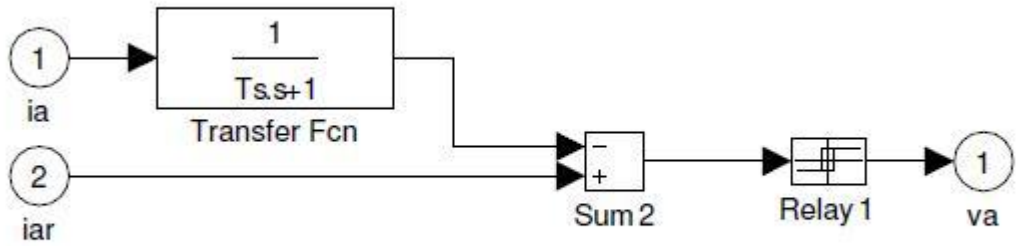

Figure 31. Current comparator

5.9 Switching Modulation Strategy Implementation in Simulink

The different types of switching modulation strategies have been already discussed in Section 3.3 dealing with MLIs. This thesis has been tested with both Level Shifted (LSMM) and Phase Shifted Modulation Methods (PSMM). Due amount of simulation studies and investigations were carried out in order to determine the performance, efficiency and reliability of the inverter with both modulation methods involving trade-offs. Keeping in mind the resulting THD, harmonics and efficiencies, in addition to ease of implementation in circuitry, the PSMM was chosen for 2 cells per phase implementation while LSMM was chosen for 6 cells per phase implementation. One must remember that for all practical purposes, this system at the same power level and number of levels in the MLI would work equally well with both modulation methods. As the number of levels increase, the carrier signal frequencies get closer in PSMM, while they become smaller in amplitude in LSMM.

It is to be understood that there are two cells per phase in this MLI, as also evident from both (Figure 5) and (Figure 17). Hence the six signals that are generated for two cells per phase for the three phases are shown in the switch gating control block in (Figure 32).

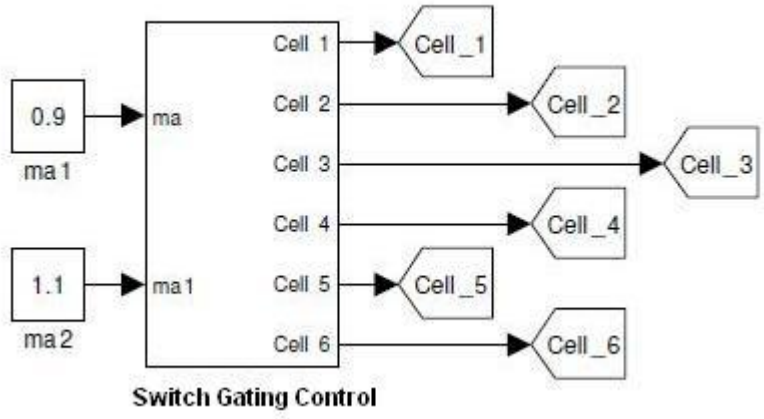

Figure 32. Switch gating control block

Each cell needs to be fed by its respective reference gating signal. This reference signal is converted into equivalent PWM gating signals for each switch of the cell. The two inputs in the above figure are the modulation indices for the upper and lower cells of each phase. These modulation indices denoted by ma1 and ma2 measure 0.9 and 1.1 respectively. The importance of value of modulation index is well explained in the book by Ned Mohan [32]. The extension to deliver a practical solution by employing 6 cells per phase requires control block to provide 6 times 3 equaling 18 signals. The following (Figure 33) shows a LSMM implementation of the 6 cells per phase MLI.

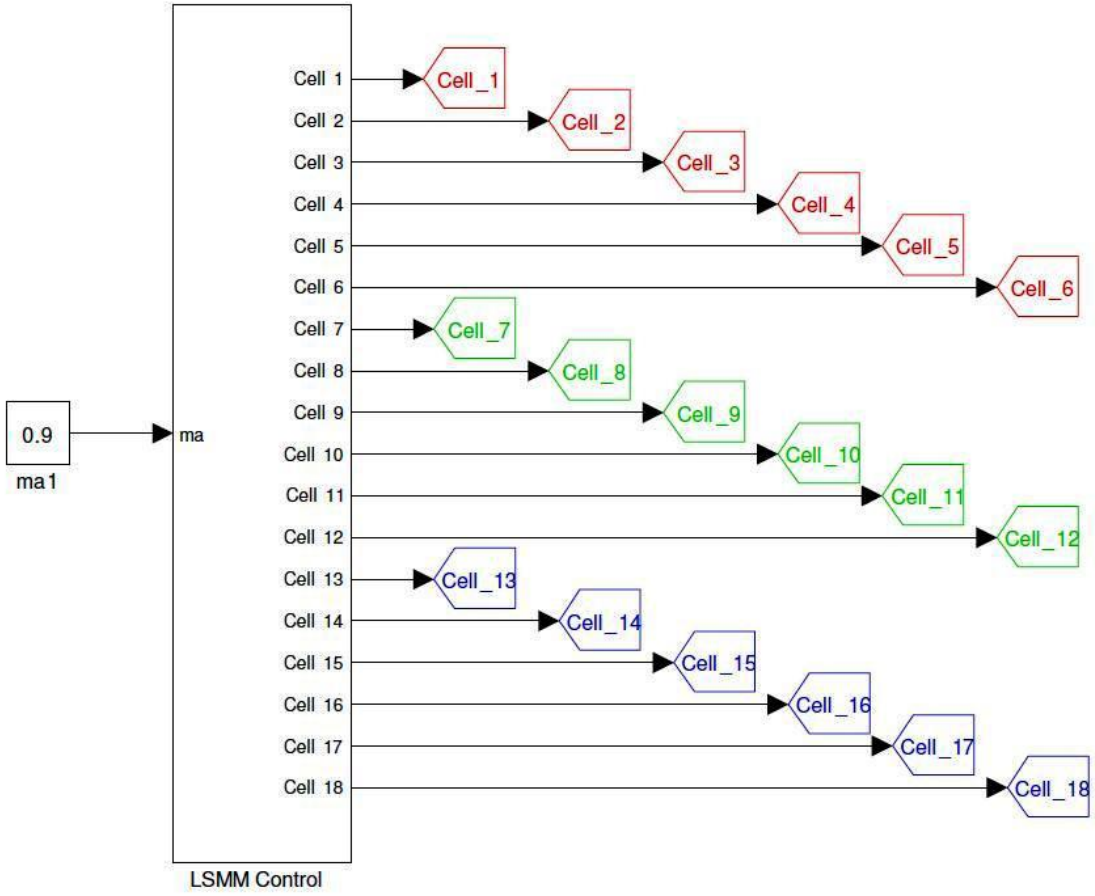

Figure 33. Masked sub-system model of switch gating control block for 6 cells per phase MLI

The colors red, green and blue illustrate the three phases that are fed by the gating signals. One must duly note that this particular simulation was implemented using LSMM, and a single modulation index unlike the previous case. It is purely for reasons of convenience, and it is understood that PSMM or multiple modulation indices can also be easily employed.

The illustration (Figure 34) deals with the masked sub-system model under the switch gating control block previously shown in (Figure 32). It is seen that this sub-system has three blocks meant for each of the three phases. The outputs shown in green connection ports are the signals that go to each phase. Cell 1 and Cell 2 signals feed the upper and lower cells of phase A, Cell 3 and Cell 4 feed phase B while Cell 5 and Cell 6 handle phase C.

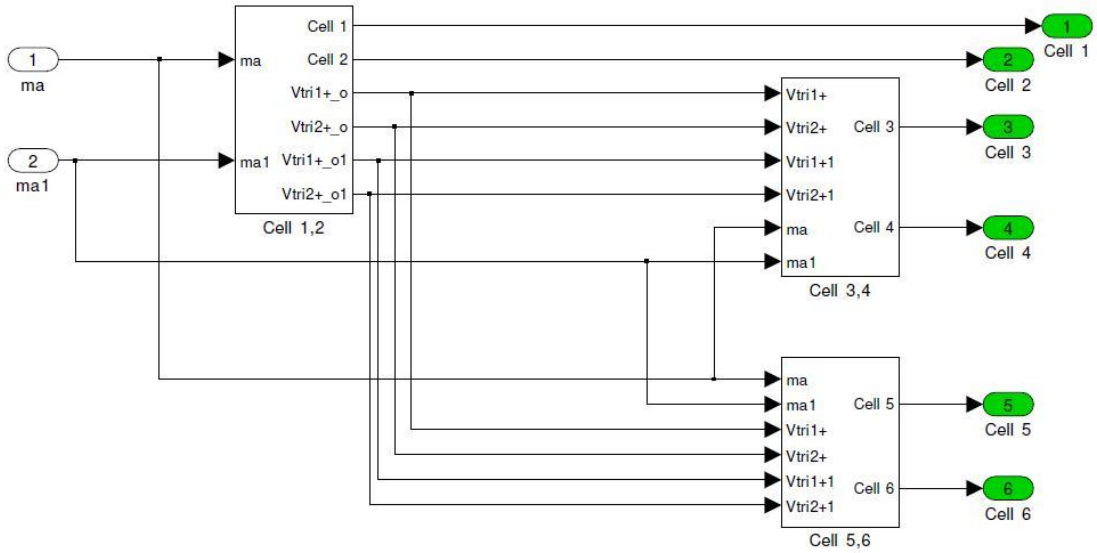

Figure 34. Masked sub-system model of switch gating control block

The gating control for phase A titled ‘Cell1, 2’ in (Figure 34) is constructed as shown in its sub-system model in (Figure 35). The two inputs on the left are the modulation indices. The other important input is the GateA signal which is coming from the Simulink model shown in (Figure 30). The modulation index ma is multiplied with the GateA signal by the product block to produce the modulation signal to be compared with the triangular carrier signal. The block denoted by ≥ processes the comparison of the modulation and carrier signals.

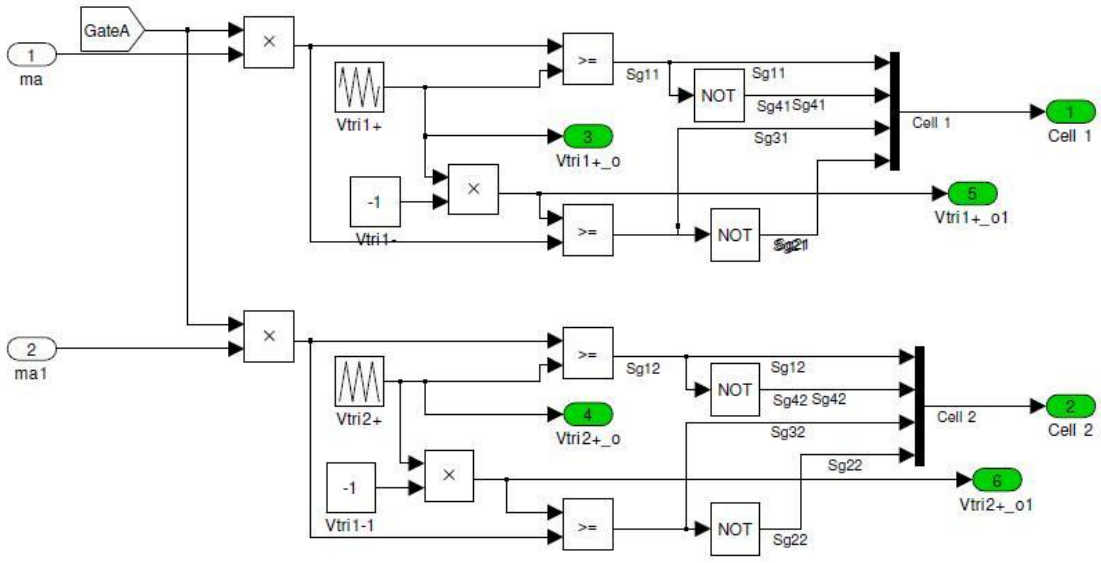

Figure 35. Sub-system model of gating control for phase A

As is evident from the above figure, there are two sets of gating signals being generated. The upper portion producing Cell 1 feeds the upper cell of phase A, while the lower portion generating Cell 2 is for the lower cell. The Boolean logic being implemented in addition to the signal comparison and conditioning is obvious from the basic theory of triggering a H-Bridge inverter. The 2 signals for each cell are toggled to complimentary values by the NOT gates in order to generate a total of 4 signals for each cell.

The switching modulation being PSMM, there are in effect 4 triangular waves for this system. An example of PSMM in implementation was explained previously in (Figure 7). The two triangular signals vtri1+ and vtri2+ are apart by 90 degrees, and each when multiplied by -1 produces its respective negative counterpart. The triangular signals are the same for all three phases hence sent to the connection ports denoted by vtri1+_01 and vtr2+_01. These go to the remaining two blocks on the right hand side of (Figure 34). Thus six gating signals are generated, all of which feed the cells of the three phases in the CHB MLI block.

For the sake of completeness, the masked sub-system model of the switch gating control block for the 6 cells per phase MLI implementation is shown in (Figure 36).

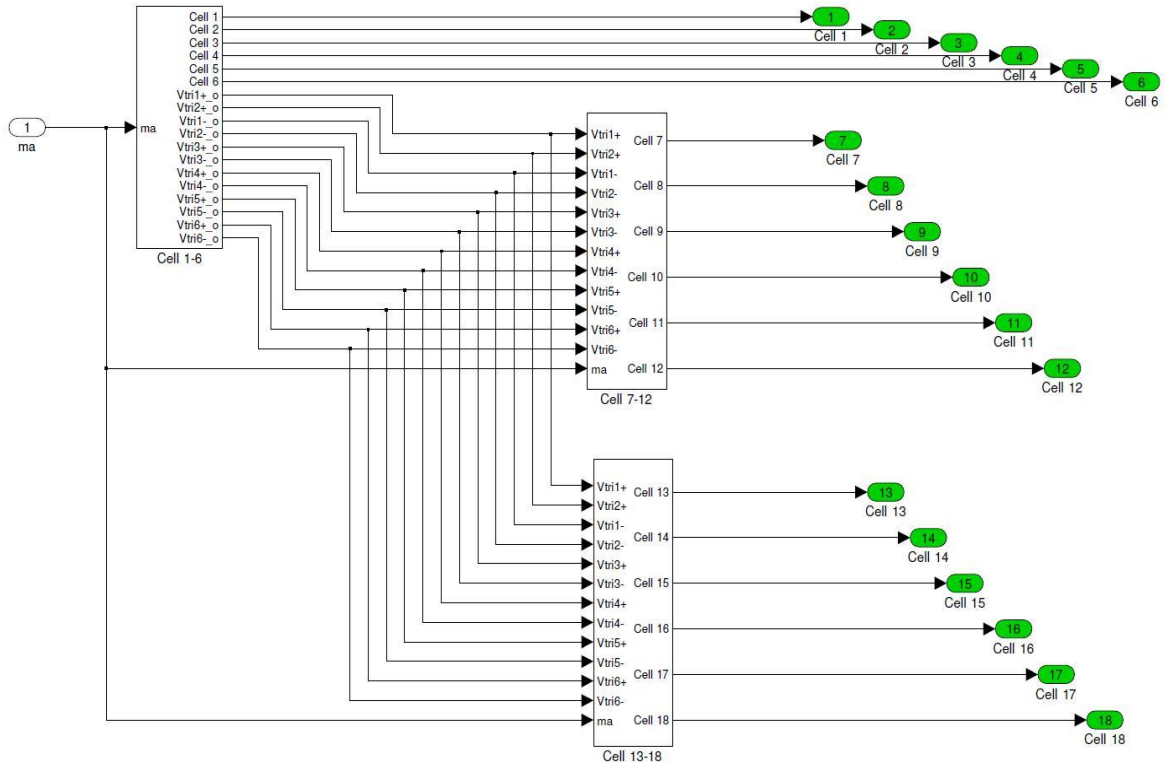

Figure 36. Masked sub-system model of switch gating control block for 6 cells per phase MLI

The blocks described in (Figure 36) are constructed as shown in (Figure 37).

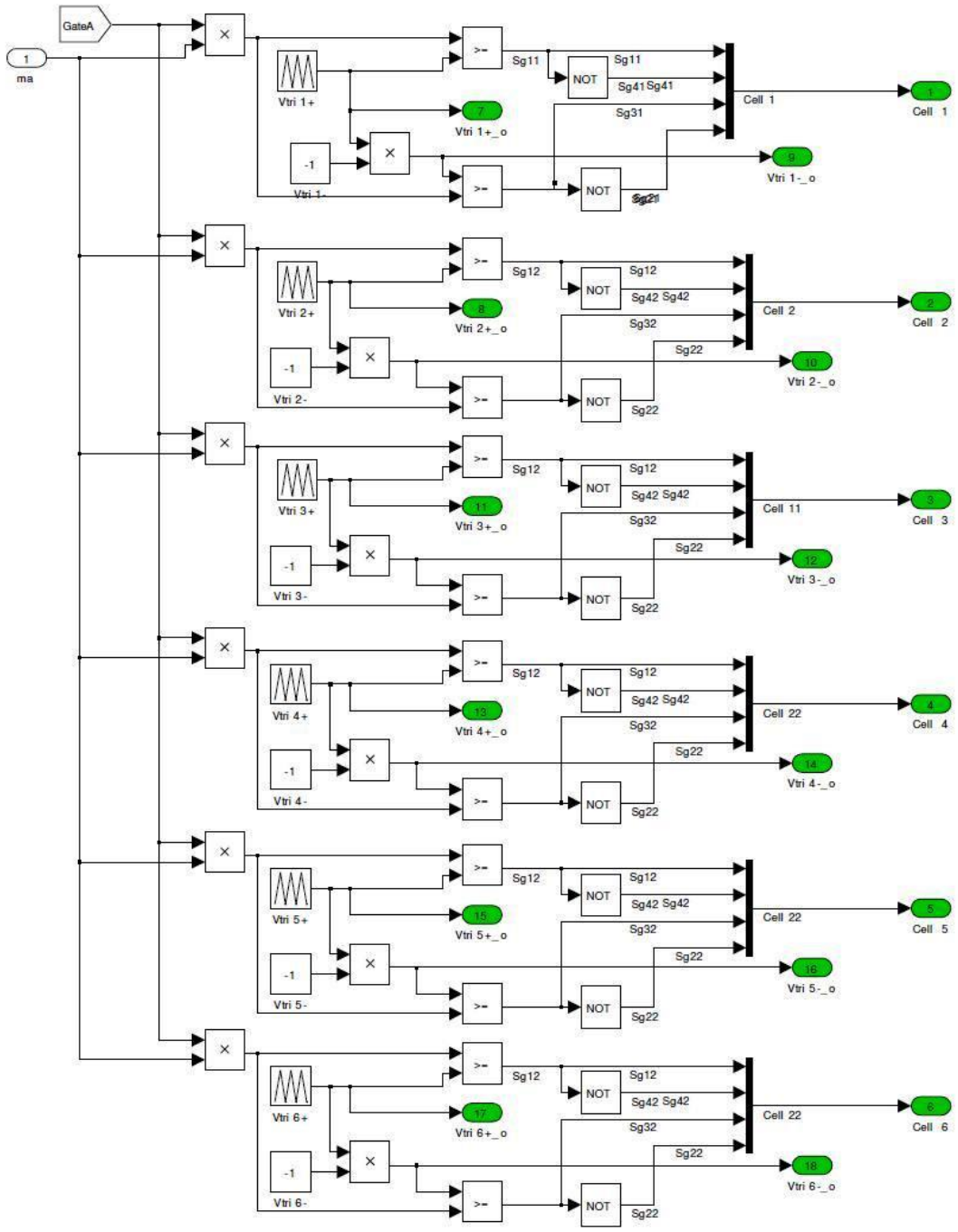

Figure 37. Sub-system model of gating control for phase A in 6 cells per phase MLI implementation

One must remember that this is a LSMM implementation. In LSMM implementation, the triangular carrier waves are level-shifted or shifted in amplitude. This was explained in greater detail in part (b) of Section 3.3. The six triangular waves are vtri1+ through vtri6+ while their respective negative counterparts are vtri1- through vtri6- as shown above. In this implementation, six gating signals are produced to feed each phase, hence a total of 18 signals for the entire system. In a bid to keep the simulation simple to show its viability and proof of operation, a single modulation index has been utilized. It is obvious that different modulation indices for different cells in each phase can be used.

There is an importance attached to employing LSMM because it can be used to selectively discharge the batteries connected to particular cells. Varying the modulation index value according to the SOC of the battery pack across a phase allows for longer battery life. It also facilitates a charge rotation and charge balance scheme which increases life and reduces vehicle running costs.

In summary, this section discussed the simulation implementation of the system designed in Section 4. The various simulation models describing the blocks such as the inverter, motor and closed loop speed control were explained in detail. The theory of operation and vector control was explained and shown in simulation modeling. The complicated switching circuitry for this MLI implementation was explained with elaborate illustrations and models. The simulation model was subjected to an input reference driving cycle, and its performance characteristics like speed, torque, closed loop speed control, and acceleration response are explained in great detail. The response to the driving cycle also helps study the regenerative capability of the system. The reverse power flow to recharge the batteries during deceleration and/or coasting has been explored. The detailed modeling and simulation implementation in this section leads the way to discussing the results in the next section.

6. RESULTS

The results of the simulation implementation described in Section 5 are discussed here. Appropriate designs were made, and carried out in simulation in order to imitate real time operation and study system performance. These results aided by many self-explanatory illustrations are discussed in this section.

6.1 Summary of System Design

The design of electric vehicle was discussed. The calculated machine ratings and other design parameters are presented herewith.

Electric Motor (BLDC)

Power Rating : 90 kW

Torque Rating : 350 Nm

Force/Effort : 8 kN

Speed Rating : 10000 RPM

Base Speed : 2500 RPM

X factor : 4

Transmission

Single Gear Transmission assumed

Gear Ratio of Transmission : 7.07

Gear Ratio of Final Drive : 1

Efficiency of the whole drive from motor to wheels : 96.04%

Battery (Li ion)

Power Capacity : 100 kW

Energy Capacity : 9 kWh

Weight : 83.33 kg

The following are some of the several important observations from this work:

- Output voltage of the MLI
- Acceleration, constant speed, coasting, deceleration
- Closed loop speed response
- Electromagnetic torque
- Three phase stator currents
- Stator back-emf
- Regenerative capability
- Fault sensing and diagnostics
- Fault monitoring and control

6.2 Output Voltage of the MLI

It was explained in the Multi Level Inverter sub-system model of Section 5.4 and illustrated in (Figure 17) as to how the upper and lower cells respectively build up the phase voltage. The outputs measured at each cell and the phase of 2 cells per phase implementation is shown in (Figure 38). It should be noted that the first and second graphs show the upper and lower cell voltages respectively. The third one shows the sum of the above two, which is the phase voltage. One should remember that the value of the DC voltage at the terminals of the battery is 700V. The output phase voltage for the 6 cells per phase MLI implementation is shown in (Figure 39).

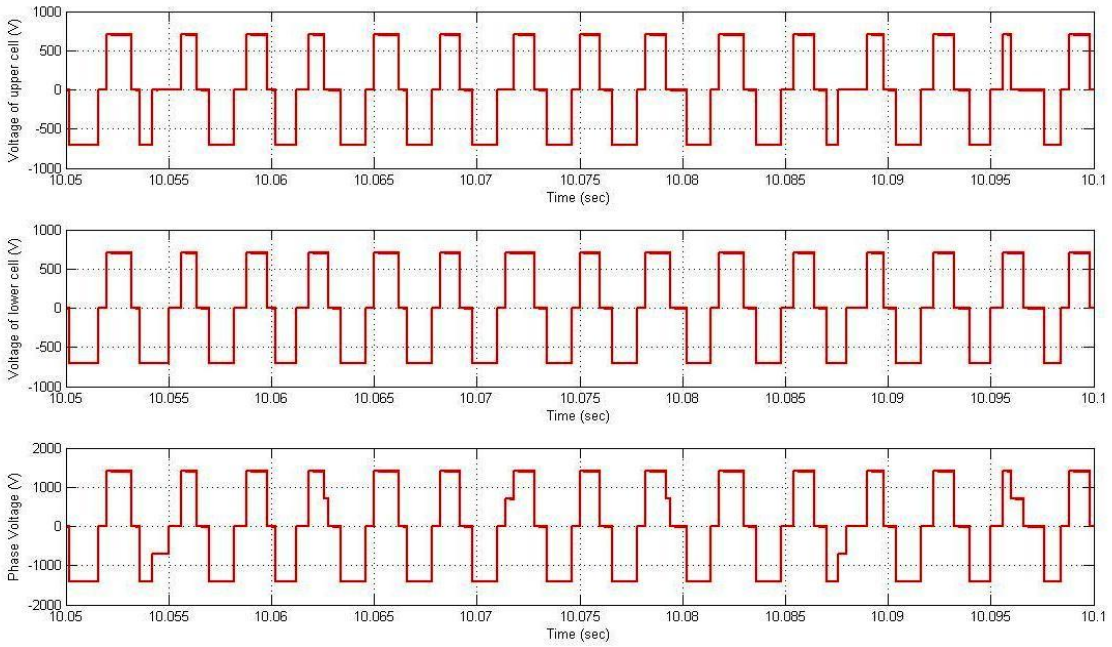

Figure 38. Upper and lower cell voltages adding to produce phase voltage

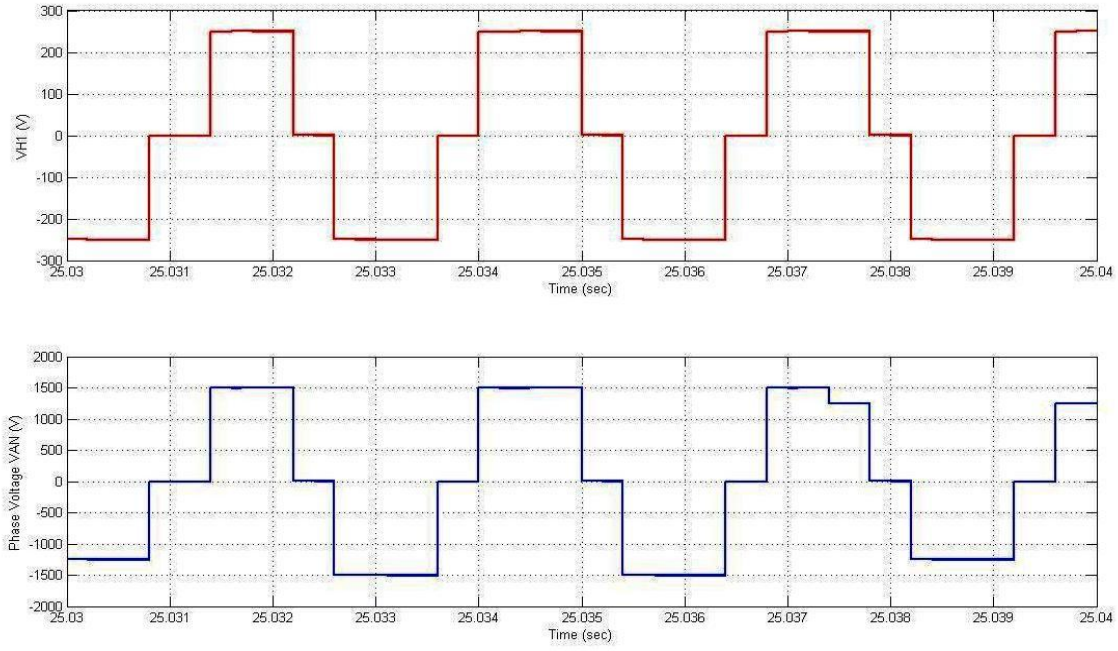

Figure 39. Cell voltages adding up to produce phase voltage in 6 cells per phase MLI implementation

It is seen in the (Figure 39) that the peak output voltage of one cell VH1 equals 250V. Six of the cells' respective output voltages add up to produce the peak amplitude of 1500V as the value of the output phase voltage measured between node A and neutral N. This result demonstrates the feasibility of adding any number of required cells to produce the desired output voltage. The implementation can help reduce voltage stresses across each switch, and facilitates the usage of standard power devices readily available in the market.

6.3 Typical Speed Response and Acceleration Performance

The resulting response of the system to inputs such as step inputs in order to study its acceleration performance is discussed here. In the illustration (Figure 40), the first plot depicts the input reference. For various step input changes, the vehicle's speed response is shown in blue in the second plot. The last plot also in blue shows the corresponding graph of electromagnetic torque.

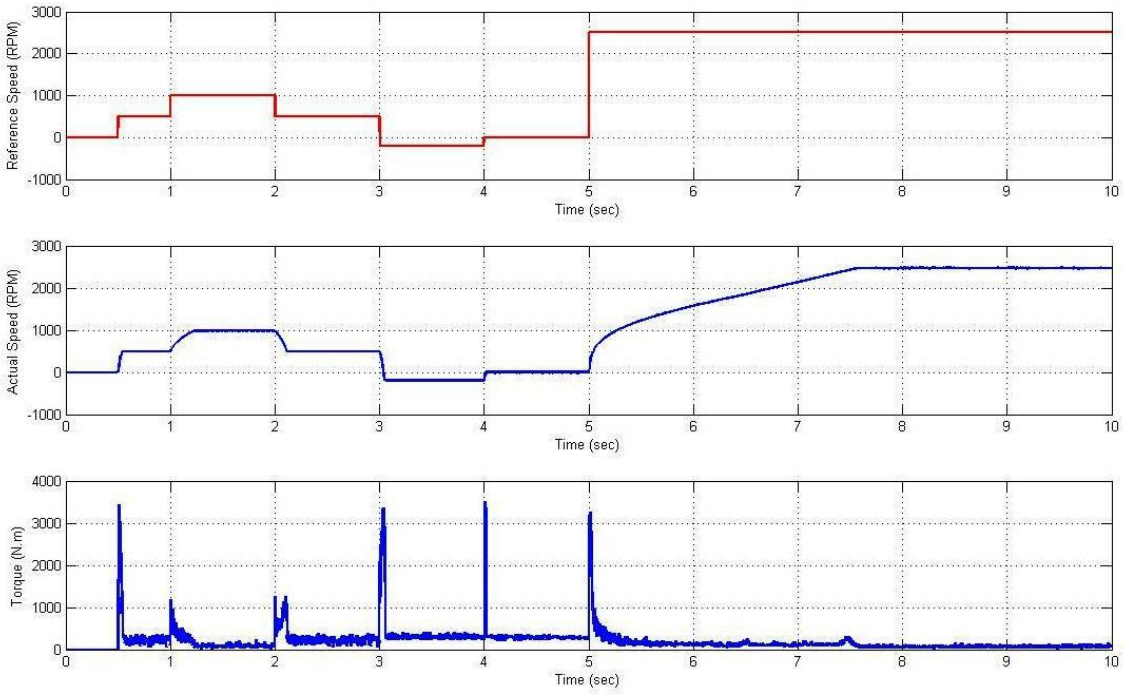

Figure 40. Vehicle's response to a typical speed profile to study acceleration performance

6.4 Closed Loop Speed Response

The results of this work help draw many vital conclusions. The importance of the reference driving cycle has been already covered. The reference drive cycle in consideration for the current simulation implementation is the FTP-75 cycle. It is also popularly known as the New York Urban driving cycle. This was explained in the Section 5.5 and illustrated in (Figure 23). The output measurements from the BLDC motor drive system consist of the speed and electromagnetic torque. The output speed (in blue) as compared to the input reference speed (in red) in RPM is seen in (Figure 41). It is immediately observed that it closely follows the input reference speed. This is an extremely important result of this work because it displays the viability of the system that its output follows the input reference very closely.

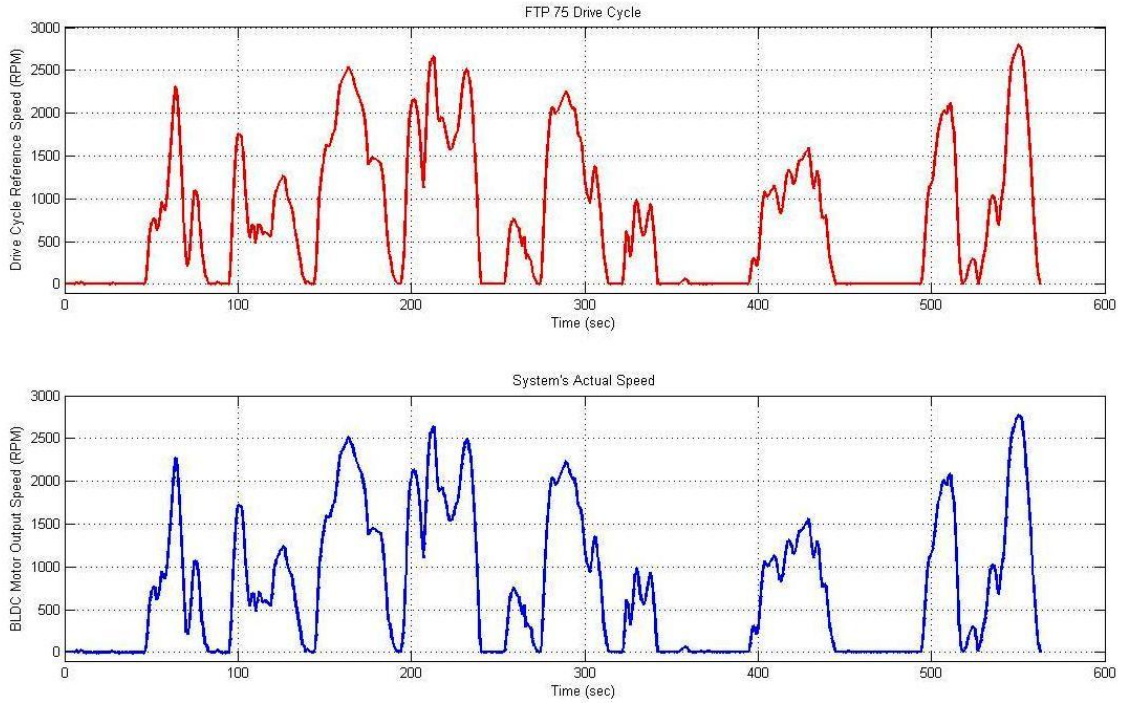

Figure 41. Input reference speed and output speed

6.5 Electromagnetic Torque

The behavior of the generated electromagnetic torque is also of vital importance. The trend of the torque as the speed varies is shown in (Figure 42). It shows the output torque along with its ripple. One can immediately observe that the torque value is high when the speed is low, and torque is low when the speed is high keeping in line with the constant power mode of the traction motor.

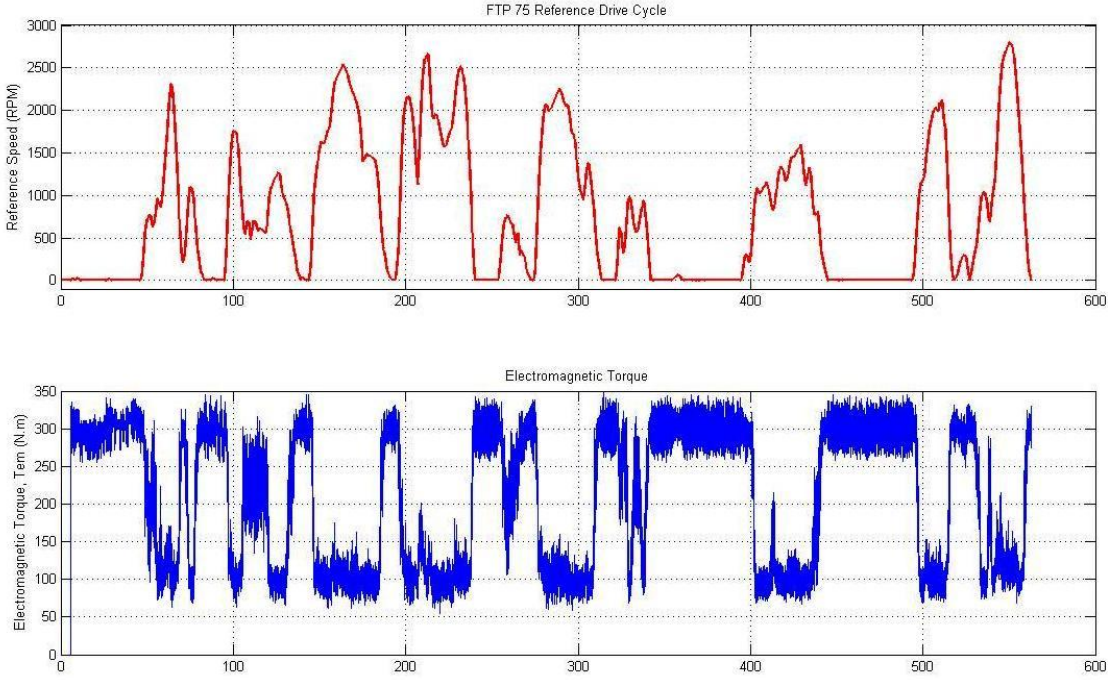

Figure 42. Output speed and generated electromagnetic torque

6.6 Three-Phase Stator Currents

Another measured output are the stator three-phase currents as shown in the following illustration (Figure 43). It should be noted that though the stator currents are actually sinusoidal they look stepped here because of the relative step size. In other words, when the step size of the simulation is made smaller (making the simulation much slower and inoperable due to software package limitations), the currents look smoother.

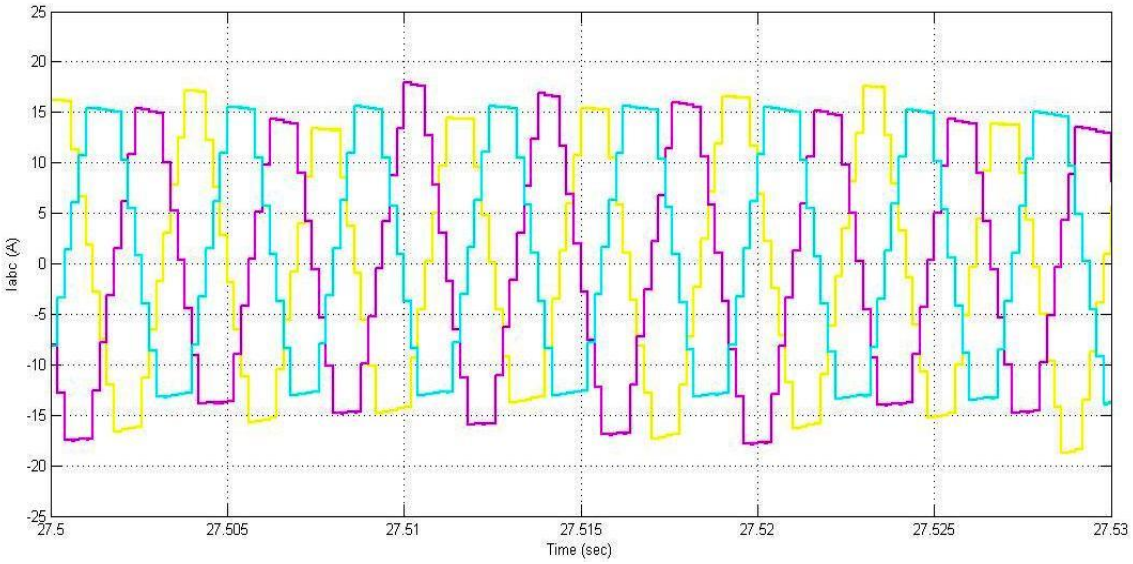

Figure 43. Three phase stator currents

6.7 Stator Back-emf

The stator back-emf for each phase as shown in (Figure 44), varies with the reference, and behaves similar to the stator currents.

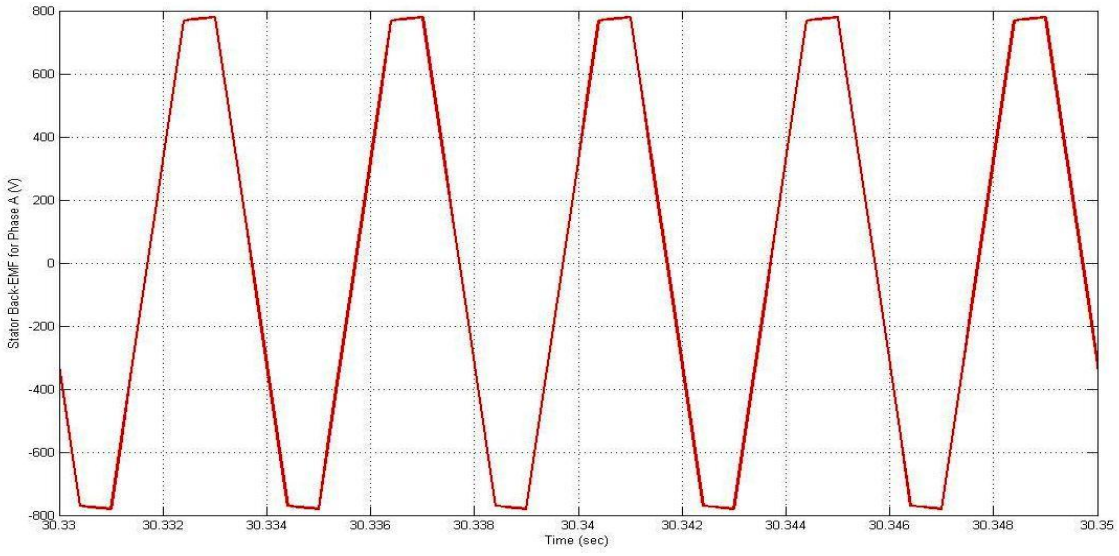

Figure 44. Stator back-emf for phase A

It is seen in the above figure that the back-emf is in trapezoidal shape. This back-emf is also important because the torque constant is designed assuming that the machine is driven by an inverter which provides a perfect synchronization between the stator's current and back-emf. In the case of the trapezoidal machine, a square wave current is assumed.

6.8 Regenerative Capability of the Implemented System

The EV achieves its high efficiency mainly due to conserving energy during braking or deceleration and coasting. During this process, the power electronic converter reverses the flow of power from the output load (vehicle is a load to the motor) to the input power source i.e. the batteries. A sample portion (about 50 seconds) of the actual driving cycle is chosen to show the regenerative capability of the system. This is illustrated in (Figure 45). It is seen that the State-Of-Charge (SOC) of one battery changes with the speed. The SOC should be particularly observed during the acceleration and deceleration portions.

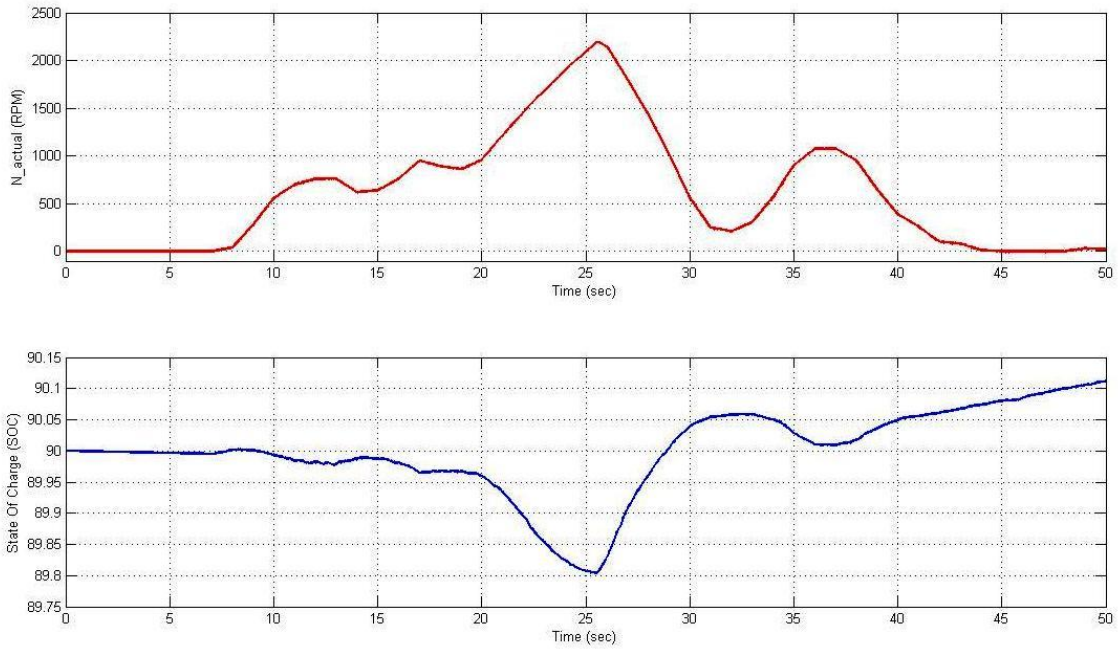

Figure 45. Variation of the battery SOC with actual speed

6.9 Fault Analysis

Fault analysis involves investigation of the system in the presence of faults. Most common faults are cell short circuit, phase-to-phase short circuit etc. Some of these faults were artificially created in the simulation to imitate an actual real-time scenario. The above faults are introduced in the MLI sub-system model.

Broadly speaking, the cell failure could be an open-circuit fault or short-circuit fault. By open-circuit fault, it is meant that the particular cell in the phase under consideration does not produce any voltage or indeterminate voltage because all the 4 switches in the inverter are off. This rare event would occur only when a fault in the control circuitry triggers them to remain off. The cell ceases to generate a voltage, and since being in series the whole string or phase is compromised. Although a cascaded MLI has the ability to tolerate a fault for some cycles, it would be better if the fault type and its location can be detected and cleared as soon as possible. Upon fault detection in one cell, the switching patterns and the modulation index of other active cells of the MLI can be adjusted to maintain the operation under balanced load condition.

A short circuit fault is introduced in the simulation system as shown in (Figure 46). In this event, the short circuit happens at the output of the MLI between any two phases (say A and B). The block titled ‘ref1’ inputs a time based signal of 1 and 0 as a gate control signal to the circuit breaker. The circuit breaker operates in Normally Open (NO) condition, and closes to simulate a short circuit fault. At the bottom of the figure, one can observe two inputs titled as input reference 1 and 2 respectively. Both feed through a switch case logic controller (titled ‘Switch’) to produce the input driving cycle reference speed. The switch case logic controller allows the input 1 to flow under normal circumstances, and would switch over to make input 2 to flow in the event of a fault. Thus it can switch between two different inputs to flow through depending on the control signal that it receives, which is the event of a fault. It is built such that the input remains the same while the fault lasts for a short period of time say 5 seconds, so that the system can continue normal operation. It is to be understood that the entire system i.e.

vehicle should not come to a halt because of a fault. The basic idea is to test the fault tolerance, ruggedness and reliability of the system. One should remember that the input current drawn by the MLI from the batteries is proportional to the magnitude of the speed. Hence in the presence of a fault, the vehicle is forced to run at a lower speed instead of normal driving cycle speed so as to discharge the batteries slower, the life increases, and the SOC does fall too low. This is called limp-home capability wherein the vehicle limps home at a slow speed but is functional until the vehicle gets fixed or the fault is cleared by other means. The lower speed value of 500 RPM for input reference for the system is shown by the constant block.

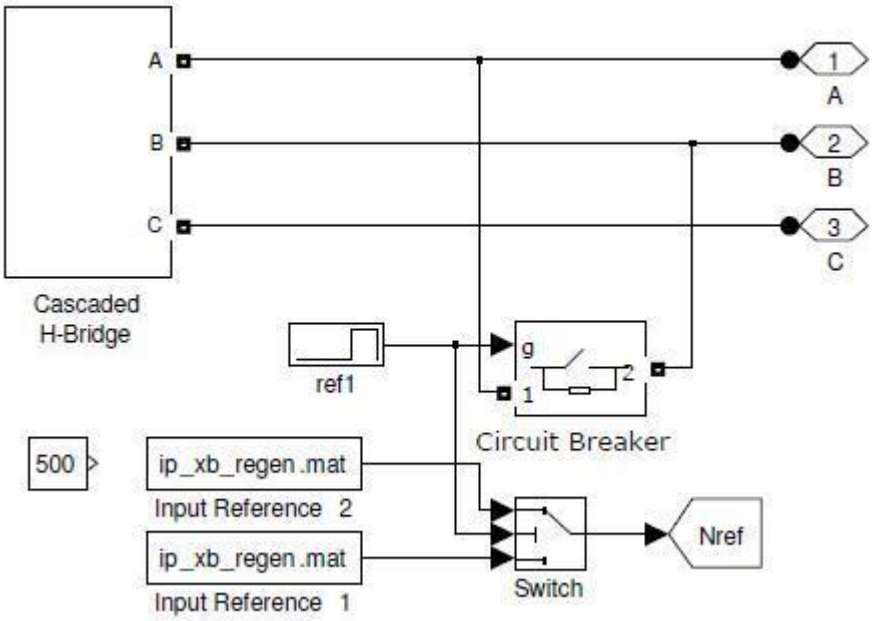

Figure 46. Introducing a phase-to-phase fault at output of the multi level inverter

6.10 Fault Diagnostics and Control

One of the first things to be dealt with is the detection or sensing of the fault. It was seen from an earlier illustration (Figure 20) in Section 5.4.2 where the battery measurements were done. The three important measurements are SOC, current and voltage. A short

circuit fault in a phase would immediately cause a huge current to be drawn from the battery. The SOC drops slower than the rate of increase of current, and so does the voltage because of the battery's equivalent circuit especially its internal resistance. Hence the RMS value of current is measured and compared with a reference value in order to actuate a relay block as shown in (Figure 47). The circuit breaker would be in Normally Closed (NC) condition during steady state. In the event of a fault, the relay would produce a 0 to actuate the circuit breaker to open. The fault monitoring and control system is shown by the red box in the following figure.

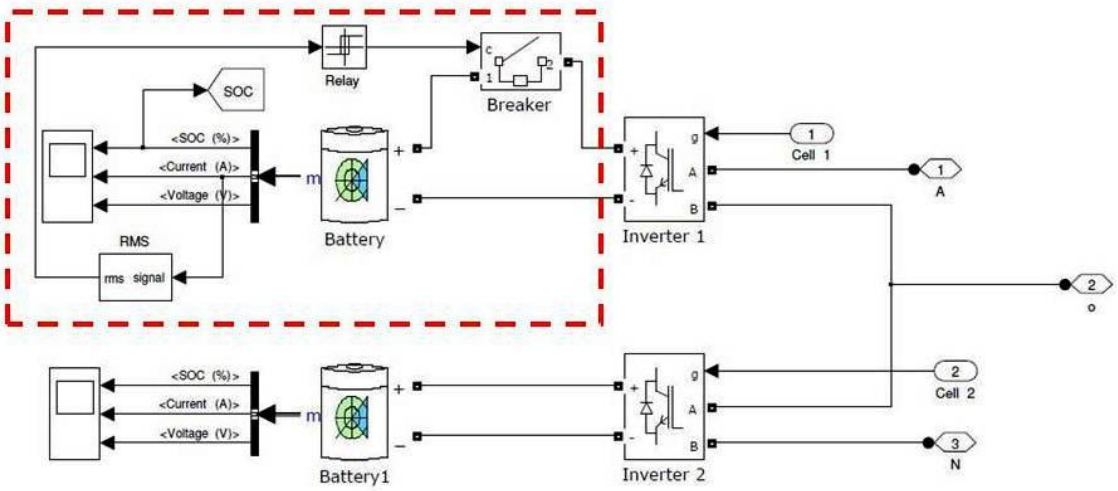

Figure 47. Fault monitoring and control system for a single battery

The result of employing the above illustrated system as a means of fault monitoring and control for a battery is explained as follows. As seen from the above example, the control system has been used for one battery but not for the other. The above schematic clearly shows how the sensing, relay and fast-acting circuit breaker blocks are involved in controlling the fault current for the upper battery. The measurements of the battery in the presence and absence of the fault monitoring and control system are to be compared.

Hence in the absence of a fault control system, the measurements of the lower battery in the schematic (Figure 47) are shown in the graph (Figure 48). Please note that these measurements are for the system employing 5-level 2 cells per phase MLI. Therefore the cell voltages are 750V here and the following analysis can be extrapolated to the other system employing 13-level 6 cells per phase MLI. It is observed in the plot that the SOC drops rapidly from 90% to about 85%, while the current oscillates very fast between 0A and 450A. The battery terminal voltage oscillates between approximately 5V and 800V. The lower end of the voltage, here 5V is a result of the internal resistance chosen. The battery model needs to be improved to include easy changes in internal resistance without simulation errors. From literature survey of industry standards and datasheets, the range of internal resistance is expected to be of the order of 1-10 mΩ. If such a value is chosen, then during a fault event the lower end of the voltage that the battery falls is around 500V. This means the voltage oscillations are between 500 and 800V while the current dissipated due to short circuit is lower too. An important consideration is also the on-time resistance R_{on} (the lower, the better) of the circuit breaker. Now the measurements of the upper battery are to be seen since it displays the performance of the fault monitoring and control system as marked by the red box. The above mentioned measurements are shown in the graph (Figure 49). In direct comparison with (Figure 48), it is easily seen that the fault current is chopped in such a way that it stays at zero for longer periods. The net power loss is seen to be much lower if one can visualize the area under the curve. By tuning the parameters of the RMS block and the relay block, one can optimize the system performance in the presence of a fault to be even better.

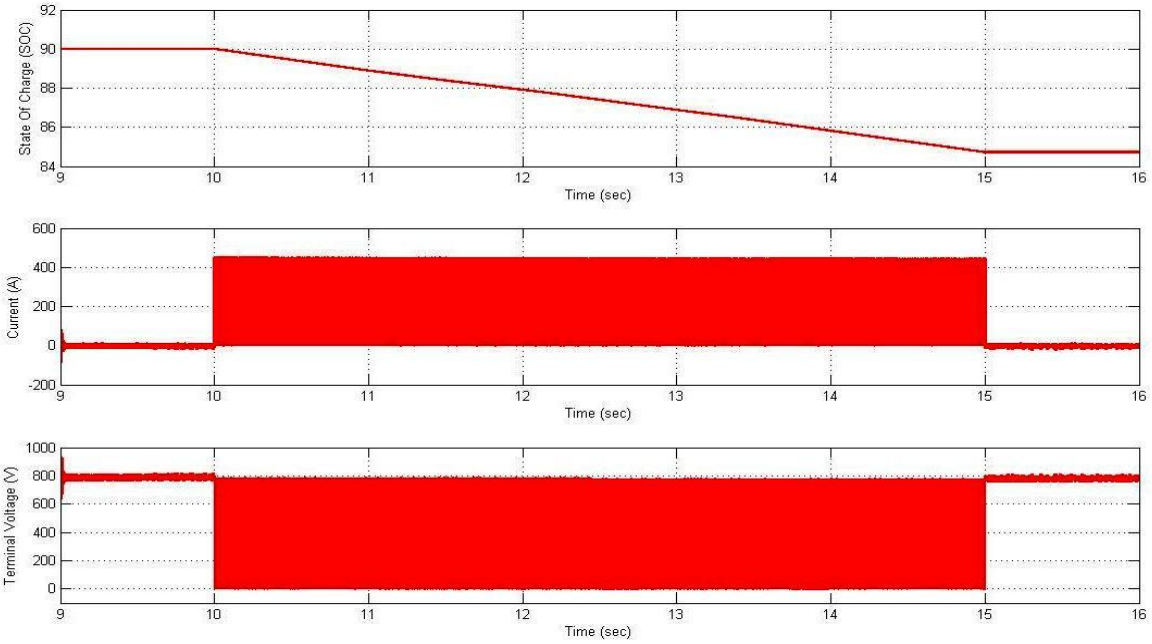

Figure 48. Battery measurements - SOC, current and voltage, in the absence of a fault control system

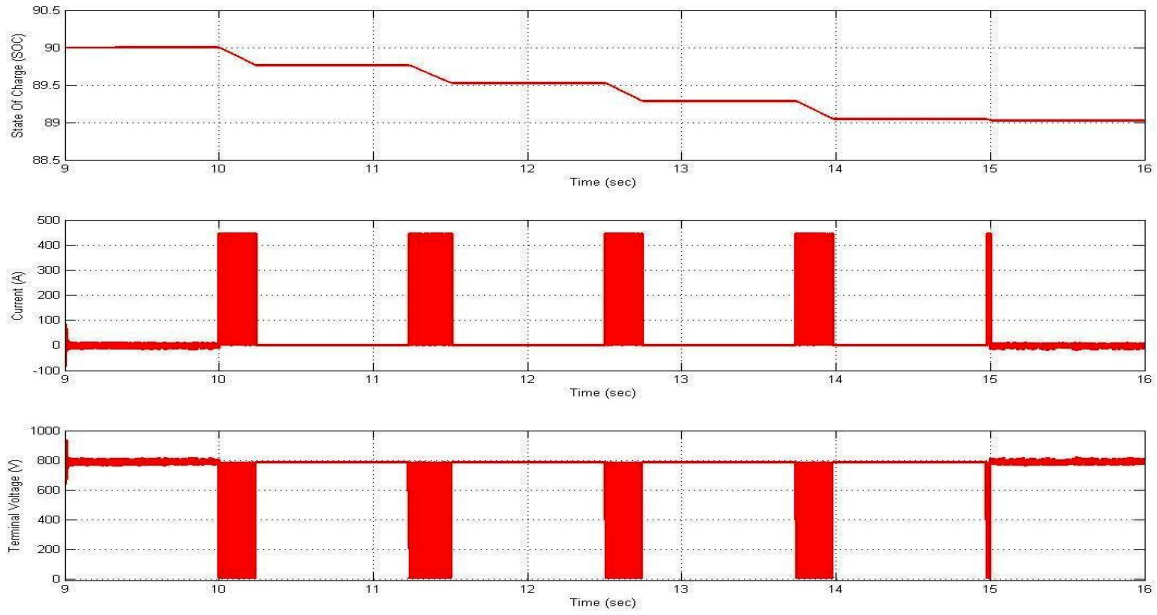

Figure 49. Battery measurements - SOC, current and voltage, in the presence of a fault control system

It is also seen that the terminal voltage does not fall to its lowest allowed value as frequently as before, which is very good for the battery life. Since the currents don't discharge and voltage does not drop as badly as before, the upper battery shall have a longer life. The SOC which was falling from 90% to about 85% in the lower battery is seen to reduce to a mere 89% in the upper battery. This clearly demonstrates a winner since it displays a performance improvement by 4 times because it has limited the fall in SOC to only 1% instead of 5%. This is perceived to be one of the most significant results of this thesis. As a result, the fault monitoring and control system is employed for all the batteries in each phase of the MLI. One phase of the MLI would look as shown in (Figure 50). The red box marks the control system for the first battery, the blue for the second and so on. At a system level implementation, the control signals can be generated by a master controller for each phase in order to simplify computation.

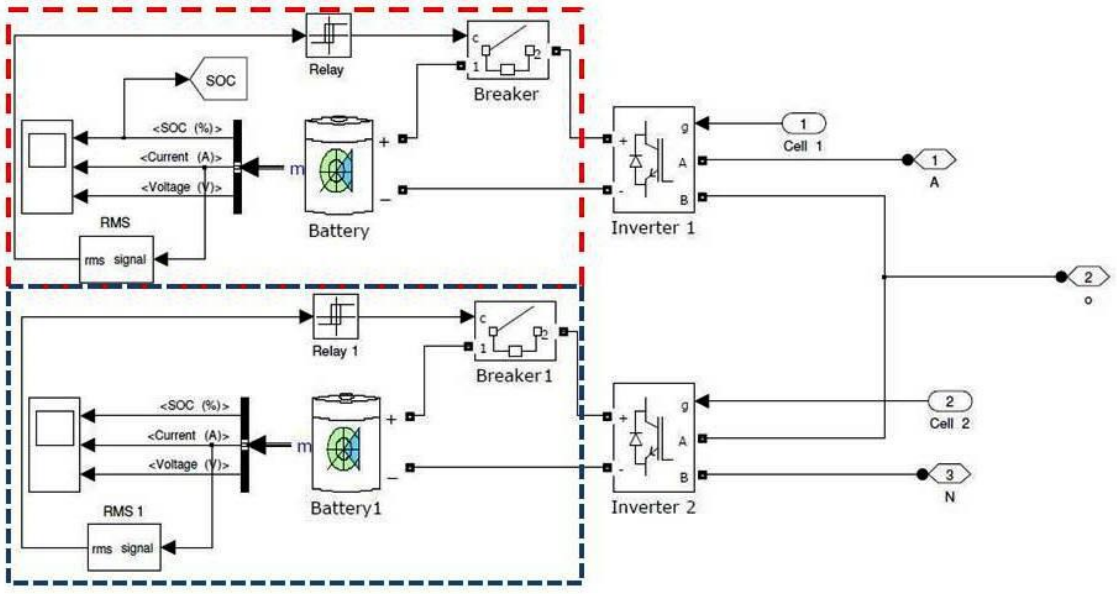

Figure 50. Fault monitoring and control system for all batteries in a phase

After utilizing the fault control systems for all the batteries, the simulation was run to observe performance for the experimental 50 second driving cycle. This is the same

driving cycle that was shown earlier in (Figure 45). In the presence of a fault for 5 seconds between the 10 and 15 second instants, the measurements have been already shown. The following figure (Figure 51) shows the battery measurements for the entire 50 second interval. The SOC drops to about 89% mainly due to the fault, and stays around the same value. The battery currents and voltage return to their nominal values after the fault is cleared.

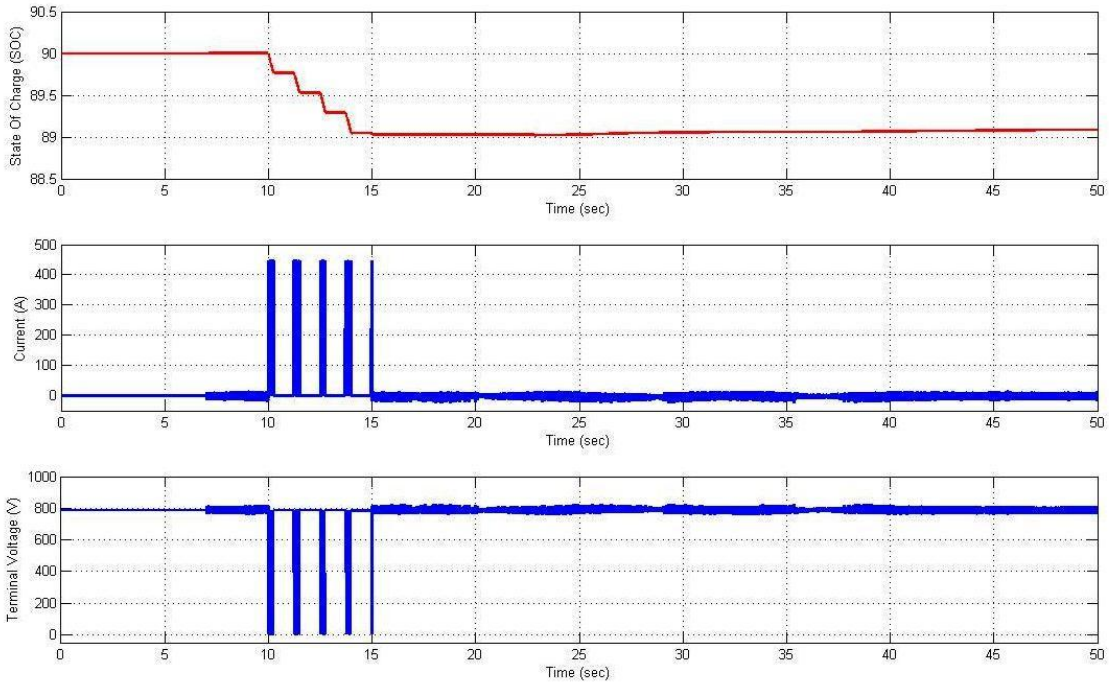

Figure 51. Battery measurements - SOC, current and voltage, in the presence of a fault control system for the entire driving cycle

One must remember that the output speed matches the input reference driving cycle speed perfectly even in the presence of the fault. This is shown in (Figure 52). The battery's capacity to withstand high current for short periods of time is understood from the parameter Cold Cranking Amperes (CCA) as borrowed from its datasheet. Most automotive batteries are built to withstand a couple of thousand amperes for 30 seconds.

The fault period is currently the 10-15 second interval as shown in (Figure 52). As long as the fault period is small, say 1 to 30 seconds; faults can be managed, cleared or avoided to be in limp-home mode. This is also called abuse testing or failure testing of batteries. However the longer the fault stays, the faster the batteries discharge, and the vehicle would eventually come to a stop. This control system would definitely work towards giving the much required range even though a fault occurs.

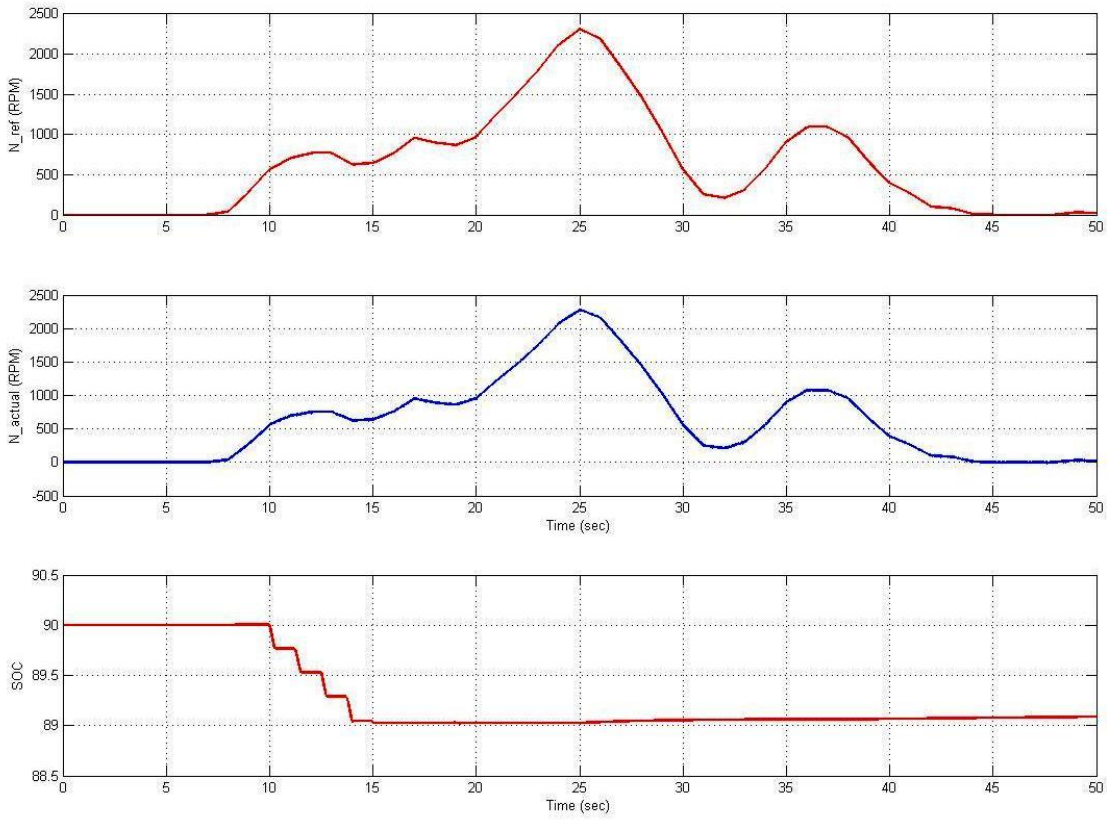

Figure 52. Reference speed, actual speed and SOC of one battery

6.11 Fault Tolerance of the Implemented System

A more careful observation of the graph (Figure 52) shows that the SOC falls in a stepped fashion. If the steps can be made wider, then the depth of the step would be smaller which in turn means the oscillatory parts of the fault period would be even smaller. Alternatively it means, the zero current portions of the fault period can be increased which obviously reflects in further improvement in performance. This is done by introducing a time delay block in the battery fault control system as shown in (Figure 53).

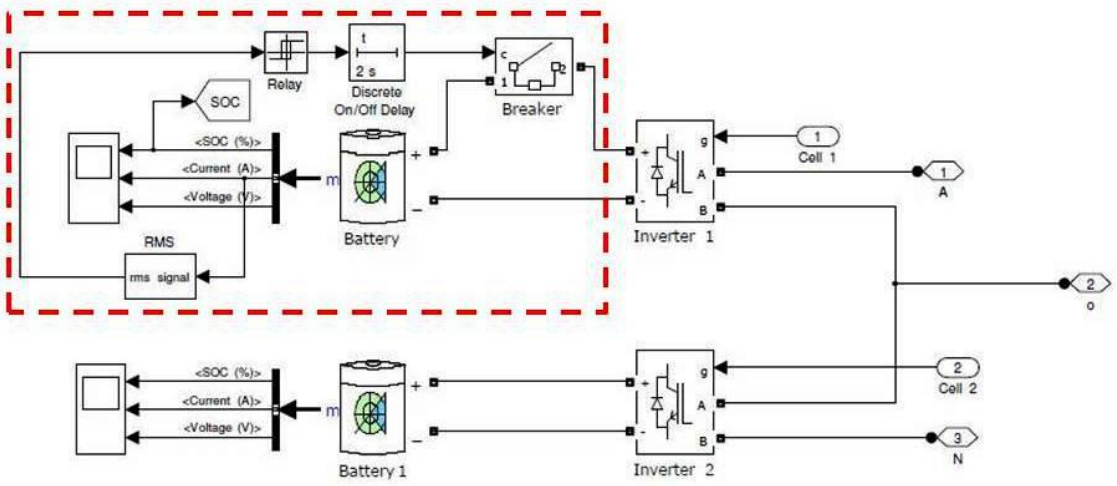

Figure 53. Fault monitoring and control system employing time delay block for a single battery

The result of introducing a time delay block in the fault control system is shown in the measurements graph (Figure 54). A direct comparison with an earlier result (Figure 52) shows that the zero current portions have increased. The main reason in employing a control system to keep the faults under check is to improve system performance and efficiency, while increasing battery life.

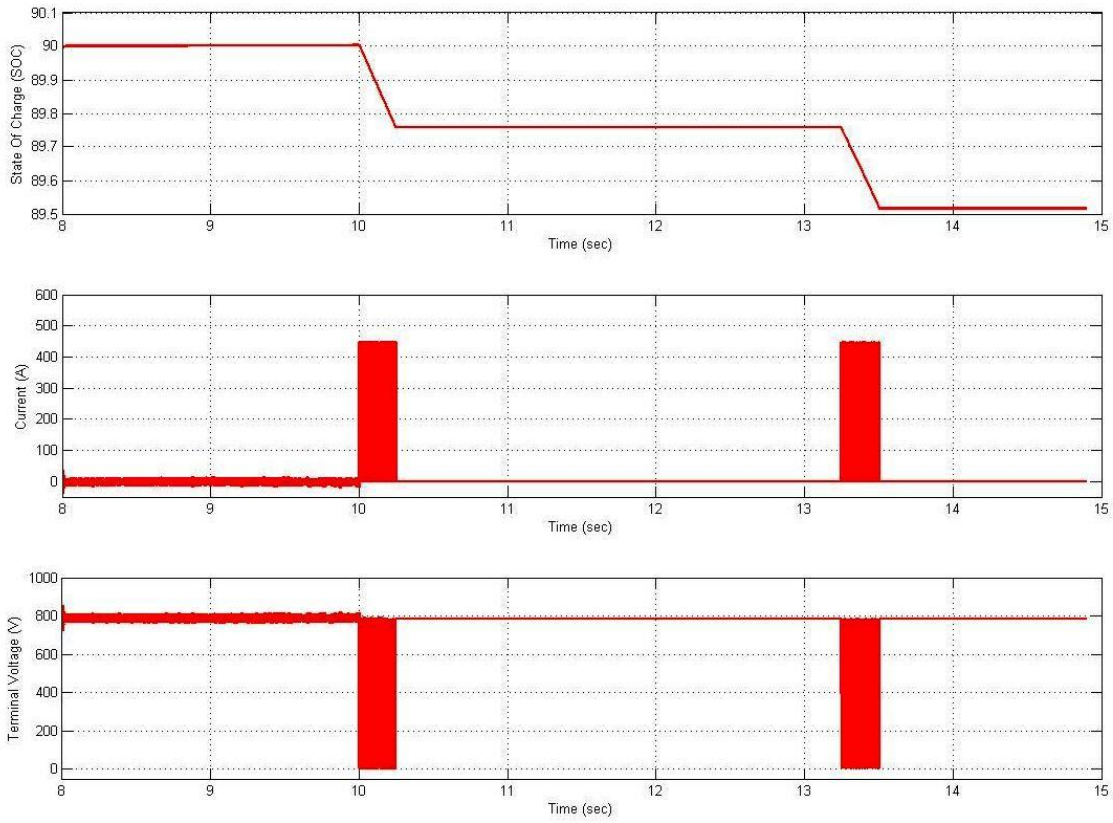

Figure 54. Battery measurements - SOC, current and voltage, in the presence of a fault control system with a time delay block

This section discussed the results of the simulation implementation described in Section 5. The main observations such as output voltage, closed loop speed response and acceleration performance were illustrated and explained. Other observations such as back-emf, stator currents and electro-magnetic torque were also demonstrated. Fault analysis was performed in order to test the implemented system's tolerance, and appropriate modifications in control were done to make it more rugged and tolerant system.

7. CONCLUSIONS

This section discusses the conclusions drawn from this thesis, and briefly summarizes the implications of the results shown in Section 6. The scope of future research and recommendations are provided at the end of this section.

7.1 Conclusions

This thesis mainly demonstrated the successful implementation of a Cascaded H-Bridge multi level inverter to drive a BLDC motor in an electric vehicle. The viability of the system to operate when subjected to realistic driving cycles is shown. This work is primarily an engineering design study and is meant to lead the way for it to be practically implemented. The results as explained in the earlier section discuss the implications of various factors that play into the system design and integration. Since using a multi level inverter to feed a BLDC motor has not been done before for an electric vehicle, this is potentially a new application area.

The Electric Vehicle was designed in great detail to suit real world parameters including the electrical, mechanical and physical specifications. This meant the sizing of the energy sources i.e. battery packs, traction motor, voltage and current levels of the system according to the driving range. The design of the multi level inverter involved choosing the number of cells per phase. This in turn decided the number of voltage levels and power capacity of the inverter. Though the CHB MLI is limited to applications where the individual energy sources are isolated DC sources, this becomes a boon in disguise for the current system since it consists of batteries at the front end.

The design of the system helped understand that the driving range and acceleration performance are very important input considerations. According to the city or type of driving cycle, the vehicle specifications would change. The peak power of the motor and battery are designed with the above considerations in mind. EVs are expected to serve localized solutions better, instead of being envisaged as vehicles that can traverse the entire country. For example, if the EV designed in this thesis were to be meant for purely

the New York city and adjoining areas, it would be great for example as a cab (or taxi). The FTP-75 being a very transient driving cycle, displays the ruggedness of the design because it can handle the ups and downs. Since rapid accelerations and decelerations are present in this driving cycle, it means the designed vehicle can rise up to its maximum speed fast enough and brake in as fast as required. If the implemented design can work for the FTP-75 transient cycle, then it is imagined to work for most other cycles especially highway driving cycles.

The use of a MLI provides some very useful advantages (as perceived from a system level performance point of view) which are mentioned as follows:

- Longer battery life and better battery utilization
- Smaller/lighter batteries
- Improved power management and system reliability
- Avoid no-start and fault conditions (like phase-to-phase short circuit)
- Reduced electrical requirements
- Improved fuel economy
- Decreased warranty costs

To sum up, the main benefits of using multi level converters for the primary traction drive in electric vehicles include:

1. Being suitable for large VA-rated motor drives and traditional 230 V or 460 V motors can be used.
2. Higher efficiency is expected for these MLI fed drive systems due to use of higher voltages and minimum possible switching frequency.
3. Switching devices with lower voltage and current ratings can be used.
4. No EMI problem or common-mode voltage/current problem exists.
5. No charge imbalance problem in either charge mode or drive mode.

The simulation implementation of the system involved modeling the individual components and their respective interconnections. The models mainly consisted of the MLI, traction motor (BLDC), input reference driving cycle, closed loop speed control, vector control, switch gating control blocks and the measurements, Another important model is the Battery Management System which performs fault diagnostics, monitoring and control. The control technique that was implemented for the motor drive was Field Oriented Control, which was explained briefly in basic theory and implemented in simulation model.

The fault analysis forms an important part of this work because it demonstrated the tolerance in the presence of a fault. The system's behavior with and without the fault control scheme were compared. The Battery Management System devised is simple and easily conceivable in hardware, and helps in sensing and clearing the fault. In real time operation, this system provides for a limp-home capability by not having to halt the vehicle because of a short circuit fault. Instead by continuing to run on the intended driving cycle or at a lower speed depending on the level of SOC, the vehicle can be made to run much longer until it can reach the nearest help to be repaired. This battery diagnostic and control system along with the MLI's modularity and scalability greatly improves the viability of the implementation. The SOC was kept in check in order to maintain the life of the batteries and improve the system's fault tolerance.

Device failure constitutes the most significant contingency in a multi level inverter. Loss of devices in certain locations in the string restricts the inverter operation more severely than in other cases. However one must remember that failure probability can be reduced by connecting more cells in series but at an increased cost. Following a fault, the generated THD and DC capacitor voltage ripple is increased because some switching states are lost. It is possible to run the inverter at reduced DC bus utilization. The MLI thus offers a degree of robustness with respect to cell failure or device failure.

7.2 Future Work and Recommendations

This study investigated a simulation model of using a multi level inverter to feed a BLDC motor drive in an electric vehicle. Although the simulations show that the power electronics, motor drive and closed loop control scheme can operate satisfactorily, a hardware prototype needs to be constructed and tested. This is vital to understand for real time operation before it can be made available as a consumer product. The RMS value of current is not an accurate measure of the SOC but has been used here to control the battery during fault. The battery's charge capacity degrades with use, so more accurate methods to estimate and control the battery during fault periods will eventually need to be developed.

One of the biggest advantages of using MLIs in EVs is the hybridization of different energy sources such as a fuel cell, battery, and ultra-capacitors etc. Thus this system can possibly be expanded to hybridize multiple power sources. Variations of the motor drive techniques presented in this thesis could also be employed for better performance. As briefly mentioned in Section 6, another control strategy using time delay can be developed to cater to the battery and use it sparingly. The objective of the BMS control in this thesis was to achieve limp-home capability while preserving battery life.

Since this thesis established proof of principle that MLIs can be used to run BLDC motor drive in EVs, this opens doors to employing them in Hybrid Electric Vehicles. The control of power electronics would be more complicated since it involves the state of the engine in addition to the motor. This would be an interesting research problem to be dealt with in the future.

REFERENCES

[1] J. Rais and M. P. Donsion, "Permanent magnet synchronous motors (PMSM) - parameters influence on the synchronization process of a PMSM," *The International Journal for Computation and Mathematics in Electrical and Electronic Engineering*, vol. 27, pp. 946 - 957, 2008.

[2] L. Chang, "Comparison of AC drives for electric vehicles-a report on experts' opinion survey," *IEEE AES Systems Magazine*, vol., pp. 7-11, 1994.

[3] L. Hao and H. A. Toliyat, "Bldc motor full speed operation using hybrid sliding mode observer," in *Proc. IEEE APEC '03*, 2003, pp. 286-293.

[4] G. S. Buja and M. P. Kazmierkowski, "Direct torque control of PWM inverter-fed AC motors—a survey," *IEEE Transactions on Industrial Electronics*, vol. 51, pp. 744 - 757, 2004.

[5] F. Blaschke, "The principle of field-orientation as applied to the transvector closed-loop control system for rotating-field machines," *Siemens Rev*, vol. 34, pp. 217 - 220, 1972.

[6] M. P. Kazmierkowski, R. Krishnan, and F. Blaabjerg, *Control in power electronics*. 1 ed., San Diego, CA: Academic, 2002.

[7] M. Pietrzak-David and B. de Fornel, "Non-linear control with adaptive observer for sensorless induction motor speed drives," *European Power Electronics and Drives (EPE)*, vol. 11, pp. 7-13, 2001.

[8] M. F. Rahman, L. Zhong, and K.W. Lim, "An investigation of direct and indirect torque controllers for PM synchronous motor drives," in *Conf. Rec. PEDS '97*, Singapore, 1997, pp. 519-523.

[9] M. F. Rahman, L. Zhong, and K.W. Lim, "A direct torque controlled interior permanent magnet synchronous motor drive incorporating field weakening," in *Conf. Rec. IEEE-IAS Annual Meeting*, New Orleans, USA, 1997, pp. 67-74.

[10] M. E. Haque, L. Zhong, and M. F. Rahman, "A sensorless speed estimator for application in a direct torque controller of an interior permanent magnet synchronous motor drive, incorporating compensation of offset error," in *Proc. IEEE PESC'02*, Cairns, Australia, 2002, pp. 276–281.

[11] M. R. Zolghadri and D. Roye, "Sensorless direct torque control of synchronous motor drive," in *Proc. ICEM '98*, Istanbul, Turkey, Sep 2-4, 1998, pp. 1385–1390.

[12] Y. Liu, Z. Q. Zhu, and D. Howe, "Direct torque control of brushless DC drives with reduced torque ripple," *IEEE Transactions On Industry Applications*, vol. 41, pp. 599-608, 2005.

[13] T. S. Low, K. J. Tseng, T. H. Lee, K. W. Lim, and K. S. Lock, "Strategy for the instantaneous torque control of permanent-magnet brushless DC drives," *Proc. IEE—Electric Power Applications*, vol. 197, pp. 355–363, 1990.

[14] T. S. Low, T. H. Lee, K. J. Tseng, and K. S. Lock, "Servo performance of a BLDC drive with instantaneous torque control," *IEEE Transactions On Industry Applications*, vol. 28, pp. 455–462, 1992.

[15] S. K. Chung, H. S. Kim, C. G. Kim, and M. J. Youn, "A new instantaneous torque control of PM synchronous motor for high-performance direct-drive applications," *IEEE Transactions on Power Electronics*, vol. 13, pp. 388-400, 1998.

[16] S. B. Ozturk and H. A. Toliyat, "Direct torque control of brushless DC motor with non-sinusoidal back-emf," in *Proc. IEEE IEMDC '07*, 2007, pp. 165-171.

[17] Akira Nabae, I. Takahashi, and H. Akagi, "A new neutral-point-clamped PWM inverter," *IEEE Transactions on Industry Applications*, vol. 1A-17, pp. 518-523, 1981.

[18] R. H. Baker and L. H. Bannister, "Electric power converter," U.S. Patent 3867643, 1975.

[19] J. Rodriguez, J. S. Lai, and F. Z. Peng, "Multilevel inverters: A survey of topologies controls and applications," *IEEE Transactions on Industrial Electronics*, vol. 49, pp. 724 - 738, 2002.

[20] E. Cengelci, S. U. Sulistijo, B. O. Woom, P. Enjeti, R. Teodorescu, and F. Blaabjerge, "A new medium voltage pwm inverter topology for adjustable speed drives," *IEEE Transactions on Industry Applications*, vol. 35, pp. 628-637, 1998.

[21] A. F. Nnachi, A.A Jimoh, and D.V Nicolae, "Multilevel high power converters for reversible power flow between utilities and power pool transmission corridor," in *IEEE AFRICON 07*, Windhoek, Namibia, 2007.

[22] J. S. Lai and F. Z. Peng, "Multilevel converters - a new breed of power converters," *IEEE Transactions on Industry Applications*, vol. 32, pp. 509-517, 1996.

[23] F. Z. Peng, "A generalized multilevel inverter topology with self voltage balancing," *IEEE Transactions on Industry Applications*, vol. 37, pp. 611-618, 2000.

[24] L. M. Tolbert, F. Z. Peng, and T. G. Habetler, "Multilevel converters for large electric drives," *IEEE Transactions on Industry Applications*, vol. 35, pp. 36-44, 1999.

[25] L. M. Tolbert, F. Z. Peng, and T. G. Habetler, "Multilevel inverters for electric vehicle applications," in *WPET '98*, Dearborn, Michigan, October 22-23, 1998, pp. 79-84.

[26] G. Sinha and T. A. Lipo, "A four-level rectifier inverter system for drive applications," *IEEE Industry Applications Magazine*, vol. 4, pp. 66-74, 1998.

[27] Tim Cunnyngham, *Cascade multilevel inverters for large hybrid-electric vehicle applications with variant dc sources*. Master's Thesis, Electrical Engineering, The University of Tennessee, Knoxville, 2001.

[28] L. M. Tolbert, F. Z. Peng, "Multilevel inverters for large automotive drives," *All Electric Combat Vehicle Second International Conference*, vol. 2, pp. 209-214, 1997.

[29] Bin Wu, *High-power converters and AC drives*. Illustrated ed., Hoboken, NJ: Wiley-IEEE. 333, 2006.

[30] Mehrdad Ehsani, Y. Gao, S. E. Gay, and A. Emadi, *Electric vehicles*, in *Modern electric,hybrid electric, and fuel cell vehicles - fundamentals, theory, and design*, Ch 4, Boca Raton, FL: CRC Press, 2005.

[31] James Larminie, and J. Lowry, *Electric vehicle technology explained*, Ch 2, West Sussex, England: John Wiley & Sons Ltd, 2003.

[32] Ned Mohan, T. M. Undeland, and W. P. Robbins, *Power electronics: Converters, applications, and design*. 2 ed., New York: Wiley, 1995.

APPENDIX A

INPUT REFERENCE DRIVING CYCLE CODE

```
% INPUT REFERENCE DRIVING CYCLE
% read data points from standard driving cycle, create a suitable input file for the system simulation
clear all;clc;
% read the datapoints for speed vs time from a data file to a vector
x=fopen('C:\Documents and Settings\Sriram\My Documents\MATLAB\MSP\project\nyc\nyc.txt');
y=fscanf(x,'%15f');
% create the time variable
t=linspace(0,563,564);
y=y';
% the multiplication factor of 62.5 comes from product of 5/18 and 225, 225 comes from gear ratio formula
y=y*62.5;
y=horzcat(0,y);
% here x is the input reference driving cycle
x=[t;y];
% the data points stored in variable x are stored as a 2 column vector in a MAT file
save('nyc.mat','x');

% for the purpose of ease of simulation, the data range is split into 4 portions each of which can be simulated separately
% the results are joined together later
t_period=564;
tb1=t(1:150); tb_bal=t_period-3*length(tb1);
b1=y(1:150); xb1=[tb1;b1];
b2=y(150:300); xb2=[t(1:151);b2];
b3=y(300:450); xb3=[t(1:151);b3];
b4=y(450:564); xb4=[t(1:tb_bal+1);b4];

% for purpose of evaluating regenerative capability of the system, a new variable is created with only 50 seconds portion of the actual cycle, this data is saved in a new MAT file which is the input to the simulation
b_regen=y(40:90); xb_regen=[t(1:51);b_regen];
save('ip_xb_regen.mat','xb_regen');
```

APPENDIX B

SPLIT SIMULATION

```
% Splitting simulation into parts for faster run time
clear all; clc;
% for the purpose of ease of simulation, the data range is split into 4 portions each of which can be simulated separately
% the results are joined together later
t_period=564;
tb1=t(1:150); tb_bal=t_period-3*length(tb1);
b1=y(1:150); xb1=[tb1;b1];
b2=y(150:300); xb2=[t(1:151);b2];
b3=y(300:450); xb3=[t(1:151);b3];
b4=y(450:564); xb4=[t(1:tb_bal+1);b4];

% here xb1, xb2, xb3, xb4 are the input reference driving cycles
% the data points stored in variable x are stored as a 2 column vector in a MAT file
save('nyc1.mat','xb1');
save('nyc2.mat','xb2');
save('nyc3.mat','xb3');
save('nyc4.mat','xb4');

% generating outputs
% reading the time base
t1=Nref_Nactual.time;
y1=Nref_Nactual.signals(1,1).values;
y2=Nref_Nactual.signals(1,2).values;
t1=t1'; y1=y1'; y2=y2';

% saving the output in a MAT file
save('op_xb7_1.mat','y1');
save('op_xb8_1.mat','y2');

% loading the output MAT file to a variable
x11=load('op_xb1_1.mat','y1');
x12=load('op_xb2_1.mat','y2');
x21=load('op_xb3_1.mat','y1');
x22=load('op_xb4_1.mat','y2');
x31=load('op_xb5_1.mat','y1');
x32=load('op_xb6_1.mat','y2');
x41=load('op_xb7_1.mat','y1');
```

```
x42=load('op_xb8_1.mat','y2');


% concatenating the 4 output variables to combine into a single variable
% xa and xb are the input and the output respectively
xa=horzcat(x11.y1,x21.y1,x31.y1,x41.y1);
xb=horzcat(x12.y2,x22.y2,x32.y2,x42.y2);

% the step time of the simulation
Ts=20e-5;
% creating a time base
t=linspace(0,563,564/Ts);
t=horzcat(0,0,0,0,t);

% generating input and output vectors, plotting them together
ya=[t;xa];
yb=[t;xb];
subplot(2,1,1); plot(t,xa); grid on;
subplot(2,1,2); plot(t,xb); grid on;
```

APPENDIX C

INPUT PARAMETERS FOR THE SIMULATION

```
% Input parameters for the simulation
clear all; clc;
% simulation time step
Ts=20e-5;
% DC terminal voltage of each battery
V=250;
% number of cells per phase, for use in LSMM control
% the number of cells decides the number of levels for the control signals
n=6;
% switching frequency
f=60;
% Ampere hour capacity
Ah=10;
```

VITA

Sriram Sarma Emani received his Bachelor of Technology degree in electrical and electronics engineering from the Jawaharlal Nehru Technological University at Hyderabad, India in 2006. He worked as a Junior Project Officer at The Indian Institute of Technology, Kharagpur during 2006-2007 where he developed pulse generators for specialized applications such as nano-material compaction and food sterilization.

He graduated with a Master of Science degree in Electrical Engineering specializing in Power Electronics, Motor Drives and Electric Vehicles at Texas A&M University in 2010. He has worked as an intern in TECO-Westinghouse Motor Company. He pursued another internship working on solar PV inverters at eIQ Energy Inc. His other research interests include power electronic control topologies, power system engineering, smart vehicles, control systems and renewable energy applications. His ambitions are to work on power electronic converter applications in the energy industry.

Mr. Emani may be reached via email at: esriramsarma@tamu.edu or by mail at: Department of Electrical Engineering, Texas A&M University, 109 WERC, College Station, TX 77843.